MISSOURI S&T | CURTIS LAWS WILSON LIBRARY
MISSOURI UNIVERSITY OF SCIENCE AND TECHNOLOGY

Scholars' Mine

Masters Theses | Student Theses and Dissertations

Fall 2012

Effects of coal comminution in relation to waterjet and selected feed properties

Yaqing Li

Follow this and additional works at: https://scholarsmine.mst.edu/masters_theses

 Part of the Mining Engineering Commons

Department:

Recommended Citation

Li, Yaqing, "Effects of coal comminution in relation to waterjet and selected feed properties" (2012). *Masters Theses*. 5288.
https://scholarsmine.mst.edu/masters_theses/5288

This thesis is brought to you by Scholars' Mine, a service of the Curtis Laws Wilson Library at Missouri University of Science and Technology. This work is protected by U. S. Copyright Law. Unauthorized use including reproduction for redistribution requires the permission of the copyright holder. For more information, please contact scholarsmine@mst.edu.

www.manaraa.com

المنارة للاستشارات
www.manaraa.com

EFFECTS OF COAL COMMINUTION IN RELATION TO WATERJET AND SELECTED FEED PROPERTIES

by

YAQING LI

A THESIS

Presented to the Faculty of the Graduate School of the

MISSOURI UNIVERSITY OF SCIENCE AND TECHNOLOGY

In Partial Fulfillment of the Requirements for the Degree

MASTER OF SCIENCE IN MINING ENGINEERING

2012

Approved by

Grzegorz Galecki, Advisor
Jerry Tien
Kwame Awuah-Offei
Sen Sezai

www.manaraa.com

المنارة للاستشارات
www.manaraa.com

ABSTRACT

The necessity to develop a viable alternative to oil means that the development of coal-water fuels (CWF) has become increasingly important. However, the existing methods of comminution to prepare ultrafine particles for CWF are very inefficient. Consequently, a number of novel methods of comminution have been investigated in order to increase the efficiency of the process.

In this research, a new method of comminution using a high-pressure waterjet has been tested to produce ultrafine particle sizes necessary for efficient CWF process. To establish the fundamental performance of the waterjet mill, the influence of the operational pressure, standoff distance, feed size, mode (dry/wet) of feed material, and ash content of feed material were evaluated. The comminution products were characterized in terms of particle size, surface area change, particle size distribution (PSD), and morphological properties.

The experimental results show that this new comminution method offers a promising means for achieving the size reduction required for use in CWF. It was also found that the waterjet-mediated comminution of coal was strongly affected by all these operating parameters. Higher operational pressure led to finer products that were more spherical shaped, while the energy efficiency of the mill strongly depended on the initial feed size and standoff distance. Since there is currently no accurate mode assessing the size of the comminution products, a volume-based fractal model was deduced to characterize the particle size distribution of the comminution products through a single and exact parameter.

www.manaraa.com

ACKNOWLEDGMENTS

Great appreciation is expressed to my advisor, Dr. Greg Galecki, for his encouragement and guidance throughout my master's program at Missouri University of Science and Technology. Special thanks are given to Dr. Gul Akar, and Dr Sezai Sen for their invaluable suggestions, guidance and assistance at various stages of my thesis.

I would like to acknowledge and express my gratitude to my committee members, Dr. Jerry Tien, and Dr. Kwame Awuah-Offei. I am thankful for their valuable suggestions, feedbacks and interests in this research.

I wish to say thanks to the Mining Engineering Department of Missouri University of Science and Technology and my fellow graduate students in the department.

Lastly but not least, I would like to thank my parents for their continued encouragement over the years. Abundant thanks are given to my husband Yutao Zhang, and son Daniel Zhang for their continued love and sacrifices which made this endeavor possible.

www.manaraa.com

TABLE OF CONTENTS

Page

ABSTRACT iii

ACKNOWLEDGMENTS iv

LIST OF ILLUSTRATIONS ix

LIST OF TABLES xiv

NOMENCLATURE xv

SECTION

1. INTRODUCTION 1

1.1. BACKGROUND AND MOTIVATION 1

1.2. OBJECTIVES 5

1.3. THESIS OUTLINE 6

2. LITERATURE REVIEW 7

2.1. GENERAL INTRODUCTION 7

2.2. BALL MILLS 9

2.3. HAMMER MILLS 10

2.4. VERTICAL SPINDLE MILLS 12

2.5. HIGH-PRESSURE WATERJET MILLS 13

2.6. FRACTAL THEORY 18

3. METHODOLOGY 20

3.1. DESIGN OF EXPERIMENTS 20

3.1.1. Variables of WaterJet 20

3.1.2. Variables of Feed Materials. 20

www.manaraa.com

3.1.3. Experimental Procedure. 21
3.2. SAMPLE PREPARATION 21
3.3. EXPERIMENTAL APPARATUS 22
4. TEST RESULTS AND DISCUSSION 25
4.1. GENERAL INTRODUCTION 25
4.2. WATERJET-BASED COMMINUTION OF C1 COAL 27
4.2.1. Particle Size Analysis. 27
4.2.2. Surface Area Change. 32
4.2.3. Particle Size Distribution. 33
4.2.4. Morphological Properties of Feeds and Comminution Products 35
4.3. WATERJET-BASED COMMINUTION OF C2 COAL 38
4.3.1. Particle Size Analysis.. 39
4.3.2. Surface Area Change. 44
4.3.3. Particle Size Distribution. 46
4.3.4. Morphological Properties of Feeds and Comminution Products 47
4.4. WATERJET-BASED COMMINUTION OF C3 COAL 51
4.4.1. Particle Size Analysis 51
4.4.2. Surface Area Change. 57
4.4.3. Particle Size Distribution. 58
4.4.4. Morphological Properties of Feeds and Comminution Products 60
4.5. OVERVIEW OF SECTIONS 4.2, 4.3, AND 4.4 64
4.5.1. Particle Size Analysis. 64
4.5.2. Surface Area Change. 71

www.manaraa.com

4.5.3 Particle Size Distribution. 71

4.5.4. Morphological Properties of Feed and Comminution Products 71

4.6. WATERJET-BASED COMMINUTION OF C3 COAL IN THE FEED FORM OF COAL-WATER SLURRY 72

4.6.1. Particle Size Analysis. 72

4.6.2. Summary of Section 4.6. 76

4.7. THE EFFECT OF STANDOFF DISTANCE ON WATERJET-BASED COAL COMMINUTION 78

4.7.1. C3 Coal Comminution with 100 Millimeter Standoff Distance. 78

4.7.1.1 Particle size analysis. 78

4.7.1.2 Particle size distribution. 80

4.7.2. C3 Coal Comminution with 98 Millimeter Standoff Distance 81

4.7.2.1 Particle size analysis. 81

4.7.2.2 Particle size distribution 83

4.7.3. C3 Coal Comminution with 3 Millimeter Standoff Distance. 85

4.7.3.1 Particle size analysis. 85

4.7.3.2 Particle size distribution. 86

4.7.4. Section Summary. 87

5. APPLICATION OF THE FRACTAL THEORY FOR EVALUATING EFFECTS OF WATERJET-BASED COAL COMMINUTION 90

5.1. GENERAL INTRODUCTION 90

5.2. FRACTAL MODEL FOR PARTICLE SIZE DISTRIBUTION 90

5.3. CHARACTERIZATION OF THE COMMINUTION PRODUCTS BY THE PROPOSED MODEL 93

5.4. SUMMARY OF SECTION 5 98

www.manaraa.com

6. CONCLUSIONS AND RECOMMENDATIONS FOR FUTURE WORK 100

6.1. CONCLUSIONS 100

6.2. RECOMMENDATIONS FOR FUTURE WORK 101

6.2.1. Construction of Mathematical Models for Waterjet-Based Comminution 101

6.2.2. Conduction of Comparative Experiments. 101

6.2.3. Energy Consumption Analysis. 101

BIBLIOGRAPHY 102

VITA 109

www.manaraa.com

LIST OF ILLUSTRATIONS

Figure Page

2.1. Required Energy for Size Reduction In Comminution Process 8

2.2. Cross-Section Diagram Of The Mixing Chambers Used In Experiments By Hlaváč et al 16

3.1. Basic Flow-Sheet of the Experimental Procedure 21

3.2. Basic Flow-Sheet of the Sample Preparation 22

3.3. Schematic of the High-Pressure Waterjet Mill 23

3.4. Conventional Abrasive Waterjet Cutting Head 23

3.5. Cavitating Jet 24

4.1. CVUSCs of C1FM and Mono-Sized Subsamples (C1FR1through C1FR4) 27

4.2. CVUSCs of Products for C1FR1 Comminuted at Different Operational Pressures 28

4.3. CVUSCs of Products for C1FR2 Comminuted at Different Operational Pressures 29

4.4. CVUSCs of Products for C1FR3 Comminuted at Different Operational Pressures 30

4.5. CVUSCs of Products for C1FR4 Comminuted at Different Operational Pressures 31

4.6. CVUSCs of Products for C1FM Comminuted at Different Operational Pressures 31

4.7. CSARs versus Operational Pressures for Mono-Sized Subsamples of C1FM 33

4.8. PSD Curves of C1FM as a Function of the Operational Pressure 34

4.9. Morphological Properties of the Original Feed Material (C1FM) 35

4.10. Morphological Properties of the Product Obtained from C1FM (10,000 psi Operational Pressure) 36

www.manaraa.com

4.11. Morphological Properties of the Product Obtained from C1FM (20,000 psi Operational Pressure) 36

4.12. Morphological Properties of the Product Obtained from C1FM (30,000 psi Operational Pressure) 37

4.13. Morphological Properties of the Product Obtained from C1FM (40,000 psi Operational Pressure) 38

4.14. CVUSCs of C2FM and Mono-Sized Subsamples (C2FR1through C2FR4) 39

4.15. CVUSCs of Products for C2FR1 Comminuted at Different Operational Pressures 40

4.16. CVUSCs of Products for C2FR2 Comminuted at Different Operational Pressures 41

4.17. CVUSCs of Products for C2FR3 Comminuted at Different Operational Pressures 42

4.18. CVUSCs of Products for C2FR4 Comminuted at Different Operational Pressures 43

4.19. CVUSCs of Products for C2FM Comminuted at Different Operational Pressures 44

4.20. CSARs versus Operational Pressures for Different Feed Sizes of C2 Coal 45

4.21. PSD Curves of C2FM as a Function of the Operational Pressure 46

4.22. Morphological Properties of the Original Feed Material (C2FM) 47

4.23. Morphological Properties of the Product Obtained from C2FM (10,000 psi Operational Pressure) 48

4.24. Morphological Properties of the Product Obtained from C2FM (20,000 psi Operational Pressure) 49

4.25. Morphological Properties of the Product Obtained from C2FM (30,000 psi Operational Pressure) 49

4.26. Morphological Properties of the Product Obtained from C2FM (40,000 psi Operational Pressure) 50

4.27. Morphological Properties of the Product Obtained from C2FM (40,000 psi Operational Pressure, Higher Magnification) 51

www.manaraa.com

4.28. CVUSCs of C3FM and Mono-Sized Subsamples (C3FR1through C3FR4) 52

4.29. CVUSCs of Products for C3FR1 Comminuted at Different Operational Pressures 53

4.30. CVUSCs of Products for C3FR2 Comminuted at Different Operational Pressures 54

4.31. CVUSCs of Products for C3FR3 Comminuted at Different Operational Pressures 55

4.32. CVUSCs of Products for C3FR4 Comminuted at Different Operational Pressures 56

4.33. CVUSCs of Products for C3FM Comminuted at Different Operational Pressures 57

4.34. CSARs versus Operational Pressures for Mono-Sized Subsamples of C3FM 58

4.35. PSD Curves of C3FM as a Function of the Operational Pressure 59

4.36. Morphological Properties of the Original Feed Material (C3FM) 60

4.37. Morphological Properties of the Product Obtained from C3FM (10,000 psi Operational Pressure) 61

4.38. Morphological Properties of the Product Obtained from C3FM (20,000 psi Operational Pressure) 62

4.39. Morphological Properties of the Product Obtained from C3FM (30,000 psi Operational Pressure) 62

4.40. Morphological Properties of the Product Obtained from C3FM (40,000 psi Operational Pressure) 63

4.41. C1 Coal: Median Particle Sizes of the Products as a Function of Operational Pressures 66

4.42. C2 Coal: Median Particle Sizes of the Products as a Function of Operational Pressures 66

4.43. C3 Coal: Median Particle Sizes of the Products as a Function of Operational Pressures 67

4.44. Temperature of the Comminution Products as a Function of the Operational Pressure 67

www.manaraa.com

4.45. Photomicrograph of C2 Coal 70

4.46. Wet Feed: CVUSCs of C3FM and Mono-Sized Subsamples (C3FR1through C3FR4)..... 73

4.47. Wet Feed:CVUSCs of Products for C3FR1 Comminuted at Different Operational Pressures..... 74

4.48. Wet Feed:CVUSCs of Products for C3FR2 Comminuted at Different Operational Pressures..... 74

4.49. Wet Feed:CVUSCs of Products for C3FR3 Comminuted at Different Operational Pressures..... 75

4.50. Wet Feed:CVUSCs of Products for C3FR4 Comminuted at Different Operational Pressures..... 76

4.51. CVUSCs of C3FM and Mono-Sized Subsamples (C3FR1through C3FR4)..... 79

4.52. 100 mm Standoff Distance: CVUSCs of Products Obtained from Mono-Sized Subsamples Comminuted at 10000 psi..... 79

4.53. 100 mm Standoff Distance: CVUSCs of Products Obtained from C3FM Comminuted at Different Operational Pressures..... 80

4.54. 100 mm Standoff Distance: PSD of C3FM as a Function of the Operational Pressure..... 81

4.55. 98 mm Standoff Distance: CVUSCs of Products Obtained from Mono-Sized Subsamples Comminuted at 10000 psi..... 82

4.56. 98 mm Standoff Distance: CVUSCs of Products Obtained from C3FM Comminuted at Different Operational Pressures..... 83

4.57. 98 mm Standoff Distance: PSD of C3FM as a Function of the Operational Pressure..... 84

4.58. 3 mm Standoff Distance: CVUSCs of Products Obtained from Mono-sized Subsamples Comminuted at 10000 psi..... 85

4.59. 3 mm Standoff Distance: CVUSCs of Products Obtained from C3FM Comminuted at Different Operational Pressures..... 86

www.manaraa.com

4.60. 3 mm Standoff Distance: PSD of C3FM as a Function of the Operational Pressure 87

5.1. Regressive Curves of PSDs for Products Comminuted at Different Pressures 93

5.2. Fractal Dimensions of Particle Size Distribution versus Operational Pressure 98

www.manaraa.com

LIST OF TABLES

Table Page

3.1. Codes And Properties of Coal Samples ....…..20

3.2. Characteristics of the High-Pressure Waterjet Mill ....…..24

4.1. C1 Coal: The Median Particle Sizes of the Products Comminuted at Different Comminution Conditions ....…..65

4.2. C2 Coal: The Median Particle Sizes of the Products Comminuted at Different Comminution Conditions ....…..65

4.3. C3 Coal: The Median Particle Sizes of the Products Comminuted at Different Comminution Conditions ....…..65

4.4. C1 Coal: Particle Size Reduction Ratios of Different Comminution Conditions…..69

4.5. C2 Coal: Particle Size Reduction Ratios of Different Comminution Conditions…..69

4.6. C3 Coal: Particle Size Reduction Ratios of Different Comminution Conditions…..69

4.7. C3 Coal-Wet Feeding: The Median Particle Size of the Products Comminuted at Different Comminution Conditions ....…..77

4.8. C3 Coal-Wet Feeding: Size Reduction Ratios Obtained at Different Comminution Conditions ....…..77

4.9. Mono-Sized Samples: Size Reduction Ratios as a Function of the Standoff Distance ....…..88

4.10. The Original Feed Material (C3FM): Size Reduction Ratios as a Function of the Standoff Distance ....…..89

5.1. Fractal Dimensions Calculated From the Slopes of the Best Fitting Lines ....…..96

www.manaraa.com

NOMENCLATURE

Symbol	Description
CWS	Coal Water Slurry
SSA	Specific Surface Area
CSA	Calculated Surface Area
CSAR	Calculated Surface Area Ratio
PSD	Particle Size Distribution
CVUSC	Cumulative Volume Undersize Curve

www.manaraa.com

1. INTRODUCTION

1.1. BACKGROUND AND MOTIVATION

According to a report by the International Energy Agency (IEA), coal is the world's most abundant and widely distributed fossil fuel (Anonymous, 2011).When compared to both oil and natural gas, the price of coal is more stable and much lower. As a result, coal has been the world's most reliable energy source and also the fastest growing fuel in the past decades. In 2010, the global demand for coal increased 46% compared with 27% for natural gas, 25% for hydro, 10 % for oil and just 7% for nuclear (Tony Hayward Group Chief Executive, 2010). Currently, coal fuels more than 40% of the world's electricity. This figure is much higher in many countries, such as South Africa, (93%); Poland, (92%); China, (79%); India, (69%); and the United States,(49%) (Anonymous,2011).

As an affordable and cheap energy, coal will continue to fuel the largest share of worldwide electric power production by a wide margin (Boltik, 2011). It is forecasted that in the next five years, the world will add 300 gigawatts (GW, $1GW=10X10^7KW$) of coal-fired power generation, the equivalent of the entire U.S. fleet (Richardson, 2011). As well, the world net coal-fired generation is projected to nearly double from 7.9 trillion kilowatt hours in 2007 to 15.0 trillion kilowatt hours in 2035 (Boltik, 2011). Since coal is the most abundant energy resource with significant remaining reserves in the United States, it will remain as a key component in the power generation industry. It has been forecasted by the Energy Information Administration (EIA) that, under current policies, fossil fuels will provide 78 percent of U.S. energy in 2035, and 43 percent of net electricity will be from coal (Karmis, 2011). Developing countries tend to have an even higher percent of net electricity powered by coal. Kost (2011) stated that approximately 80% of newly installed electric generation in developing countries is projected to be coal. However, there are some significant problems associated with the utilization of coal due to its complex composition.

Coal is full of hazardous substances that, when burned, can contaminate the air, the land, and the water. Environmentalists claimed that coal burning is a leading cause of smog, acid rain, and introduction of toxic solid waste into the environment. In addition to

www.manaraa.com

environmental impact, ash/impurities from coal can form deposits on heat transfer surfaces as the coal burns. These deposits not only lower the efficiency of a boiler but may also cause safety hazards, e.g. explosion. As a result, removal of those toxins is the core issue for effective utilization of coal for power generation.

The successful reduction of those toxic components from coal depends on directly the degree of liberation from coal. The degree of liberation is known to improve with a decrease in particle size. Recent findings have already proven that most of the minerals in coal, down to the micron particle size range, can be liberated by fine grinding (Lackowski, 2001). As the cost of emission control emerged as a new barrier for coal-fired power generation, reduction of coal to micron particle size for advancing coal cleaning technology has become increasingly important. Additionally, the utilization of coal as the fuel for compression combustion engines has already shown its viability (Caton, 1993). The successful conversion of coal-water fuel (CWF) to a diesel fuel strongly depends on effectively reducing coal to a micron size level. Consequently, it is quite clear that the sustainable development and utilization of coal relies to a large extent on the comminution processes to produce ultrafine coal particles.

As a result of the comminution mechanism employed, conventional comminution processes are very inefficient for preparation of ultrafine coal particles. It has been shown that more than 96% of energy spent in current comminution process is wasted (Cui et al., 2006). Based on the work of Zulfiquar et al. (2006), the current industrial scale comminution processes are typically less than 1% efficient based on the energy required for the creation of the new surface. Currently, ball mills are commonly used for coal pulverization. According to Cui et al. (2006), it takes at least two hours on average to reduce the coal particles from 2 mm to 20 μm using a conventional ball mill. When the coal particle sizes are reduced to about 15 microns in diameter, a dynamic balance between pulverization and aggregation occurs (Cui et al., 2008). As a result, when coal particles are smaller than 15 microns, there will be no further particle size reduction in ball mills but the energy consumption dramatically increases. For these reasons, a search for novel grinding methods is of great importance.

The inefficiency of the conventional comminution methods for ultrafine grinding attributes to the fact that conventional comminution devices rely too much on the

www.manaraa.com

exertion of compressive forces on the feed materials. However, most brittle materials are weaker in tension than in compression. This is particularly true for coal as a result of its internal structure which is pervaded by small micro-cracks and fissures (Galecki et al., 2011). Thus, fragmentation of coal through the development of tensile stresses within the particles is more economical. However, this fact has not been utilized until high-pressure waterjets were applied for coal comminution in the 1980s (Galecki and Mazurkiewicz, 1987; Galecki and Mazurkiewicz, 1988).

In addition to a change in failure-inducing forces from compressive to tensile, waterjet-based mineral comminution offers other distinctive advantages. In a high-pressure waterjet mill, mineral particles are injected into a conventional abrasive cutting head and then exposed to high-speed waterjets. These waterjets penetrate into the existing cracks of mineral particles, resulted in external stresses within existing flaws. Further crack growth is thus promoted by these external stresses and finally results in fragmentation. In this way, minerals are liberated along the grain boundaries of different constituents. Along the same lines, since these small waterjets move so fast that they can effectively penetrate into the material almost as quickly as the crack tip can propagate, most mineral particles in a high-pressure waterjet mill are rapidly broken into smaller ones. For this reason, the original crystalline shapes and surface glossiness of minerals are retained without any surface modification and contamination. Consequently, the natural hydrophilic or hydrophobic properties of different components of coal are preserved. This will significantly benefit the subsequent separation process and greatly expand the application of this technique.

Attracted by these unique advantages, high-pressure waterjet comminution technique was quickly adopted by many researchers as an ultrafine grinding method to generate contaminant free products. After more than 25 years of development, many valuable experiences about the high-pressure waterjet comminution have been presented. Detailed information on this is given in Section 2, the literature review. Currently, the application of the high-pressure waterjet comminution technique has covered a large spectrum. Rock crushing, coal grinding and material micronization are all listed as processes benefitting from waterjet comminution. In 2007, Cui et al. (2007) used a high pressure waterjet for ultra-clean micronized coal slurry preparation. The encouraging

www.manaraa.com

results from this research led him to propose a process for preparation of ultra-clean superfine coal-oil slurry (Cui et al., 2008). Using results obtained from his studies, Cui et al. was able to validate the unique advantages of high-pressure waterjet comminution for the development of coal water slurries as a viable alternative energy resource.

Although waterjet-based coal comminution has led to many advances in grinding processes, all findings on this problem were empirical. No model currently has been constructed to either predictively or quantitatively assess the performance of the waterjet mill for coal comminution. The main reason for this is that the size reduction process in the high-pressure waterjet mill is strongly affected by a variety of operating parameters and feed properties. Further, effects of these factors are not constant but may undergo rapid changes with the parameters of the water jet and feed properties. This phenomenon further complicates the comminution process of waterjets. As a result, an extensive, detailed study on the effects of these water jet's parameters and feed properties is essential to fully understand the process of waterjet-based coal comminution.

To quantitatively evaluate the effect of these testing factors, quantifying the particle size of the comminution product is critically important. The particle size analysis results are usually graphically presented using a cumulative particle size distribution plot to characterize the process of particles segregation into predefined categories (Hyslip and Vallejo, 1997). This is a very useful and widely accepted method for presenting the particle size distribution of granular materials. However, quantification of particle size of comminution products by only considering a few points such as D_{80} or D_{50}, or a limited portion of the particle size distribution curve has inherent limitations. Therefore the search for a more versatile method of presenting comminution results is of interest. A solution to this problem was fractal theory which provides a means by which the entire particle size distribution (PSD) of comminuted materials could be quantified through a specific and exact value.

Fractal theory was proposed by Benoit B. Mandelbrot (1977) to characterize some irregular, unsmooth, and non-differentiable objects or shapes in nature. The concept of fractal theory and its applications were systematically described by Mandelbrot (1982). Different from Euclidean geometry, fractal theory states that the dimension (D) of an object is not necessarily an integer but also can be a specific fraction varying from 0 to 3

www.manaraa.com

depending on true fractal sets (Mandelbrot, 1982). More information on this theory will be given in Section 2, literature review. Since the self-similarity of coal comminution using fractal PSD analysis was demonstrated by Zeng et al. (2002), self- similar fractal is widely used in comminution engineering. Cui et al (2006) employed fractal PSD to analyze the fineness of comminution products by a waterjet. He demonstrated the use of a single parameter applied for comminution characterization. Tasdemir (2009) proved that the fragmentation processes of chromite ores can be quantified by using the fractal dimension of the PSDs. At the moment, most applications of the fractal concept for PSD analysis are based on the fragmentation model developed by Turcotte (1986). In this model, the fractal dimension appears as an exponent in the relationship for expressing the cumulative mass of particles as a function of particle sizes (Cui et al., 2006; Tasdemir, 2009). The mass-size distribution of fragments is obtained by sieving and/or sedimentation. Theoretically, dry sieving is preferred because fewer assumptions would be involved (Perfect, 1997). However, in practical applications, this method is mostly affected by human and inconvenient to operate for ultrafine particles. More importantly, waterjet comminution is a suspension-based process. Consequently, laser particle size analyzers, which give accumulated volume information, are the most widely particle size analysis method for fine and ultrafine coal particles fragmented by the waterjet mill. For this reason, constructing a volume-based model that can accurately evaluate the particle size of the comminution products is of importance for optimizing the waterjet-based coal comminution process.

1.2. OBJECTIVES

The overall objective of this research was to establish the fundamental performance capabilities of the waterjet mill for ultrafine coal comminution. The measurable objectives for achieving this objective were as follows:

- Determine the effects of operating parameters and feed properties on the particle size reduction and distribution of products comminuted by a high-pressure waterjet mill;

www.manaraa.com

- Investigate the comminution mechanism of the waterjet-based coal comminution process.
- Propose a model that can quantitatively characterize the particle size of the products comminuted by the waterjet mill through a specific and exact parameter.

1.3. THESIS OUTLINE

This thesis is organized into five sections. The first section, Section 1, describes the objective of this research.

The literature review is performed in the second section (Section 2) to give an overview of the current coal comminution technologies and throw lights on the work have been done in the field of the high-pressure waterjet comminution.

A series of experiments are designed, executed, and discussed in the third section (Sections 3 and 4).

In the fourth section (Section 5), a volume-based fractal model is developed to characterize the sizes of coal products comminuted in the high pressure waterjet mill through a specific and exact value.

The fifth section (Section 6) describes the conclusion drawn from this work. Recommendations for future work are also given in this section.

This research provides a deeper insight into the high pressure water jet comminution for coal comminution and a basis for process parameter optimization.

www.manaraa.com

2. LITERATURE REVIEW

2.1. GENERAL INTRODUCTION

Comminution is a process whereby particulate materials are reduced from the coarse feed size to the fine product sizes required for downstream or end use (Kwade and Bernotat, 2002). It constitutes an important part in many industrial systems, especially coal-fired power plants. Comminution is an energy-intensive stage in the overall process to provide materials in proper fine size ranges for the required properties of the final product. It is estimated that approximately 2% of all electric energy generated in the United States is used for such processes (Galecki et al., 2012). Thus, comminution processes are regarded as appropriate targets for significant energy savings.

Comminution in the mineral processing plant takes place as a sequence of crushing and grinding processes. Crushing reduces the particle size of run-of-mine ore to such a level that grinding can be carried out until the mineral and gangue can be substantially produced as separate particles. Crushing is usually a dry process, and accomplished by compression of the ore against rigid surfaces, or by impact against surface in a rigidly constrained motion path. Grinding is the last stage in the process of comminution. Also, it is the most energy intensive stage. It is reported that this unit operation uses as much as 75% of the total electrical energy consumed in a typical concentrator (Charles and Gallagher, 1982; La Nauze and Temos, 2002).

Size reduction devices are classified into crushers, cutting machines, and grinders (McCabe et al., 1993). Crushers are designed as the primary size reduction units for large pieces of solids obtained from mining. Usually, a primary crusher is accompanied by a secondary crusher. A primary crusher accepts any maximum sizes of materials and reduces them to around 250 mm in diameter. Then, secondary crusher further reduces these particles to 6 mm in size (Zulfiquar et al., 2006). Cutting machines are used to give particles of definite size and shape, about 20-10 mm in length (McCabe et al., 1993). Function of grinders is to reduce the crushed feed into powders. Grinders are further categorized into intermediate grinder, fine grinder, and ultrafine grinders. Typically, diameters of products are less than 420 μm for intermediate grinders, and 74 μm for fine

www.manaraa.com

grinders. An ultrafine grinder accepts feed particles no larger than 6 mm with a product size between 1-50 µm (Zulfiquar et al., 2006).

Due to the fact that larger particles have many flaws that are disappeared during breakage into daughter fragments, and reduced number of flaws means less chance of breakage of smaller particle, the energy input to the comminution process increases as the product size decreases. Figure 2.1 indicates that only 1kWh/t is required to produce 104 µm particles, while more than 200kWh/t is needed to obtain 1 µm particles (Wang and Forssberg, 2007). Consequently, comminution mill development is always aimed at lowering energy consumption of fine and ultrafine grinders.

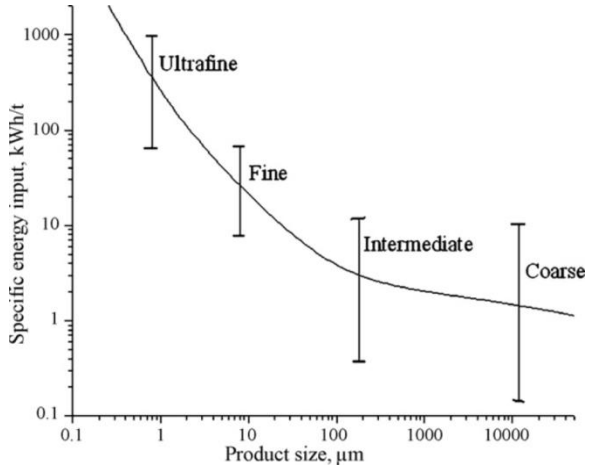

Figure 2.1. Required Energy for Size Reduction in Comminution Process (Wang and Forssberg, 2007)

Coal pulverizers, commercially, used in power plants can be classified by speed, as follows: (i) low speed e.g. tube-ball mills, (iii) medium-speed mills, e.g. vertical spindle mills, and (iii) high-speed mills, e.g. hammer mills. In general, high rank coal, which tends to have low moisture content and require the finest grinding are ground in tube/ball mills. Hammer mills are usually used to grind low rank coal with high moisture content.

www.manaraa.com

2.2. BALL MILLS

Ball mills fall under the category of tumbling mills because they use the tumbling action of several steel balls to grind coal. Rod mills, which use steel rods as the grinding medium, are another type of widely used tumbling mills. Compared to rods, balls have a greater surface area per unit weight. Moreover, ball mills are smooth-running and reliable. As a result, the ball mills are better suited for fine grinding than rod mills. Ball mills are suitable for different types of coal, especially for hard anthracite. For this reason, ball mills are the most widely used mills for producing fine and ultra -fine coal. Typically, a large ball mill can have a shell diameter of 3 m and be up to 4.5 m long (McCabe et al., 1993).

A ball mill in its simplest form is basically a cylindrical shell that is turned about its horizontal axis. It is filled with a solid grinding medium to about half of its volume together with the material to be ground (McCabe et al., 1993). The raw materials are ground into smaller sizes by the impacts between the steel medium and the raw feed as they tumble together inside the shell. Depending on the applications, ball mills may use ball charges from different material, including alumina, stainless steel or zirconium oxide with the latest high chrome material to be the heaviest and the most wear resistant. In general, the grinding efficiency of ball mills increases as the amount of raw feed increase until the voids between the ball charges are filled. Nevertheless, further increase in raw feed lowers the efficiency (Coulson and Richardson, 1980; McCabe et al., 1993; Kelly and Spottiswood, 1995). In a ball mill for coal grinding, the grinding medium is typically made of steel with 12 mm to 125 mm in diameter and occupy between 30 to 50 percent of the volume of the mill (Coulson and Richardson, 1980; McCabe et al., 1993).

Over time, the cylindrical shell and the ball charges inside the mill will start to wear and their replacement is part of the maintenance procedure. Thus, the inner surface of the cylindrical shell is usually lined with an abrasion-resistant material. Rubber is a widely used lining material for ball mills since it has the least wear and the greatest friction coefficient between ball charges and the shell. Besides, the balls can be carried further in contact with cylinder before being dropped on to the feed from a greater height if the rubber is lined in a shell. Since the efficiency of grinding in a ball mill depends on surface area of the grinding medium. Steel balls inside the cylindrical shell should be as

www.manaraa.com

small as possible and the charge should be graded such that the largest balls are just heavy enough to grind the largest and hardest particles in the feed. Moreover, to some extent, having ball charges with varieties of sizes can be considered advantageous, since the larger balls can be used to break the lumps of coal feed while smaller ones to obtain finer products (Coulson and Richardson, 1980). Thus, as long as the smallest size of ball charges is still practical, it does not need to be replaced. Usually for a full scale ball mill, smaller than 12 mm are generally considered as impractical ball charges (Coulson and Richardson, 1980; McCabe et al., 1993).

Ball mills can take feed up to about 50 mm in size and, theoretically, given time, any degree of fineness can be achieved. However, the power consumed in low speed ball mills is limited by the centrifugation occurring at speeds above the critical, and the grinding media could not be too small, for the impact energy of each ball would otherwise be insignificant. At low speed, large grinding media in a ball mill generate mainly impact and abrasive stresses, which, for micron- or sub-micron-size particles, do not work well. Consequently, ball mills are not energy efficient for fine and ultrafine coal grinding. It has been shown that less than 1% of the energy used in a ball mill is used for size reduction (Galecki et al., 2011). Also, it was reported that it takes at least two hours on average to reduce the coal particles from 2 mm to 20 μm for conventional ball mills (Cui et al, 2006). According to interpretation of Cui et al. (2008), there will be no particles to fragment when the coal particles sizes are reduced to about 15 μm in diameter due to the occurrence of dynamic balance between pulverization and aggregation. Specific power consumption of ball mills is typically recognized to be 22kWh/ton (McCabe et al., 1993). Depending on applications, ball mills can be used in a continuous or in a batch model either as dry and wet grinding. For the purpose of stable combustion, continuous flow of powdered dry fuel is required. Consequently, the continuous dry grinding process is more preferable for coal pulverization the in power industry.

2.3. HAMMER MILLS

Hammer mills operate on the principle that most materials will grind or crush upon the impact of swinging hammers. It is an impact mill employing a high speed

www.manaraa.com

rotation disc to which are fixed a number of hammer bars which are swung outwards by centrifugal force. The main working part of a hammer crusher is the high speed rotor with hammers. The rotor consists of main shaft, disk, hinge pin and hammers. The rotor shaft is usually in the horizontal position (McCabe et al., 1993) or at some angle to the horizontal (Coulson and Richardson, 1980). The material is fed into a hammer mill from the top of the casing and falls in to grinding chamber by gravity. Feed particles entering the grinding chamber are struck by a series of rotating hardened hammers and shatters into pieces, which, in turn, fly against a stationary anvil plate inside the casing and break into other smaller fragments. These fragments are rubbed into powder by the hammer and pushed through a screening plate under the rotor. Materials with size smaller than the screen mesh will be screened out and others are left to be further hammered and ground until they are suitably sized to pass through perforated screen applied. According to the customers' requests, in theory, the size of the final product can be adjusted to reach various discharged granularity by changing the screening plate.

Hammer mills are suitable for medium-hard or brittle materials with hardness not more than 300Mpa and 15% moisture, such as coal, cement, gypsum, brick, and so on. Depending on the applications, a hammer mill may contain more than one rotor discs on a same shaft. Each rotor disc can carry three to eight hammers which may be in the form of straight bars or with ends sharpened to a cutting edge. Due to the fact that hammers could be easily damaged and swing hammers can be readily replaced as soon as they wear out, they are hinged instead of fixing on the disc when grinding hard material to make the mill more durable.

Hammer mill used for fine reduction may have linear speeds of up to 110m/s, which can reduce 0.1 to 15 ton/h of feed to sizes finer than 74 μm (McCabe et al., 1993). Typically, commercial hammer mills can reduce 60 to 240 kg of feed material per kilowatt hour (Zulfiquar et al., 2006). Since the capacity and power requirement of a hammer mill vary greatly with the nature of the feed and cannot be approximated with confidence using theoretical consideration (McCabe et al, 1993), the best way to estimate them is to use a small-scale or full-scale test of the mill using the material to be ground.

www.manaraa.com

2.4. VERTICAL SPINDLE MILLS

Vertical spindle mills represent a family of milling machines in which the material to be reduced is caught and ground between a grinding roller and a grinding surface of a ring or a casing. Bowl mills, Babcock and Wilcox Mills, and Raymond ring-roller mills are the most common types vertical spindle mills. Differences among them are the shapes of the rollers and the way grinding takes place inside the casing.

In the design of bowl mill, the grinding rolls are stationary, while the ring is rotated by a worm gear drive. The grinding pressure is produced by means of springs, which can be adjusted to give the required pressure, while the distance between the roller and the ring may be set to a predetermined clearance (Perry's, 1984). Raw coal enters the top of the pulverizer through the raw coal feed pipe and dropped on the bowl. Then, it is directed towards the periphery of the bowl where due to the centrifugal force of the bowl rotation pulverization takes place. Hot air is forced in through the bottom of the pulverizing chamber to remove unwanted moisture and transport the coal dust up through the top of pulverizer and out of the exhaust pipe directly. Coal particles that has not been pulverized into fine enough fall back to the ring and roll to be further pulverized. Typically, specific power consumption of the bowl mill is 12 kWh/ton and the capacities of bowl mills are up to 50 ton/h. (McCabe et al., 1993).

Babcock and Wilcox Mills use hydraulically loaded vertical rollers resembling large tires to pulverize raw coal fed down onto a rotating table. As the table rotates, the raw coal is pulverized as it passes underneath the rollers. Hot air forced through the bottom of the pulverizing chamber removes unwanted moisture and transports the pulverized coal dust up through the top of the pulverizer and out the exhaust pipes directly to the burner.

The Raymond ring-roller mill is an airswept vertical ring-roll mill with an integral classification system. Different from bowl mills, in the design of Raymond ring-roller mills, the rollers are moving around a vertical shaft over a stationary grinding surface. The vertical shaft rotates a "spider" assembly of arms from which are suspended free swinging journal assemblies with rolls attached. As the unit turns, centrifugal force drives the rolls against the inner surface of the vertical grinding ring. Plows, rotating with the assembly, lift feed material from the mill bottom and direct it between the rolls and the

www.manaraa.com

grinding ring where it is pulverized. Air enters from below the grinding ring and carries fine to flow upward. An air classifier is also mounted above the grinding zone to size the pulverized material and returns oversized particles to the grinding chamber for further pulverization. A Raymond ring-roller mill is available in different capacities ranging from 0.5 to 50 ton/h with power consumptions between 28 and 500 kW (Perry's, 1984). The product size of the raymond ring-roller mill depends on the type of the air classifiers used. If a fine product is required a whizzer type air classifier should be used.

As a result of the comminution mechanism employed, current comminution processes described above is recognized as being an inherently inefficient process (Austin, G.L., 1984; Fuerstenau and Abouzeid, 2002). It has been shown that more than 96% of the energy spent in current comminution process is wasted (Cui et al., 2006). The low efficiency of current grinding processes is not the result of an inability to break particles effectively, but the result of energy application when there are no particles to fragment. Energy requirements dramatically increase with a decrease in feed size or desired ground product size. For that reason, new generation grinding mills such as roller mills, stirred media mills, vibration mills, centrifugal mills, jet mills and Hicom mill were introduced as alternate low energy comminution systems. They are promising technologies for ultrafine grinding, however, only a few of these designs are suitable for preparation of CWF in terms of product quality (particle size/distribution) and energy efficiency (Cui et al., 2011).

Since most of brittle materials are weaker in tension than in compression, fragmentation of brittle minerals through the development of compressive stresses within the minerals is more economical. This is particularly true for coal, which has an internal structure that is pervaded by small micro-cracks and fissures. However, this fact has not been utilized until high-pressure waterjets were applied for the purpose of coal comminution (Galecki and Mazurkiewicz, 1987; Galecki and Mazurkiewicz, 1998).

2.5. HIGH-PRESSURE WATERJET MILLS

The high-pressure waterjet comminution technology was first introduced by Galecki and Mazurkiewicz (1987). It offers several particular advantages. The

www.manaraa.com

penetration of the water into the cracks promotes fragmentation by development of internal pressures within the existing cracks, thus promoting further crack growth. The jet is moving so fast that it effectively penetrates into the material almost as quickly as the crack tip can propagate, which leads to rapid pressurization of material discontinuities. In this process inorganic mineral constituents are liberated along the grain boundaries of the coal, easing the separation process. Then, high density slurries can be produced. The action of the jet has been enhanced by cavitation induced by the slurry (Galecki and Mazurkiewicz, 1988; Galecki et al., 2009; Vidt and Galecki, 2010) for producing a significantly better feed stock for power generation.

After 25 years development, several types of high- pressure waterjet mills have been developed and described (Pan, 1992; Huang, 1994; Liu et al., 1997; Mazurkiewicz, 2001; Sun and Hou, 2002; Liu and Sun, 2005). Although there are some differences in the structure of these mills, the basic principle remain the same. In high-pressure waterjet mill, coal particles are drawn into a mixing chamber/passage because of the pressure difference resulted from the high velocity of the water as it passes through the chamber/passage. Then the coal particle, which is mixing uniformly with water, spurts out from a nozzle and impacts against an anvil. Finally, an increasingly dense network of micro-cracks within coal particles is created resulting in fragmentation of coal particles.

Comminution mechanism by waterjets is a very complex phenomenon, and there is no uniform explanation about it, yet. However, lots of studies toward basic understanding of grinding mechanism have been presented (Sun, 1993; Gong et al., 1998; Liu and Sun, 2005; Cui et al., 2006). As presented in these studies, size reduction in waterjet mill is the combined effects of rapid dynamic shear stress developed by high velocity particle movement, cavitation bubble growth and collapse, direct impact of particles against a rigid target, water-edge effect, water-hammer effect, and interaction friction effect. Fu (2001) provided a comprehensive analysis on the comminution mechanism of waterjet mill. Based on findings from his research, he characterized high-pressure waterjet comminution as “high-efficiency, clean, low energy-consuming, and promising new comminution engineering”. Hou and Sun (2003) addressed high-pressure waterjet comminution as a selective and efficient crushing process. Cui et al. (2006)

www.manaraa.com

shared the same view. Hlavac et al. (2010a) pointed out that the waterjet comminution is a “revolution in comminution engineering”.

Effects of cavitation and pump pressure on high-pressure waterjet comminution of mica were investigated by Guo et al. (2002) via variance analysis. His experimental results indicated that the effect of cavitation was much more significant than that of collision. And the effect of pressure on comminution results becomes less with the decrease of particle size. Hou and Sun (2003) presented influencing factors on raw salt disintegration by high pressure waterjet. The authors established a hierarchy of importance of factors affecting comminution via experimental analysis. According to their opinion, the order of influencing factors from important to minor is the operational water pressure, the diameter of nozzle, and the configuration of mixing chamber. Evaluation of influencing factors on high-pressure waterjet coal comminution was presented by Cui et al. (2006). In his paper, the author introduced the fractal dimension of particle size distribution D_f to describe the fineness of the product. Based on the results of his research, the authors indicated that the more contents of the fine particle, the higher the fractal dimension and the higher degree of the particle fragmentation. This is in agreement with views presented by Xie (1996). According to the experimental results of Cui (2006), increasing the pump pressure, the diameter of feed material, the impact angle, the comminution time, and the hardness of target resulted in an increase of the fractal dimensions. However, the decrease of the standoff distance and the diameter of mixing tube led to lower fractal dimensions. Besides, the fractal dimension increased as the particle mass flow and mixing tube length increased until the peak point was reached, then the inverse tendency appeared. In 2010, influences of mixing chamber’s inner shape on comminution of garnet particle by high-pressure waterjet were experimentally evaluated by Hlaváč et al (2010b). Two configurations, which is marked as A and B in Figure 2.2, of mixing chambers were used in his tests. Based on comparison between distribution curves of the products obtained from both types of mixing chambers, he indicated that the chamber with perpendicular inlets was more efficient.

www.manaraa.com

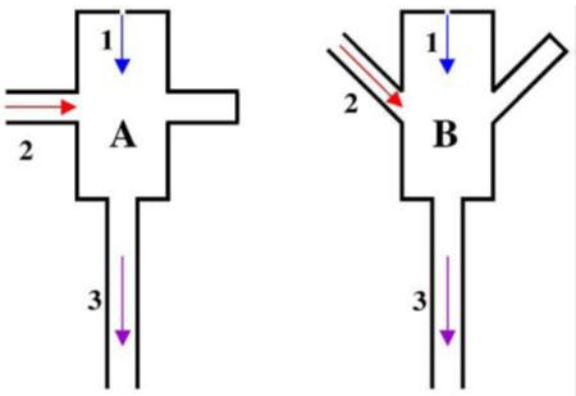

Figure 2.2. Cross-Section Diagram of the Mixing Chambers Used in Experiments By Hlaváč: 1 — Water Jet; 2 — Mix of Sucked Air and Material Particles; 3 — Outflow of The Mixed Jet; A — Mixing Chamber with the Perpendicular Inlets, B — Mixing Chamber with the Inclined Inlets.(Hlaváč et al., 2010b)

Comminution efficiency by high-pressure waterjet has been explained by different ways. In 2005, experiments of raw salt fragmentation by high-pressure fluid jet were performed by Liu and Sun (2005). Also, the author pointed out the potential of high-pressure fluid jet as a tool for comminuting thermally sensitive, inflammable, and explosive materials. Cui et al. (2007) used high- pressure waterjet for ultra-clean micronized coal slurry preparation. His studies included comparison of combustible matter recovery, ash content of the clean coal, separation efficiency, and energy consumption between the new and traditionally used comminution methods. Results gained from comparisons showed that the high - pressures waterjet can efficiently liberate pyrite, silica and other minerals from the coal with the original shapes of the fine particles remains without any surface modification and contamination. As well, the high - pressure waterjet comminution method had low energy consumption and equipment wear. The encouraging results led him to propose a process for preparation of ultra-clean superfine coal–oil slurry (Cui et al., 2008). Results obtained from this study, validated the unique advantages of high-pressure waterjet comminution for developing coal slurry as a viable alternative energy resource.

In the report of the Committee on Comminution and Energy Consumption, waterjet was characterized as low-energy consuming process compared to other

www.manaraa.com

comminution process. Influencing factors of energy consumption in the high-pressure waterjet comminution process was investigated by Galecki (unpublished work). From the author's view, the energy consumption showed a very strong dependence on jet diameter and pressure, initial coal particle size, solid concentration in slurry, and kinematics of interaction between the high pressure waterjets and coal.

Coal and other mineral comminution by high-pressure waterjet lead to many predominant advantages over mechanical grinding process. Size reduction in a cavitation cell is the result of combined effects of rapid dynamic shear stress, cavitation bubble growth and collapse, and direct impact of particles against a rigid anvil and some results of recent studies are presented in (Galecki et al., 2011). No theory, up to now, can comprehensively explain size reduction of coal in this complex process. As a result, almost all of research just provided empirical findings. Wang et al (2009) tried to use neural network method to establish predicting mathematical model for comminution productive rate by waterjet. However, the proposed models are far away from reality of this very complex problem with narrow, limited conditions. No model, so far, has been constructed to predictively or quantitatively assess the particle size distribution (PSD) of the fragments, which plays a critical role in estimating efficiency of comminution and controlling/ optimizing this comminution process of high-pressure waterjet mill.

Rittinger's Law, Kick's Law, and Bond's Law are three well-known laws of comminution for assessing comminution energy, and indirectly, the comminution efficiency. However, Kick's Law is valid when the particle size is larger than 100,000 μm in diameter, Bond's Law applies reasonably in the range of conventional rod-mill and ball-mill grinding, and Rittinger's Law is suitable for particle sizes from 75μm to 500μm. As a result, these laws cannot be used to estimate the energy consumption of the waterjet mill for ultrafine coal comminution. In 2007, the specific surface energy was successfully used by Gong and Dong (2007) to investigate the energy consumption of the ultrafine mica comminution using cavitation abrasive waterjet technology. Their research provides another mean to analyze the energy consumption of the waterjet mill.

www.manaraa.com

2.6. FRACTAL THEORY

The fractal theory was proposed by Benoit B. Mandelbrot to characterize some irregular, unsmooth, and non-differentiable objects or shapes in nature (Mandelbrot, 1977). The concept of fractal theory and its applications were systematically described by Mandelbrot (Mandelbrot, 1982). Different from Euclidean geometry, fractal theory states that a value of dimension (D) is not necessarily an integer but should be a specific fraction varying from 0 to 3 depending on true fractal sets (Mandelbrot, 1982).

One of the first applications of fractal theory was in animal and plant morphology studies to characterize the complexity of neurons and glia cells shapes (Smith et al., 1989; Neal et al, 1993; Smith and Neale 1994; Corbit and Garbary, 1995). On a larger scale, the fractal theory was used to characterize the complexity of the habitats (Morse et al, 1985; Gunnarsson 1992; Gee and Warwick, 1994). Fractal theory was successfully applied for characterization of particle, pore, and aggregate size distribution in soils (Bartoli et al., 1991; Rieu and Sposito, 1991; Perfect et al., 1992; Crawford et al., 1993, Wu et al., 1993; Kozak et al., 1996). More recent successful applications of the fractal theory were in roughness, pore size distribution, and adsorption behavior characterization of porous media such as coal (Friesen and Ogunsola, 1995; Zhang and Li, 1995; Hyslip and Vallejo, 1997; Huang et al., 2003; Zhou et al, 2004). As defined by Mandelbrot, fractals are hierarchical and very often highly irregular, geometric systems (Mandelbrot, 1982) and as a novel tool for comminution products analysis, the fractal theory was applied for homogeneous and heterogeneous materials (Carpinteri and Pugno, 2003). A different aspect of the fractal theory use was its application for quantitative of fractures and faults (Seacy and Sammis, 1991; Boadu and Long, 1994).

Basically, there are two types of fractal theories which are self-similar fractal and self-affine fractal. The self-similarity and scale invariant are the characteristics of the self-similar fractal. Based on the experimental studies on ball mills, Zeng et al., (2002) concluded that the PSD of comminution products at different grinding time were similar. This conclusion denoted the self-similar fractal theory can be used to characterize the self-similarity of coal comminution. Then, self-similar fractal is widely used in comminution engineering. The fractal fragmentation theory to give a multi-scale interpretation of energy size effect have been developed and applied by Carpinteri and

www.manaraa.com

Pugno (2002) and Carpinteri and Pugno (2003). The proposed theory emphases how the energy dissipation in the comminution process occurs in a fractal domain intermediate between a surface and a volume. According to the authors' explanation, the damage occurs in small concentrated for finer comminution indicating that finer particles are the result of the surface-dominated breakage. Since the damage for larger particles are spatially distributed, the breakage model is the volume-dominated phenomenon. Further, authors indicated that the fractal dimension of the surface-dominated phenomenon should be close to 2. Additionally, for volume-dominated phenomenon, the fractal dimension should be close to 3. Cui et al. (2006) employed fractal PSD to analyze the fineness of comminution products by waterjet. He demonstrated the use of a single parameter applied for comminution characterization. Tasdemir (2009) proved that the fragmentation processes of chromite ores can be quantified by using the fractal dimension of the PSDs.

At the moment, most applications of the fractal concept for PSD analysis are based on the fragmentation model developed by Turcotte (1986). In this model, PSDs have been analyzed with power-law functions relating cumulative number of particles to diameter or mass of particles to diameter. These two types of fragmentation relations are known as number-based and mass-based approaches (Turcotte, 1992).

www.manaraa.com

3. METHODOLOGY

3.1. DESIGN OF EXPERIMENTS

The objective of this experimental study is to explore the effects of the operating conditions on the response of the coal particles to the action of the waterjet. To achieve this objective, comminution tests were carried out by varying the properties of the waterjet and the feed materials.

3.1.1. Variables of Waterjet. The operational pressure and standoff distance are parameters of the water jet.

The operational pressure is the pressure of the water stream entering into the mixing tube. In this research, the operational pressure ranges from 10,000 to 40,000 psi with a 10,000 psi increment. The standoff distance is defined as the distance from the mixing nozzle to the anvil. To investigate the effect of standoff distance on the behavior of coal particles exposed to the action of the waterjet, four different standoff distances are tested. These are: 100 mm, 98 mm, 19 mm, and 3 mm.

3.1.2. Variables of Feed Materials. Effects of the feed size, feed mode, and ash content on the behavior of coal particles to the action of the waterjet were explored in this study.

Four different feed size ranges, -106 microns, - 212 + 106 microns, -355 + 212 microns, and - 850 + 355 microns, are used. Since comminution can be either a dry or wet process, two feed modes, were tested - dry and wet. To better understand coal comminution to ultrafine sizes, three coals with different ash contents were selected. Ash contents and codes for each of coals used are listed in Table 3.1.

Table 3.1. Codes and Properties of Coal Samples

Codes Of Coal Samples	C1	C2	C3
Ash Content (%)	2.83	11.00	31.00

www.manaraa.com

3.1.3. Experimental Procedure. The basic flow-sheet of experimental procedure is given in Figure 3.1. Prepared coal samples are ground in a high-pressure waterjet mill coupled with a specially designed cavitation cell. Then, the ground products are filtered, dried, and characterized. The comminution products are evaluated based on physical properties including the particle size, surface area change, particle size distribution, and morphological properties.

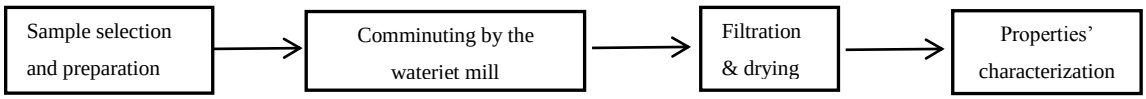

Figure 3.1. Basic Flow-Sheet of the Experimental Procedure

In order to compare the results, the experiments were performed as following:

- Keeping the same standoff distance, comminution experiments were carried out to investigate the effectiveness of coal comminution using a waterjet as a function of the operational pressure, feed size, and ash content;
- While maintaining the same waterjet parameters, wet feeding tests were conducted to show the effect of the feed form on the behavior of the coal particles subjected to the action of the waterjet;
- The location of the anvil in the cavitation cell was changed to investigate the effect of coal comminution using a waterjet mill.

3.2. SAMPLE PREPARATION

A two-step crushing process was used for sample preparation. First, run-of-mine coal was crushed with a jaw crusher to minus 5 mm. Coal was then further crushed in a hammer crusher to minus 1 mm. These samples were considered original feed material. Each sample of the original feed material was split and further classified by a dry sieving

www.manaraa.com

method into four mono-sized subsamples (- 106 microns, - 212 + 106 microns, -355 + 212 microns, - 850 + 355 microns). Figure 3.2 illustrates the basic flow-sheet of the sample preparation.

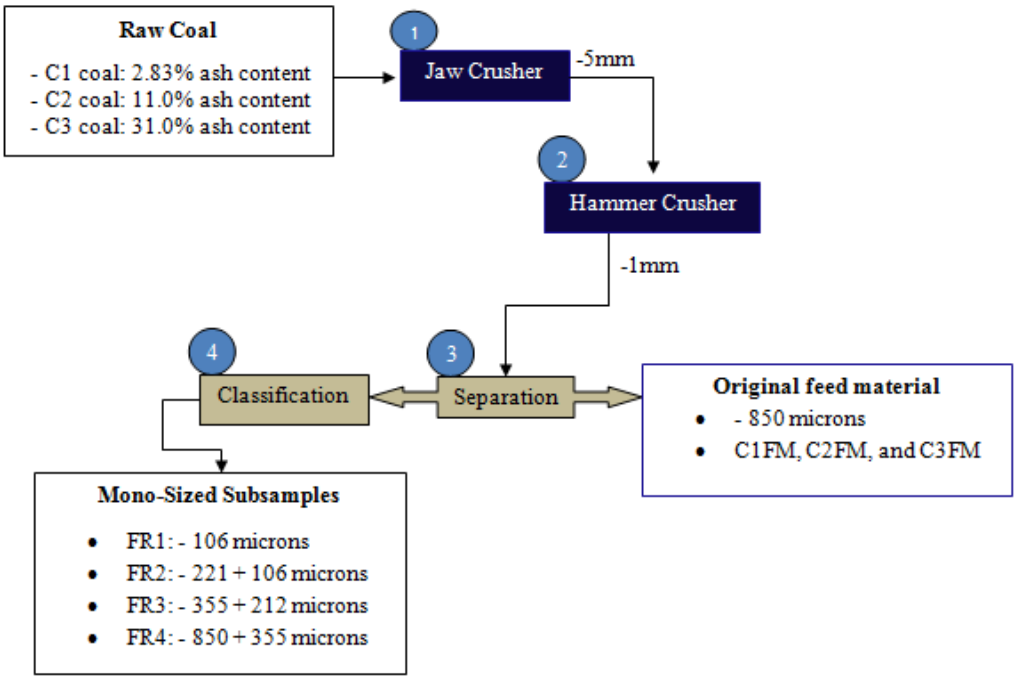

Figure 3.2. Basic Flow-Sheet of the Sample Preparation

3.3. EXPERIMENT APPARATUS

A laser diffraction Microtrac S3500 series particle size analyzer was employed to measure the particle size of the feeds and their resulting products. A Hitachi S4700 scanning electron microscope was used to determine the morphological properties of feeds and comminution products. The high-pressure waterjet mill used in the comminution experiments were designed by G. Galecki based on his previous work. The schematic and set-up of the apparatus used in this work are shown in Figures 3.2, 3.3, and

www.manaraa.com

3.4. The waterjet mill components' characteristics are given in Table 3.2. In this thesis, the operational pressure and the standoff distance were the variables of the waterjet mill.

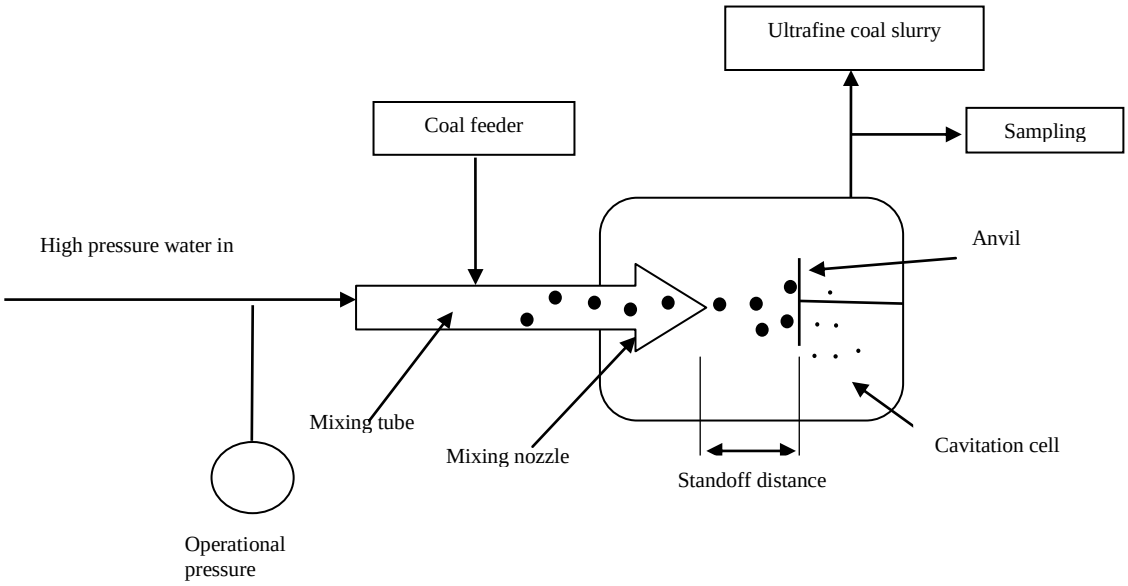

Figure 3.3. Schematic of the High-Pressure Waterjet Mill\

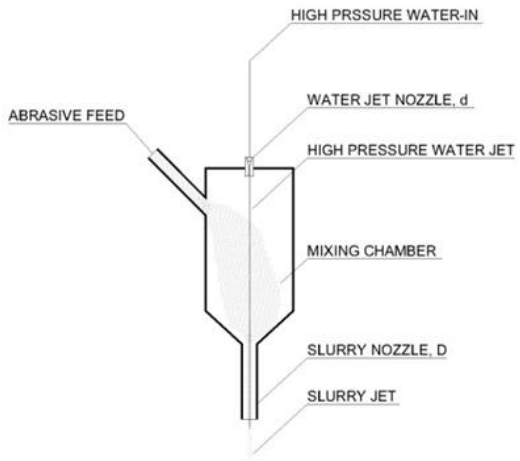

Figure 3.4. Conventional Abrasive Waterjet Cutting Head (Galecki et al., 2011)

www.manaraa.com

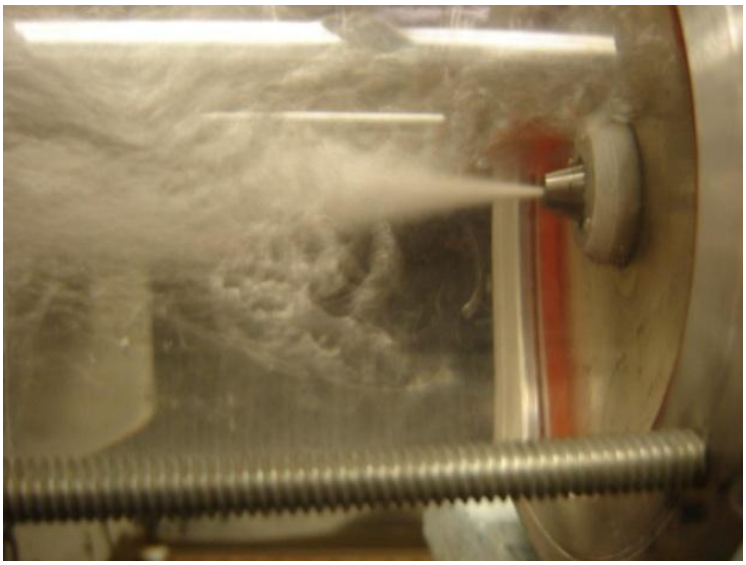

Figure 3.5. Cavitating Jet (Galecki and Mazurkiewicz, 1988)

Table 3.2 Characteristics of the High-Pressure Waterjet Mill

Mixing Tube Length	76.00 mm
Mixing Tube Diameter	0.76 mm
Cavitation Cell Inner Diameter (ID)	76 mm
Cavitation Cell Length	100 mm
Standoff Distance	3 - 100* mm
Anvil (Carbide) Dimensions	19 × 19 mm

* According to the specific objective of the individual experiment, the standoff distance varied from 3 to 100 mm along the on-axis of the cavitation cell.

www.manaraa.com

4. TEST RESULTS AND DISCUSSION

4.1. GENERAL INTRODUCTION

Particle size analysis is the most important method to assess the performance of grinding circuits. There are a variety of methods to record the particle size analysis, including cumulative undersize/oversize curves, Gates-Gaudin-Schuhmann, Rosin-Rammler, particle size distribution curves, specific surface area, and particle size distribution curves (Wills, 1997). Plotting cumulative undersize (or oversize) against particle size is the most common method to assess full significant of particle size because some valuable quantity, such as D_{50} and D_{80},for routine control of the grinding circuit, can be determined from cumulative undersize/oversize curves (Wills, 1997). The median particle size D_{50} means the value of the size that 50% of the particles are smaller than this size and 50% are larger. D_{80} refers to the size that 80% of the particles are smaller than this size and 20% are larger.

The cumulative curve can be expressed as a cumulative number curve, cumulative mass curve, cumulative volume curve, and cumulative area curve. For the same powder, each type of curve will have a different mean, a different median, etc. Thus, one must specify whether or not the accumulative curve is by number, volume, area, mass, etc. For tests purposes, all cumulative curves plotted in this thesis are cumulative volume undersize curves (CVUSCs).

Although CVUSCs are used almost exclusively, there are two serious disadvantages. 1) CVUSCs cannot express the overall size distribution of the material. 2) Points in the regions of the both finer and coarser apertures of curves tend to become congested. Thus, the surface area changes and particle size distribution curves were also employed in this thesis to characterize the particle size of feed materials and products.

Specific surface area (SSA) is a material property of particles that measures the total surface area per unit of either mass or volume. For the same amount of material, a higher SSA indicates a smaller particle size. SSA not only indicates the surface area of measured particles but also includes the surface area of both pores and cracks inside the particles. Additionally, SSA is usually measured by adsorption using the BET isotherm. Consequently, SSA differs depending on the porosity of particles, the adsorption

www.manaraa.com

specificity, or the topographical characteristics of the particles. The calculated surface area (CSA) computation assumes smooth, solid, spherical particles. It may be converted to classical units for SSA of M^2/g by dividing through value by the density of the particles. As a result, it is widely used in comminution as an indication of SSA. In this thesis, the calculated surface area ratio (CSAR) was employed to evaluate grinding characteristics of the waterjet-based comminution process. The calculated surface area ratios (CSARs) can be found by using,

$$CSAR = \frac{CS_{v,2}}{CS_{v,1}} \tag{4.1}$$

where $CS_{v,1}$ is the CSA of the feed sample and $CS_{v,2}$ is the CSA of corresponding products. A higher CSAR suggests a higher degree of grinding.

When compared to CVUSCs and CSARs, the particle size distribution (PSD) curve is often more informative. PSD allows researchers to visualize the relative frequency of occurrence of the various sizes present in material. The PSD curve is derived from first differentiating the cumulative undersize curve and subsequently plotting the gradient of the curve against the particle size. In practice, the PSD curve is obtained by plotting the retained fraction of the sieves against the size. In this research, all of the points on the frequency curve were plotted in between two sieve sizes. For example, the amount of material, which passes through 200 micron sieve is 90%, 70% however is retained on a 100 micron sieve and is consequently regarded as having a mean particle size of 150 microns with 80% of passing percentage.

Quantitative morphology analysis allows one to better evaluate the fragmentation processes (Lecoq et al., 1999). The scanning electron microscopy (SEM) studies play an important role in the determination of the particle morphology of ultrafine particles. To comprehensively evaluate the products, scanning electron microscopy (SEM) studies were also conducted in this thesis to characterize the morphological properties of feeds and their resulting products. The focus of the SEM studies was the particle shapes and surface texture.

www.manaraa.com

4.2. WATERJET-BASED COMMINUTION OF C1 COAL

To analyze the coal particle response to action of the waterjet, the original feed material labeled as C1FM in size of -850 microns and its mono-sized subsamples marked as C1FR1 (- 106 microns), C1FR2 (-212+106microns), C1FR3 (-355 + 212microns), and C1FR4 (-850 + 355microns) were used. For the purpose of these experiments the operational pressure ranged from 10,000 to 40,000 psi with the anvil located at 19 millimeters away from the mixing nozzle. Variables in these experiments are the feed size and operational pressure.

4.2.1. Particle Size Analysis. To analyze the effect of the particle size change, the cumulative volume undersize curves (CVUSCs) is first used to characterize the feeds as well as the products.

The CVUSCs of the C1FM and its mono-sized subsamples (C1FR1through C1FR4) are given in Figure 4.1.The CVUSCs of products obtained under different operating conditions are illustrated in Figures 4.2 - 4.6. To show the change in particle size as a function of operational pressure, the CVUSC of the corresponding feed is also included in Figures 4.2 - 4.6.

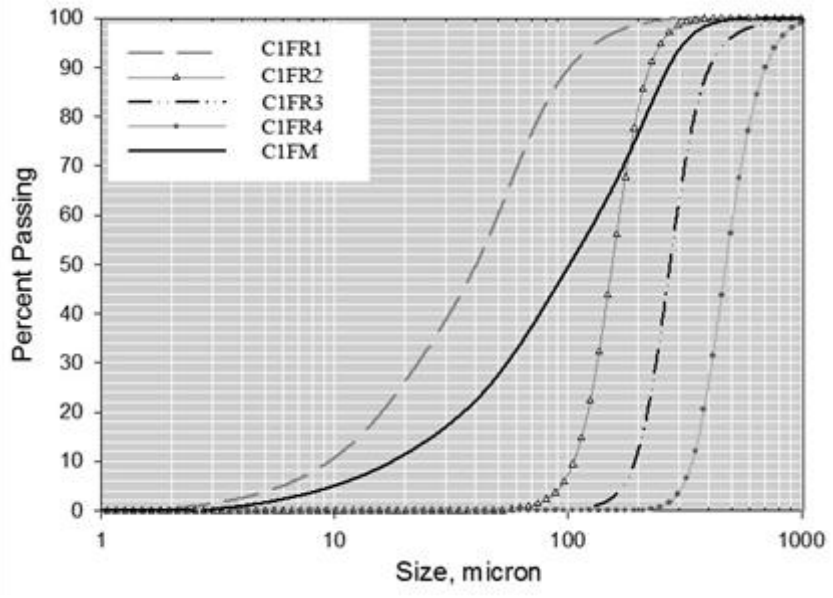

Figure 4.1. CVUSCs of C1FM and Mono-Sized Subsamples (C1FR1through C1FR4)

www.manaraa.com

Figure 4.1 depicts that the fineness of feed material from high to low were in the order of C1FR1, C1FR2, C1FR3, and C1FR4. The C1FM was the original feed material without classification. It contains coarse and very fine particles together.

C1FR1 was the finest feed sample with a median particle size (D_{50}) of 40.11 microns. The median particle sizes (D_{50}) of the products for C1FR1 ranged from 28.27 to 9.87 microns for the operational pressure varying from 10,000 to 40,000 psi (Figure 4.2). The highest size reduction ratio of 4 was obtained for the pressure of the 40,000 psi.

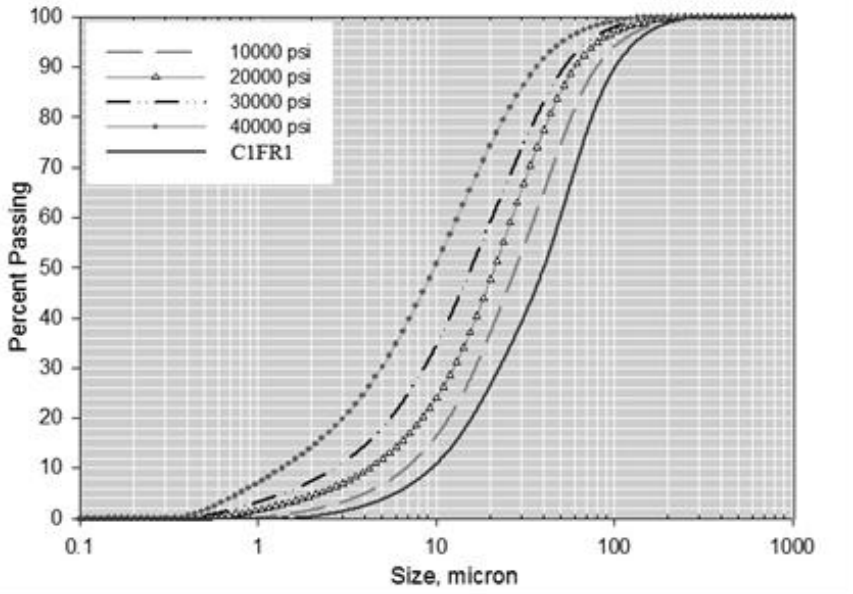

Figure 4.2. CVUSCs of Products for C1FR1 Comminuted at Different Operational Pressures

Figure 4.3 illustrates that the median size value (D_{50}) of C1FR2 was 154.7 microns. This value is almost four times larger than the same value for C1FR1, indicating the increasing coarseness of the feed. Higher size reduction ratios were obtained for this feed. The size reduction ratio for the highest operational pressure, 40,000 psi, was 13 for the feed C1FR2. The median particle sizes (D_{50}) of the comminution products varied

www.manaraa.com

from 31.98 to 11.82 microns as a function of the operational pressure increased from 10,000 to 40,000 psi (see Figure 4.3).

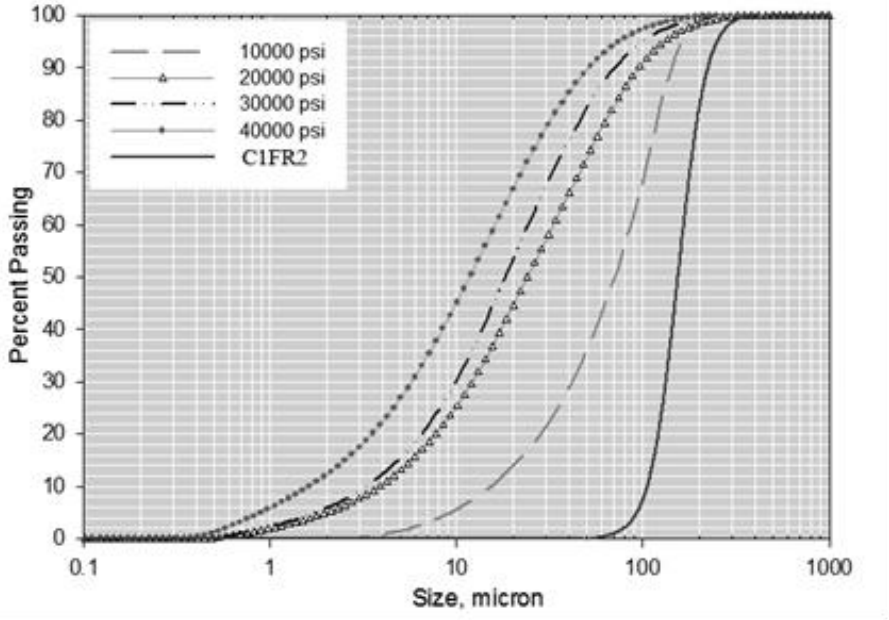

Figure 4.3. CVUSCs of Products for C1FR2 Comminuted at Different Operational Pressures

The feed C1FR3 was even coarser than the feed C1FR2. It had a median particle size (D_{50}) of 274.40 microns. The curves in Figure 4.4 indicate that a 10,000 psi operational pressure was not able to generate fine particles with diameters smaller than10 microns for this feed. However, median particle sizes (D_{50}) near 30 and 20 microns were obtained by increasing the operational pressure to 20,000 and 30,000 psi, respectively. The size reduction ratio for the highest operational pressure, 40,000 psi, was 15 for the feed C1FR3. Comparison of size reduction ratios obtain from the feeds C1FR3 and C1FR2 leads to the conclusion that the coarser feed can be more efficiently ground by the waterjet mill.

www.manaraa.com

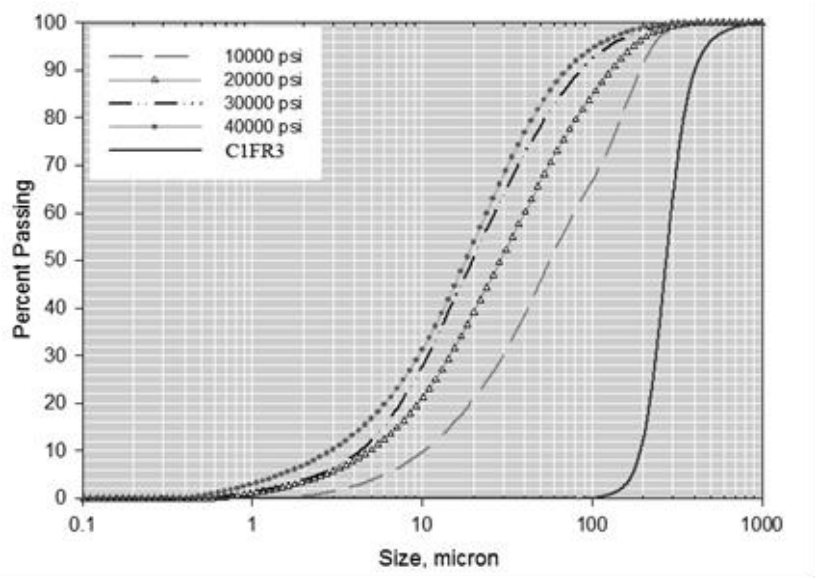

Figure 4.4. CVUSCs of Products for C1FR3 Comminuted at Different Operational Pressures

As can be seen in Figures 4.1 and 4.5, C1FR4 with a median particle size (D_{50}) of 476.50 microns was the coarsest feed. The fineness of the products from C1FR4 was very close to the products of the C1FR3. However, size reduction ratios of the feed C1FR4 were much higher than those of the C1FR3. A size reduction ratio of 23 was obtained for the feed C1FR4 when a 40,000 psi pressure was applied. The median particle sizes (D_{50}) of the ground products varied between 86.77 and 21.16 microns as the pressure increased.

Grinding in industry is a continuous process where the material obtained from crushers is fed from storage bins without classification into one end of the mill and overflowing at the other end. In order to investigate whether the size classification affects the response of the waterjet mill, the last group of grinding tests was conducted on the original feed material, C1FM. The results are presented in Figure 4.6. Data presented in Figure 4.6 indicates that the median particle size (D_{50}) of the product for the 10,000 psi operational pressure was 78.92 microns. This value was as low as 11.33 microns for the 40,000 psi operational pressure. This change trend in particle size is consistent with the results observed from the mono-size subsamples that the higher operational pressure led

www.manaraa.com

to finer products. This observation indicates that the response of coal particles to the operational pressure is independent of the size classification.

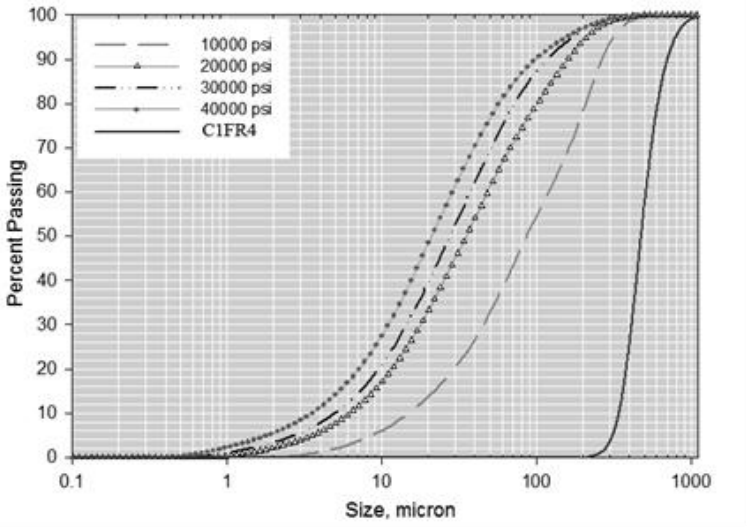

Figure 4.5. CVUSCs of Products for C1FR4 Comminuted at Different Operational Pressures

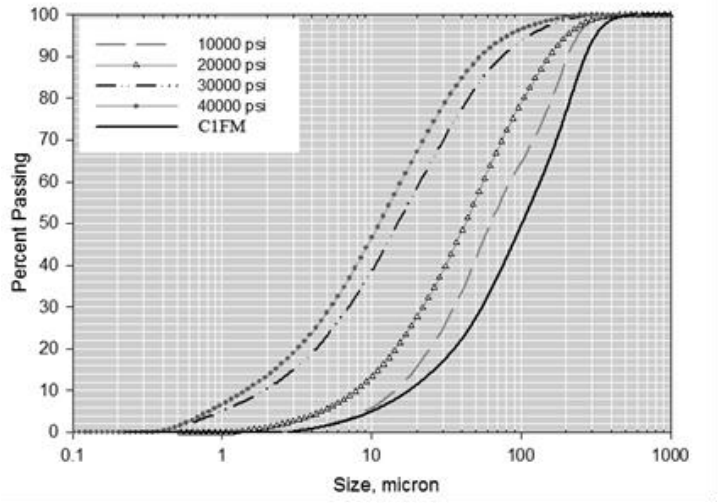

Figure 4.6. CVUSCs of Products for C1FM Comminuted at Different Operational Pressures

www.manaraa.com

Analysis of the CVUSCs indicates that the particle size change of C1 coal exposed to a waterjet strongly depends on the pressure and feed size. The dependence on the operational pressure was acutely correlated to the development of fine particles. More directly: the higher the pressure the finer the product is generated. This statement is connected with the observation that a higher particle size reduction ratio was observed for the coarser feed material. This observation indicates that smaller particles are more difficult to grind by the waterjet mill. This attributes to the lower intensity of flaws, cracks, and discontinuities in fine particles and can be explained by applying Griffith theory for brittle fractures. According to Griffith theory, the presence of cracks, flaws, and discontinuities in particles can propagate and promote the formation of new cracks under stress. As a result, lower intensity of flaws and cracks inside particles leads to increased strength. As the particle size decreases, the existing cracks progressively disappear resulting in a dramatic increase in the energy required to fracture the particles. For this reason, minimal size reduction was obtained for the finest feed C1FR1when compared to other feeds under equal pressure.

4.2.2. Surface Area Change. In order to comprehensively investigate the grinding characteristics of C1 coal comminution by a waterjet, the calculated surface area is used in this Subsection to characterize the feeds and products. The summary of results is showed in Figure 4.7.

As Figure 4.7 illustrates, the calculated surface area ratios (CSARs) proportionally increased with the operational pressure. In addition to this observation, it is noted that the highest CSARs were obtained when the coarsest feed (C1FR4) was used. According to the explanation in Section 4.1, a higher calculated surface area indicates smaller particles for the same amount of material. Additionally, higher CSARs indicate a higher degree of grinding. Following these explanations in addition to the observations obtained from Figure 4.7, leads to the conclusion that C1 coal comminution using a waterjet is strongly affected by the pressure and feed size. Finer product resulted from higher pressures for the same feed. In situations where applied pressure is equal, the high-pressure waterjet mill is more efficient for coarser feed in terms of input energy for creation of new surface area. These results strongly support the analysis of the cumulative volume undersize size curves (Section 4.2.1).

www.manaraa.com

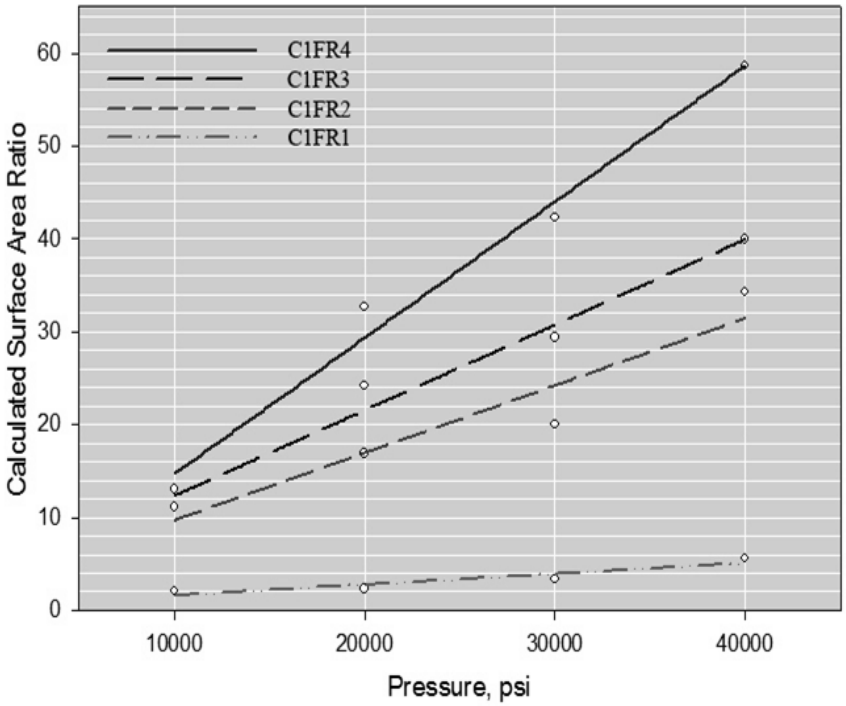

Figure 4.7. CSARs versus Operational Pressures for Mono-Sized Subsamples of C1FM

4.2.3. Particle Size Distribution. The particle size distribution (PSD) curve can visualize the relative frequency of occurrence of various sizes presented in granular material. It is commonly used in industry to evaluate the properties of comminution products. In this subsection, the original feed material and its resulting products are analyzed using the volume based particle size distribution approach. Figure 4.8 gives the summary of the results. Generation of coal particles below 10 microns with tight size distribution is becoming more important as a result of an increased need for the development of coal-water fuel. Additionally, production of coal particles with size less than 10 microns is the primary limitation of the conventional comminution methods due to serious aggregation of fine particles. Thus, 10 microns is selected as a target value.

www.manaraa.com

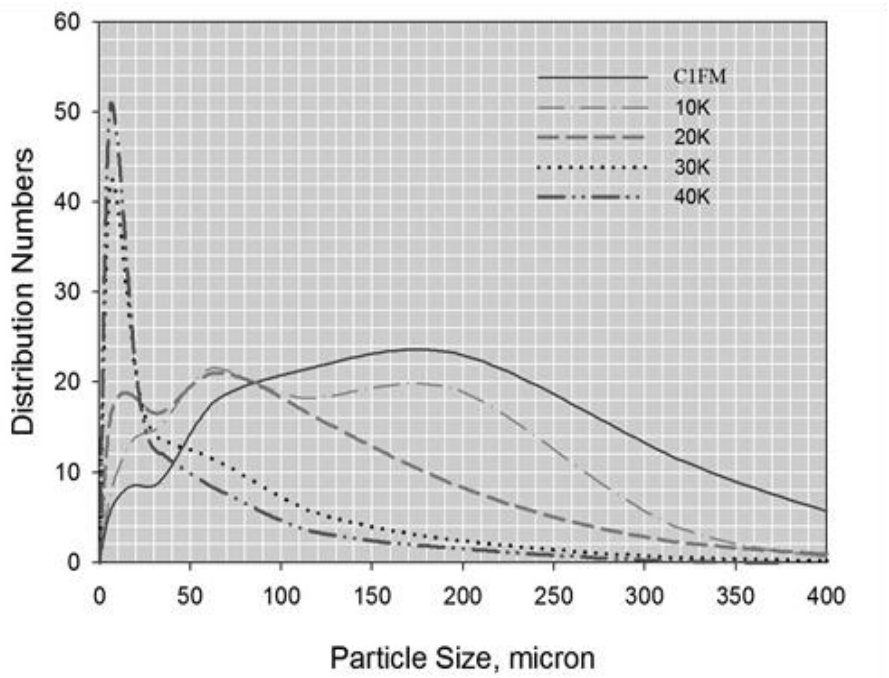

Figure 4.8. PSD Curves of C1FM as A Function of the Operational Pressure

As seen in Figure 4.8, the particle size distribution (PSD) curve labeled as C1FM displays that the particle size of the original feed material was widely distributed with coarser sizes. After undergoing a 10,000 psi pressure grinding, the size distributions of particles clearly shrank. Simultaneously, sizes of particles shifted to smaller values. No clear peak could be obtained, however (see the curve labeled as 10k). As the pressure increased to 20,000 psi, the PSD became narrower than that of the 10,000 psi. Two peaks can be found in the PSD curve. However, the values of these two peaks were greater than 10 microns. When the operational pressure increased to 30,000 psi, the PSD of particles became much narrower and a distinct peak near 8 microns was observed. Further increasing the operational pressure to 40,000 psi resulted in more particles becoming concentrated near 8 microns. This finding illustrates that the waterjet mill coupled with a cavitation cell can generate coal particles below 10 microns with a narrow size distribution for C1 coal.

www.manaraa.com

4.2.4. Morphological Properties of Feeds and Comminution Products. To analyze the morphological properties of the particles as a result of various pressures, a scanning electron microscope (SEM) was used. Data obtained in Section 4.2.2 suggests that the effects of the operational pressure on the behavior of the original feed material (C1FM) and its mono-sized subsamples were similar. For this reason, SEM studies were conducted only on the original feed material C1FM and its resulting products.

Morphological characteristics of the feed material (C1FM) captured under SEM are shown in Figure 4.9. The feed particles exhibited a variety of shapes with sharp edges and corners. It is noted that the particles of the feed material had different sizes.

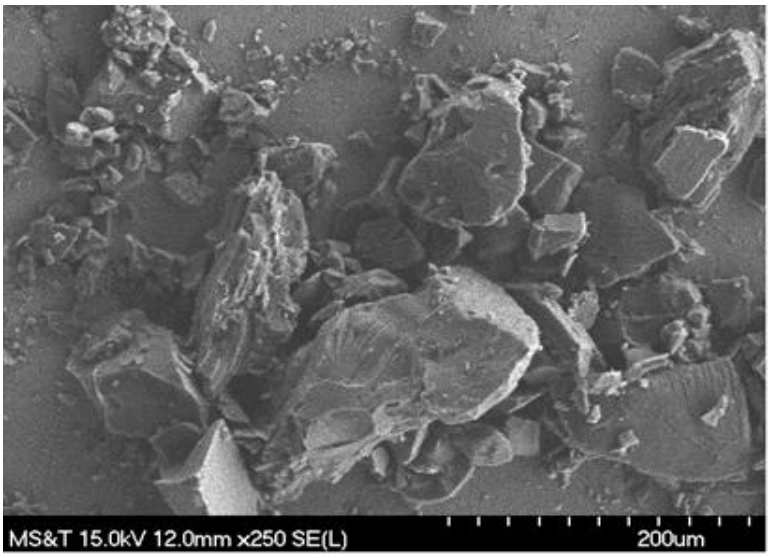

Figure 4.9. Morphological Properties of the Original Feed Material (C1FM)

The product obtained at 10,000 psi shows increased number of smaller particles. These particles still possessed different sizes and shapes, as well as relatively sharp edges and corners. As seen in Figure 4.10.

After increasing the operational pressure to 20,000 psi, chipping of edges due to the attrition between particles can be observed for the majority of the particles (Figure

www.manaraa.com

4.11). However, some particles with sharp edges are still visible suggesting some particles were not subjected to particle-particle interaction. The size of the coal particles seemed to be coarse; however the resulting product size was more homogeneous.

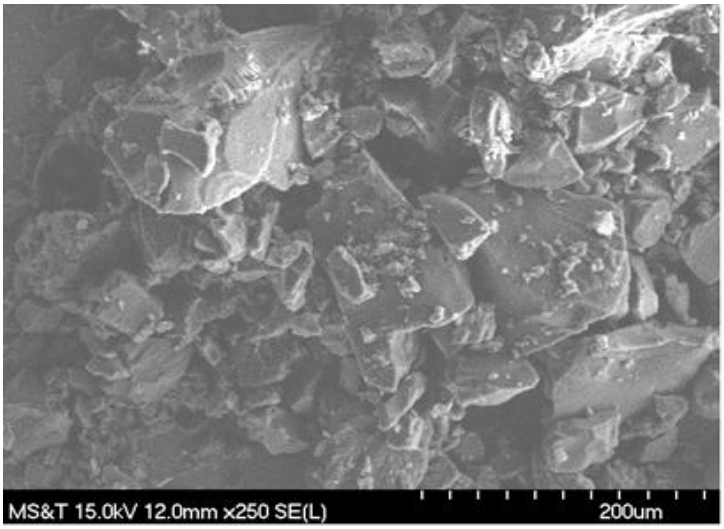

Figure 4.10. Morphological Properties of the Product Obtained from C1FM (10,000 psi Operational Pressure)

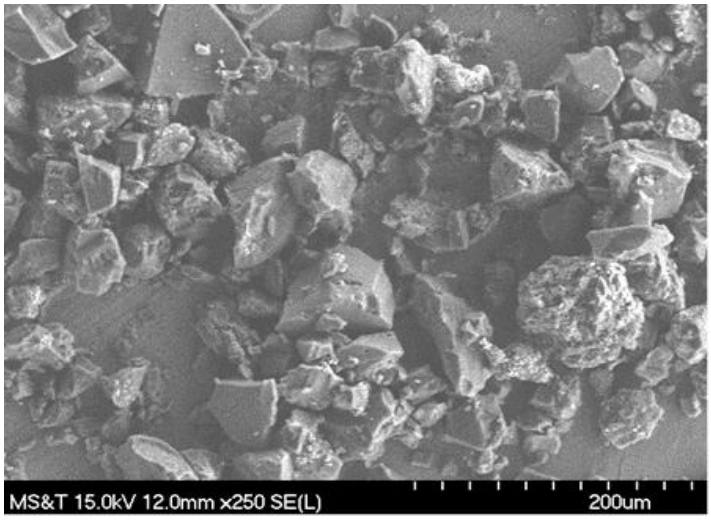

Figure 4.11. Morphological Properties of the Product Obtained from C1FM (20,000 psi Operational Pressure)

www.manaraa.com

Figure 4.12 indicates a considerable increase in fine particles. However, a few grains with larger sizes are still visible. These larger particles were likely to be composited particles (mixture of coal and minerals) or mineral particles with higher hardness values. Since the higher operational pressure induces a higher level of turbulence, the particles obtained at 30,000 psi shows more rounded edges due to higher degree of particle-particle interactions.

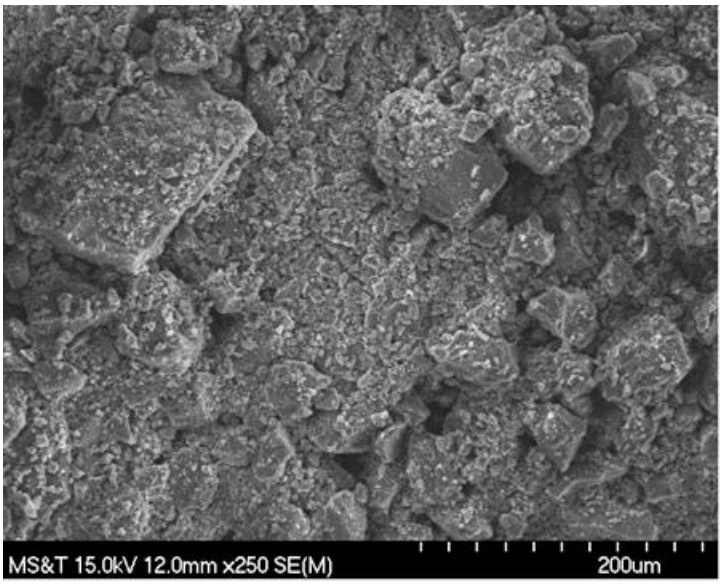

Figure 4.12. Morphological Properties of the Product Obtained from C1FM (30,000 psi Operational Pressure)

The increase of operational pressure to 40,000 psi resulted in a higher amount of fine particles (see Figure 4.13). Figure 4.6 indicates that nearly 80% volume of these particles were smaller than 20 microns. The resulting particles had a similar shape with rounded edges suggesting that the particle were subjected to more particle-particle collisions. Notice that the homogeneity of the particles size was further improved.

www.manaraa.com

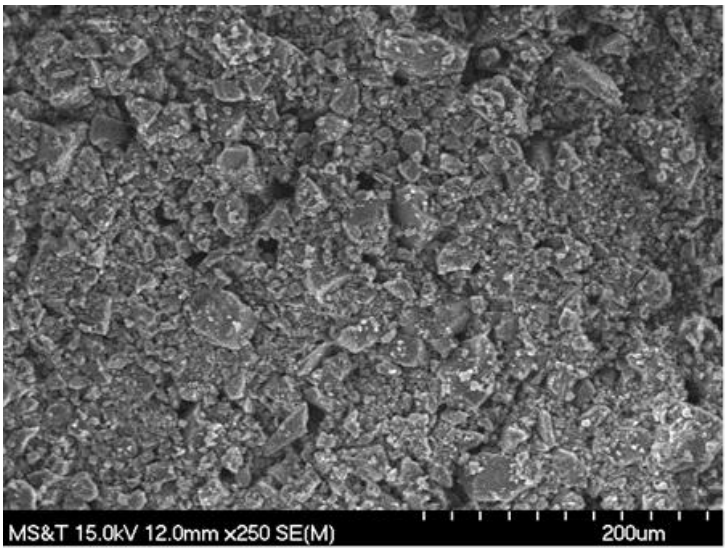

Figure 4.13. Morphological Properties of the Product Obtained from C1FM (40,000 psi Operational Pressure)

Analysis of the morphological properties indicates that the shapes of particles were altered from a high-degree of angularity to a blocky and semi-sphericity shape as a result of the operational pressure increase. Palaniandy (2008) stated that the breakage mechanism was a major factor in determining the morphological properties of the comminution particles. According to Palaniandy (2008), the destructive breakage mechanism produces particles with sharp edges while particles with rounded edges are the result of the abrasion breakage. Combining this explanation with the results of morphological analysis, it can be stated that the abrasion breakage mechanism was more pronounced in the waterjet mill as the operational pressure increased.

4.3. WATERJET-BASED COMMINUTION OF C2 COAL

In order to investigate the effects of coal properties on the behavior of coal particles subjected to the action of a waterjet, a sample of C2 coal with 11% ash content was used in this study. In a similar way as described in Section 4.2, the original feed material C2FM (-850 microns) and its mono-sized subsamples were prepared for the comminution studies. According to the size ranges, the subsamples were marked as

www.manaraa.com

C2FR1 (- 106 microns), C2FR2 (- 212 + 106 microns), C2FR3 (- 355 + 212 microns), and C2FR4 (- 850 + 355 micron). The operational pressure ranged from 10,000 to 40,000 psi with an increment of 10,000 psi. The feed size and operational pressure were the variables in these experiments. The standoff distance (the distance between the anvil and mixing nozzle exit) was still kept constant at 19 millimeters.

4.3.1. Particle Size Analysis. To quantitatively describe the coal particle size change, the cumulative volume undersize curves (CVUSCs) are used for size analysis. Figure 4.14 presents the CVUSCs of the original feed material C2FM and its mono-sized subsamples C2FR1 to C2FR4. The CVUSCs of the comminution products under different operating conditions are illustrated in Figures 4.15 - 4.19. To illustrate the response of coal particles to the value of the operational pressure, the CVUSC of the feed resulted these products are also included in these figures.

Figure 4.14 displays the CVUSCs of the feeds subjected to the comminution tests. It can be seen in Figure 4.14 that the coarseness of the feeds from low to high was in the order of C2FR1, C2FR2, C2FR3, and C2FR4. The original feed material C2FM contains coarse and very fine particles together.

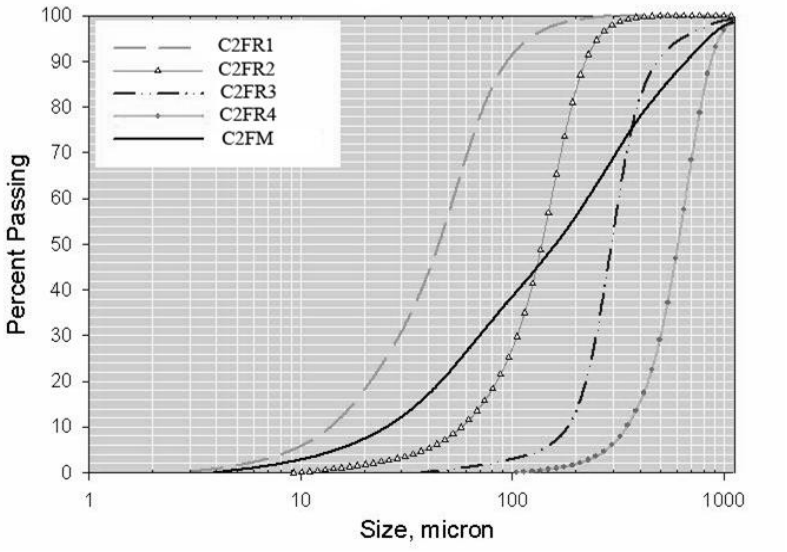

Figure 4.14. CVUSCs of C2FM and Mono-Sized Subsamples (C2FR1 through C2FR4)

www.manaraa.com

The C2FR1 was the finest feed used in the comminution experiments. It contained an abundance of fine particles. As displayed in Figures 4.14 and 4.15, half the volume of the particles in the C2FR1 was finer than 50 microns. Because smaller particles contain fewer faults, flaws, and discontinuities, the energy required to break finer particles are rather high. As a result, the particle size reduction ratios of the C2FR1 were very low when compared to other feeds. The highest size reduction ratio, obtained at 40,000 psi operational pressure, was only 3 for this feed. The median particle sizes (D_{50}) of the comminution products was reduced from 30.0 to 16.1 microns as the operational pressure increased from 10,000 to 40,000 psi.

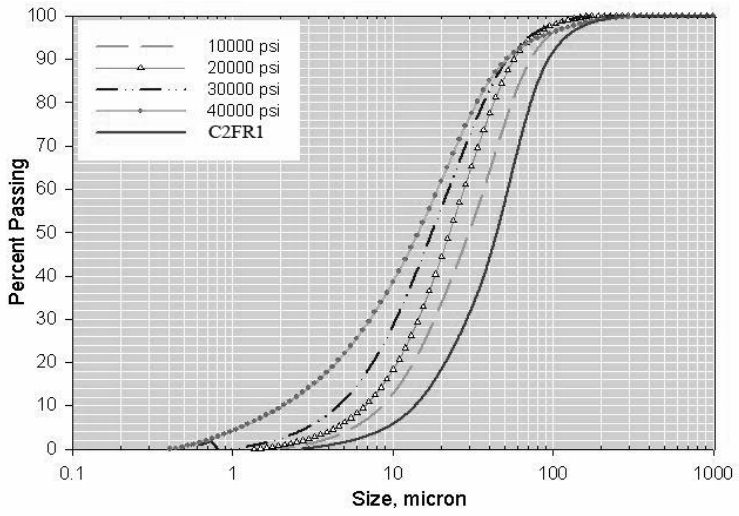

Figure 4.15. CVUSCs of Products for C2FR1 Comminuted at Different Operational Pressures

The median particle size (D_{50}) of the feed C2FR2 was 139.6 microns, almost three times larger than that of the C2FR1. The ratio of 3 is indicative of the increasing coarseness of the feed. For the same comminution conditions, the size reduction ratio obtained for the C2FR2 was higher than that of the C2FR1. The maximum size reduction ratio of 7 was obtained at 40,000 psi for C2FR2. The median particle sizes (D_{50}) of the

www.manaraa.com

products were from 70.77 to 21.32 microns as the operational pressures increased from 10,000 to 40,000 psi (Figure 4.16). Comparison of size reduction ratios obtain from the feed C2FR2 and C2FR1 indicates that the waterjet mill is more efficiently for coarser feed in terms of energy consumption for size reduction ratios.

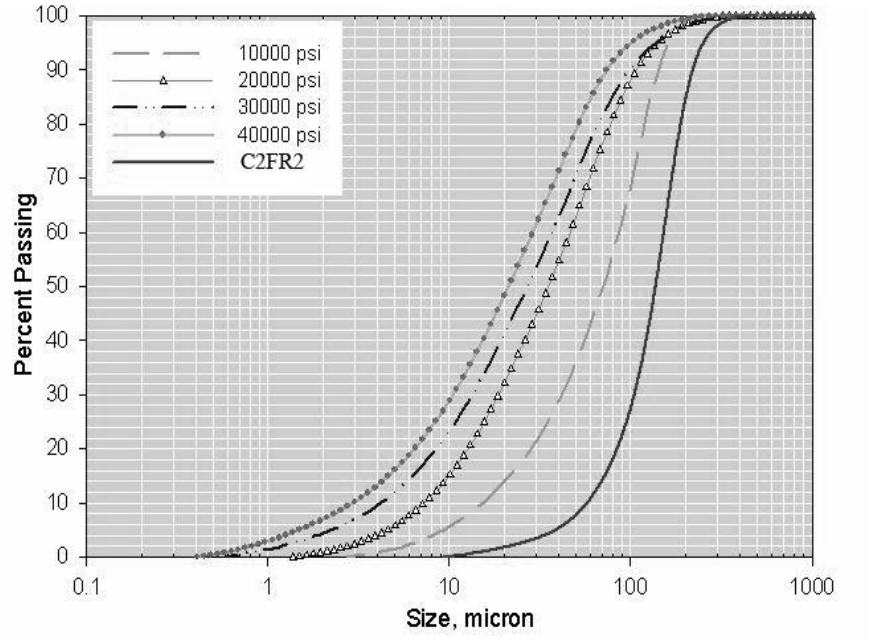

Figure 4.16. CVUSCs of Products for C2FR2 Comminuted at Different Operational Pressures

The feed C2FR3 was even coarser than C2FR2. The median particle size (D_{50}) of the C2FR3 was determined to be 294.30 microns (see Figure 4.17). The median particle size of the comminution products varied from 115.30 to 27.06 microns as the operational pressure increased from 10,000 to 40,000 psi. A size reduction ratio of 11 was obtained for the C2FR3 at 40,000 psi. It should be noted that increasing the operational pressure from 30,000 to 40,000 psi results in only marginal reduce in median particle size.

www.manaraa.com

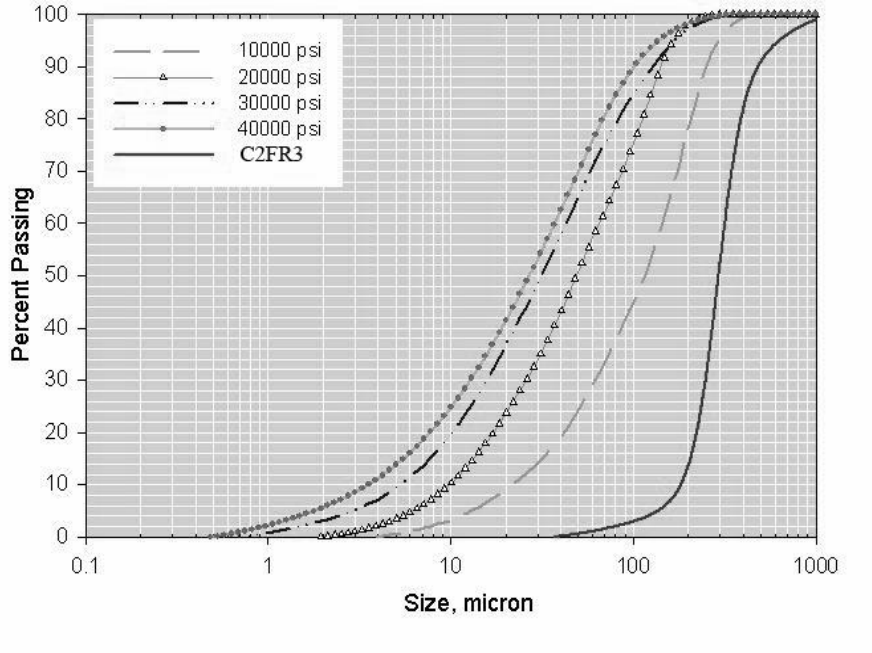

Figure 4.17. CVUSCs of Products for C2FR3 Comminuted at Different Operational Pressures

The C2FR4 was the coarsest feed used in these comminution experiments. It had a median particle size (D_{50}) of 608 microns. C2FR4's median particle size (D_{50}) was two times as large as the median particle size for C2FR3. However, the products' median particle sizes (D_{50}) of the C2FR4, varied between 129.70 and 31.40 microns, were very close to the products of the C2FR3 (Figure 4.18).This data indicates that C2FR4 resulted in much higher size reduction ratios. Under 40,000 psi, C2FR4 had a size reduction ratio of approximately 19. As a result, it can be concluded that the high-pressure waterjet mill is more efficient for coarser feed based on the energy requirement for the degree of size reduction. In addition to this finding, it was determined that increasing the pressure from 30,000 to 40,000 psi resulted in a marginal decrease in the median particle size of the products for the feed C2FR4 (see Figure 4.18).

www.manaraa.com

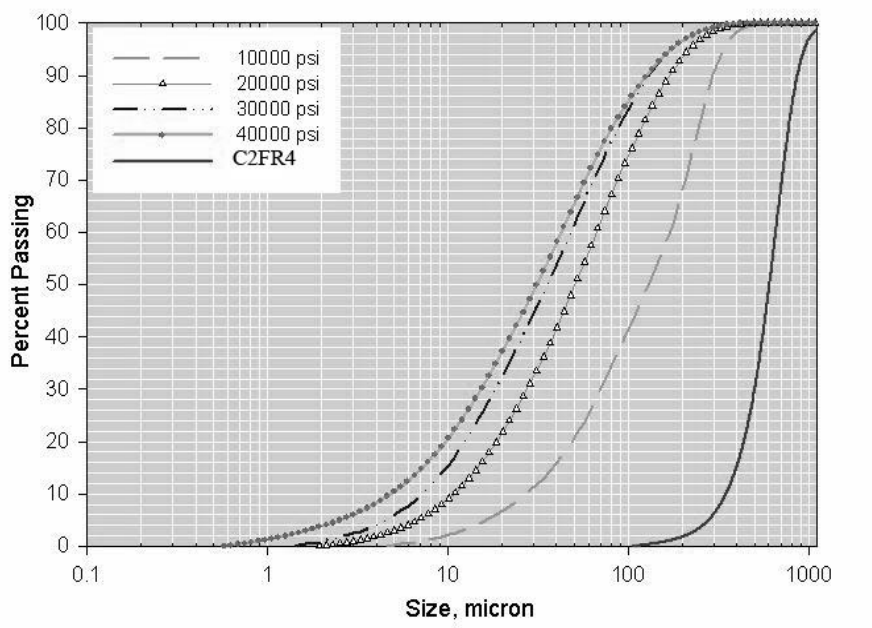

Figure 4.18. CVUSCs of Products for C2FR4 Comminuted Products at Different Operational Pressures

Similar to Section 4.2.1, the last group of experiments was conducted on the original feed material, C2FM, to investigate the effect of size classification on the response of C2 coal comminution using a waterjet. The summary of the results are given in Figure 4.19. Tests results (Figure 4.19) indicate that the median particle size (D_{50}) of the lowest operational pressure product was 58.18 microns. A median particle size (D_{50}) of 20.37 was determined at 40,000 psi. This observation supports the tests performed using the mono-sized subsamples. This finding leads to the conclusion that the behaviors of C2 coal particles responded to the value of the operational pressure are independent of size classification.

Analyzing the CVUSCs of both C1 and C2 coal samples showed that the size reduction ratios of C2 coal were lower than those obtained for C1 coal samples. This is possible a result of the fact that C2 coal has higher ash content than C1 coal. Mineral impurities are harder than coal, meaning that in general higher energy input is required to achieve the same size reduction as low-ash coal for coal samples with higher ash content. Along the same lines, results of the CVUSCs for C2 coal indicate that the effects of

www.manaraa.com

pressure and feed size on the C2 coal comminution using a waterjet are similar to that of C1 coal. Despite the fact that C2 coal has higher ash content than C1 coal, finer products resulted from higher operational pressures, while a lower size reduction ratio was observed for the finer feed.

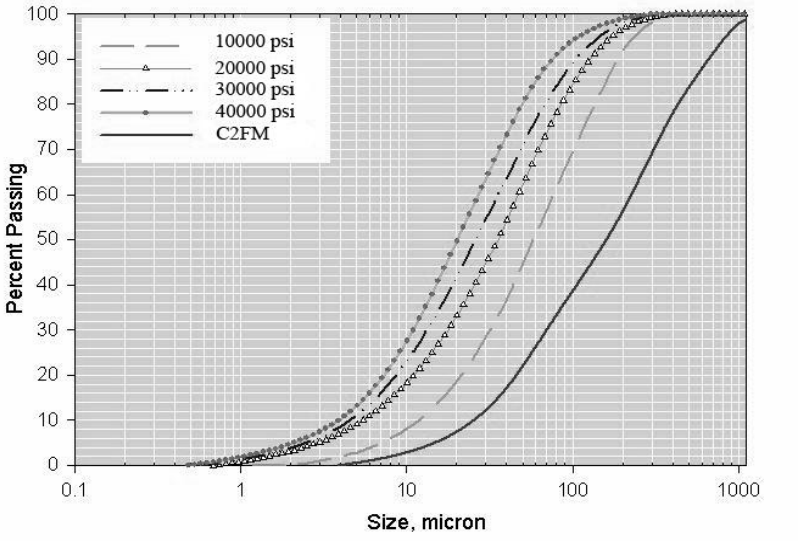

Figure 4.19. CVUSCs of Products for C2FM Comminuted at Different Operational Pressures

4.3.2. Surface Area Change. In this subsection, the calculated surface area change was used in a similar way as it was done for C1 coal to analyze the effect of C2 coal comminution using a waterjet. The results are given in Figure 4.20.

Data presented in Figure 4.20 indicates that the highest calculated surface area ratios (CSARs) were obtained for the coarsest feed, C2FR4. A minimal surface area increase was obtained for the finest feed C2FR1. This observation leads to the conclusion that it is more difficult to reduce the size of smaller particles. As explained earlier, this is a result of fewer cracks and flaws that exist in smaller particles. In addition to this observation, it was found that the CSARs were directly proportional to the value of the

www.manaraa.com

operational pressure. This finding emphasized the previous conclusion that higher operational pressures led to finer products.

As seen in Figure 4.20, increasing the pressure from 30,000 to 40,000 psi resulted in noticeable increase in the CSARs for the feeds C2FR3 and C2FR4. According to the explanation in Section 4.2.2, this observation suggests that increasing the pressure in this range resulted in a noticeable generation of fine particles. Increasing the pressure from 30,000 to 40,000 psi led to a negligible change in the median particle size, as can be seen in Figure 4.17 and Figure 4.18. According to Palaniandy (2008), the formation of fines without a noticeable change in median particle size is a characteristic of the abrasion breakage mechanism. In addition to the interpretation by Palaniandy (2008) combined with observations from Figure 4.20, 4.17, and 4.18, it can be stated that abrasion is the major mechanism of particle size reduction when the pressure exceeds 30,000 psi. Further, this statement implies that the coal particles broke due to destructive breakage rather than abrasion. This is further discussed in Section 4.3.4. The same conclusion has been made by Palaniandy (2008) for the opposed fluidized bed jet mill.

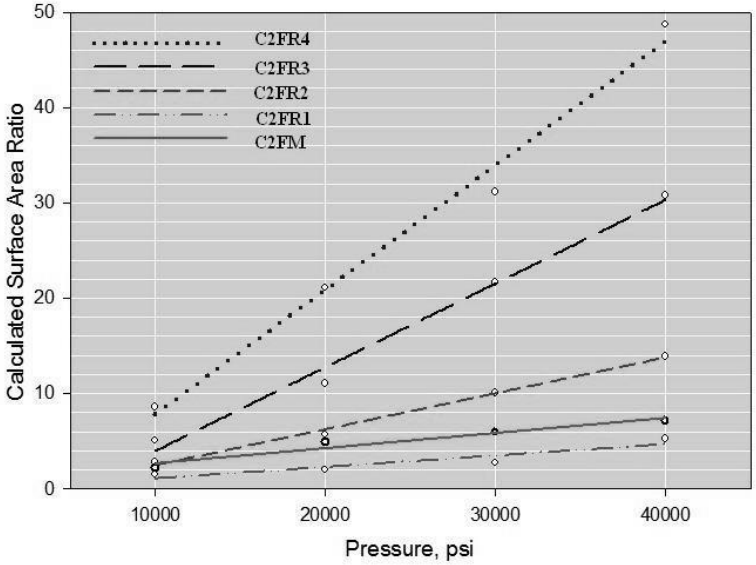

Figure 4.20. CSARs versus Operational Pressures for Different Feed Sizes of C2 Coal

www.manaraa.com

4.3.3. Particle Size Distribution. To illustrate the relative frequency of the various sizes presented in the comminuted products, the particle size distribution (PSD) approach is employed in this section. The original feed material C2FM and its products are analyzed. Figure 4.21 gives the summary of results.

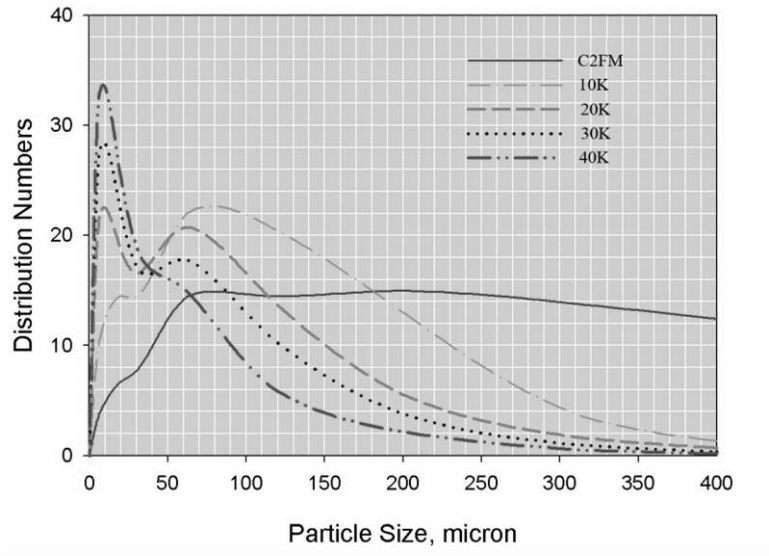

Figure 4.21. PSD Curves of C2FM as a Function of the Operational Pressures

As seen in Figure 4.21, the particles sizes of the original feed C2FM were widely distributed without any accumulation size. For the product ground at 10,000 psi, two peaks can be observed in the PSD curve. However, the sizes of these two peaks were greater than 10 microns. Additionally, it is worth mentioning the amount of particles concentrated around the peak with smaller particle size was not as significant as that of peak with larger size. As the operational pressure increased to 20,000 psi, the positions of these two peaks shifted to smaller sizes. Simultaneously, a greater population of 10 micron particles developed. The PSD of products was much narrower when the pressure further increased to 30,000 psi. A distinct peak around 8 microns was observed as well. Finally, the majority of particles were concentrated near 8 microns when a 40,000 psi jet

www.manaraa.com

was applied. Relatively coarse particles, however, still existed in the ground products. These particles are likely to be the composited particles or other mineral particles, such as pyrite and SiO_2, having higher hardness values. This finding suggests that the operational pressure of 40,000 psi was capable of producing fine particles below 10 microns with a narrow size distribution for C2 coal.

4.3.4. Morphological Properties of Feeds and Comminution Products. To completely analyze the morphological properties of C2FM as a function of the operational pressure, scanning electron microscopy (SEM) studies were conducted on the original feed material, C2FM, and its resulting products. The results are presented in Figures 4.22 to 4.27.

A SEM picture of the original feed material (C2FM) is given in Figure 4.22. Particles observed in Figure 4.22 have a variety of shapes, presenting a characteristic morphology of crushed coal with well-defined edges and corners. In addition to these observations, it is noted that the particles of the original feed materials C2FM had different sizes.

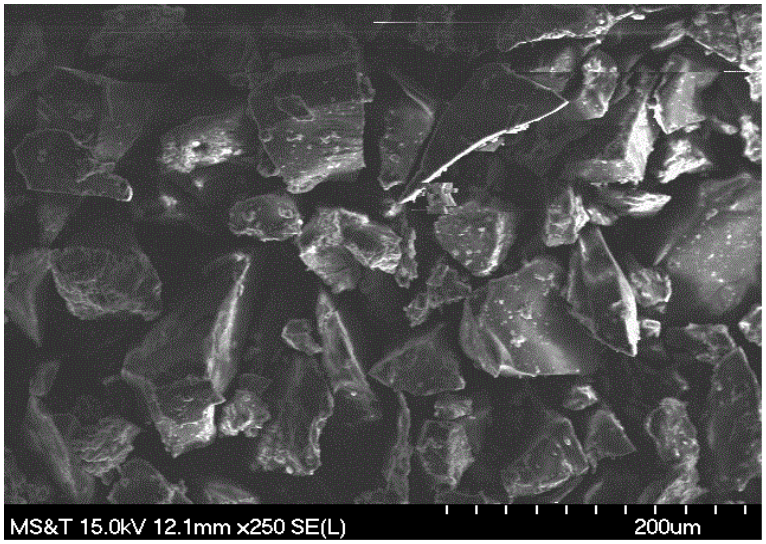

Figure 4.22. Morphological Properties of the Original Feed Material (C2FM)

www.manaraa.com

The product of the 10,000 psi operational pressure shows a reasonable increase in the amount of small particles, as seen in Figure 4.23. Slight rounding of sharp edges and corners as a result of attrition between particles can be observed for most of the particles. The shape of the particles was generally “blocky” with angular transitions.

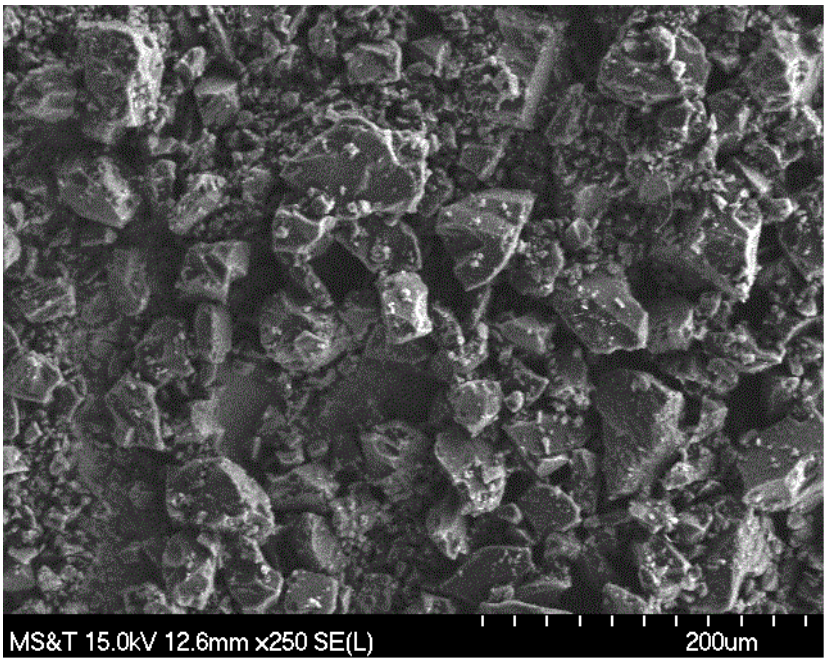

Figure 4.23. Morphological Properties of the Product Obtained from C2FM (10,000 psi Operational Pressure)

Figure 4.24 shows an increase in the amount of flaky particles. Larger particles with distinct grooves on their surface are visible. These observations are the effects of chipping of edges and corners due to increased particle-particle interaction.

In Figure 4.25, most particles had an isometric shape with rounded edges. This observation indicates that the degree of the particle-particle interaction was even higher when a 30,000 psi pressure was applied. In addition to this observation, it can be noted that these particles were reasonably uniform in size. This is evidence that the size distributions of the comminution products became narrower as the pressure increased.

www.manaraa.com

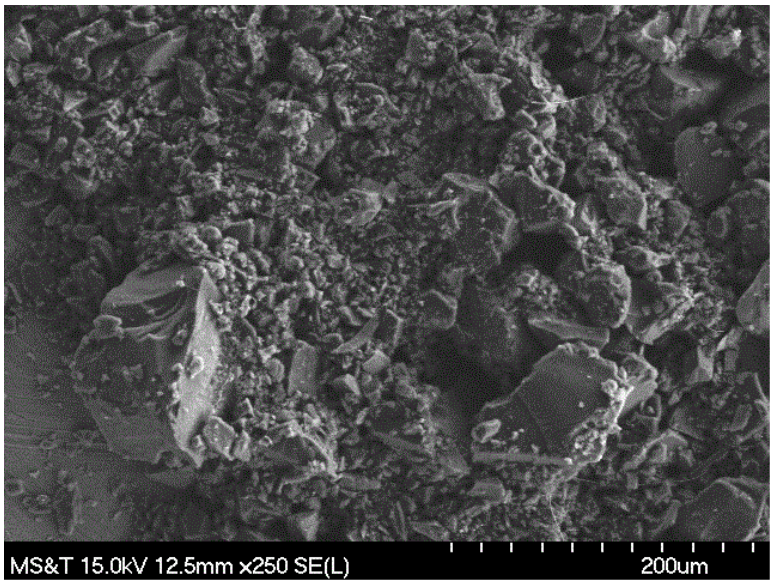

Figure 4.24. Morphological Properties of the Product Obtained from C2FM (20,000 psi Operational Pressure)

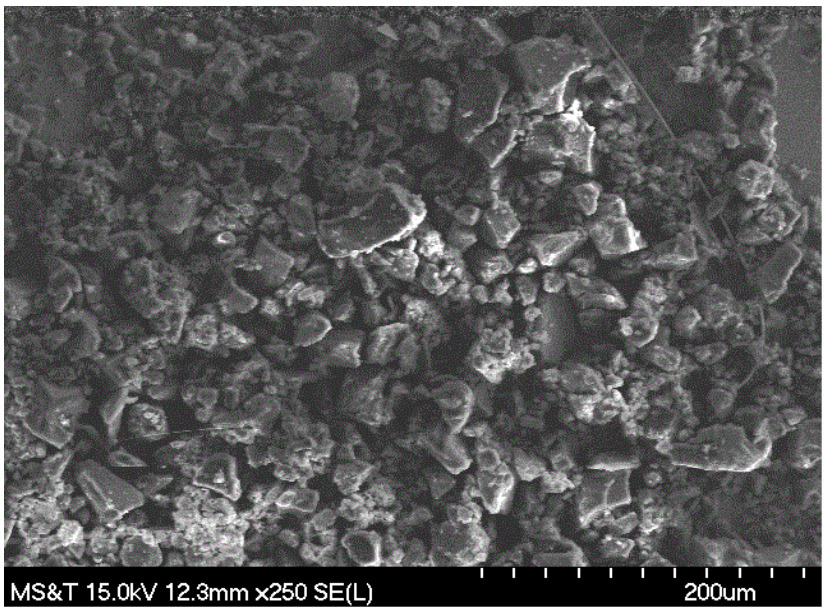

Figure 4.25. Morphological Properties of the Product Obtained from C2FM (30,000 psi Operational Pressure)

www.manaraa.com

The particles in Figure 4.26 demonstrated a medium to high degree of sphericity. There were noticeable flecks of small grains on the surface of coarser particles. A higher magnification image (Figure 4.27) exposed high electron reflectivity of these associated small particles. These small particles, thus, are believed to contain a higher concentration of metallic material, such as pyrite.

The results presented in Figures 4.22 - 4.26 demonstrate that the morphological properties of particles underwent significant change with an increase of the pressure. As the pressure increased, feed material with sharp edges became more spherical shaped. This tendency indicates that a higher degree of particle-particle interaction was involved when a higher pressure was applied. Following this logic, it can be stated that the abrasion breakage was the prominent mechanism for size reduction at higher pressures. A detailed discussion was given in Section 4.2.4. This finding well supports the result of surface area change and is consistent with the results of the SME analysis of C1 coal.

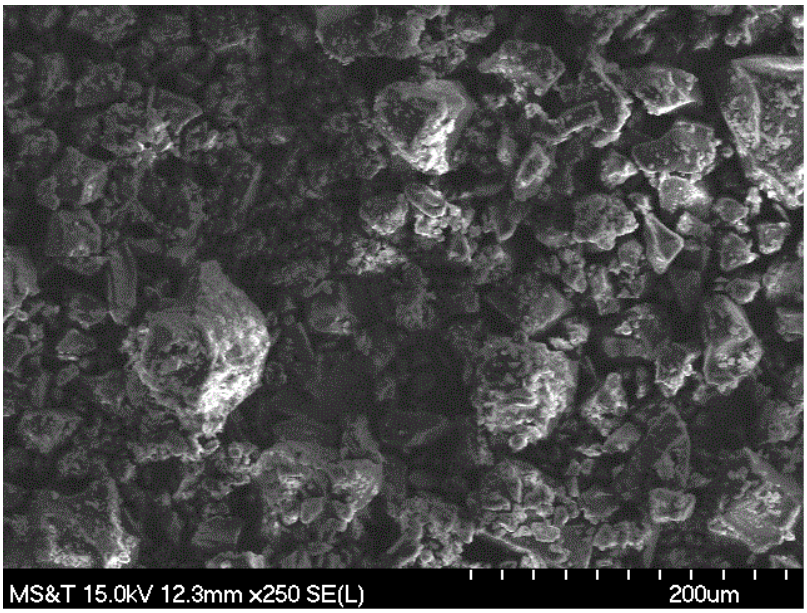

Figure 4.26. Morphological Properties of the Product Obtained from C2FM (40,000 psi Operational Pressure)

www.manaraa.com

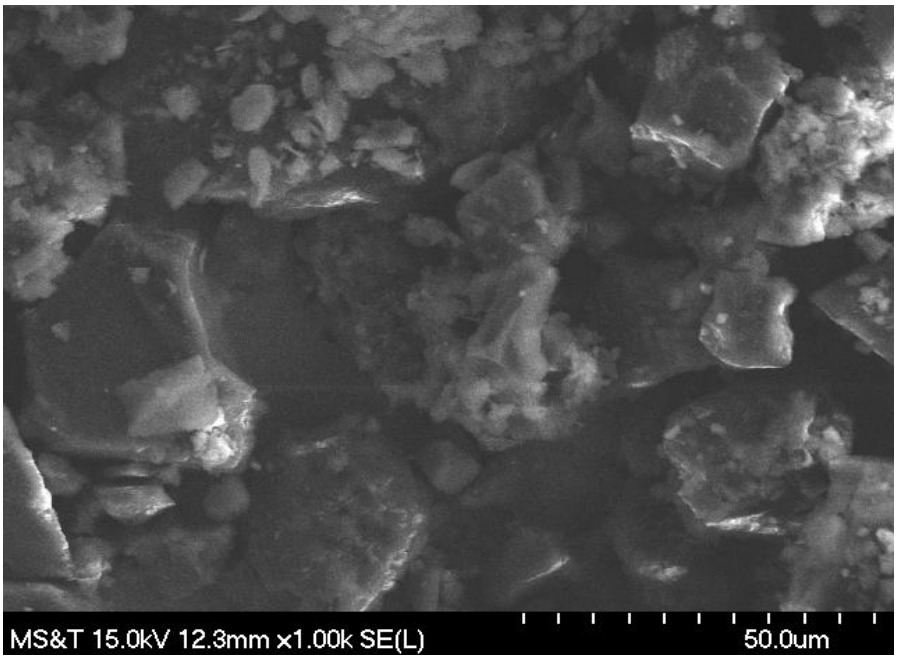

Figure 4.27. Higher Magnification: Morphological Properties of the Product Obtained from C2FM (40,000 psi Operational Pressure)

4.4. WATERJET-BASED COMMINUTION OF C3 COAL

To further analyze the effects of waterjet-based coal comminution, C3 coal with 31% of ash by mass was exposed to the action of a waterjet. To illustrate the effects of the feed properties on the behavior of coal comminution using a waterjet, a similar methodology to that employed in Sections 4.2 and 4.3 was used.

The comminution studies were conducted on the original feed material C3FM (- 850 microns) and its mono-sized subsamples labeled as C3FR1 (- 106 microns), C3FR2 (- 212 + 106 microns), C3FR3 (- 355 + 212 microns), and C3FR4 (- 850 + 355microns). Aside from the feed sizes, the operational pressure varied from 10,000 to 40,000 psi. The standoff distance was kept constant at 19 millimeters for all tests. The criteria for evaluating the comminution process were cumulative volume undersize curves, surface area change, particle size distribution, and morphological properties.

4.4.1. Particle Size Analysis. Similar to Subsections 4.2.1 and 4.3.1, the cumulative volume undersize curves (CVUSCs) are used for particle size analysis.

www.manaraa.com

The CVUSCs of C3FM and its mono-sized subsamples are given in Figure 4.28. Data presented in Figure 4.28 indicates a high content of fine particles, even in the coarsest feed C3FR4.This finding is different from that of C1 and C2 coals. The presence of these fines is believed to be caused by the dispersion of clay into water. Because the C3 coal contained a high amount of clay, the clay dispersed into water spontaneously during the particle analysis process. The ultrasonic stirring mechanism of the particle size analyzer Microtrac S3500 further enhanced the dispersion process. Some amount of fine particles, thus, was detected even in the coarsest feed C3FR4.

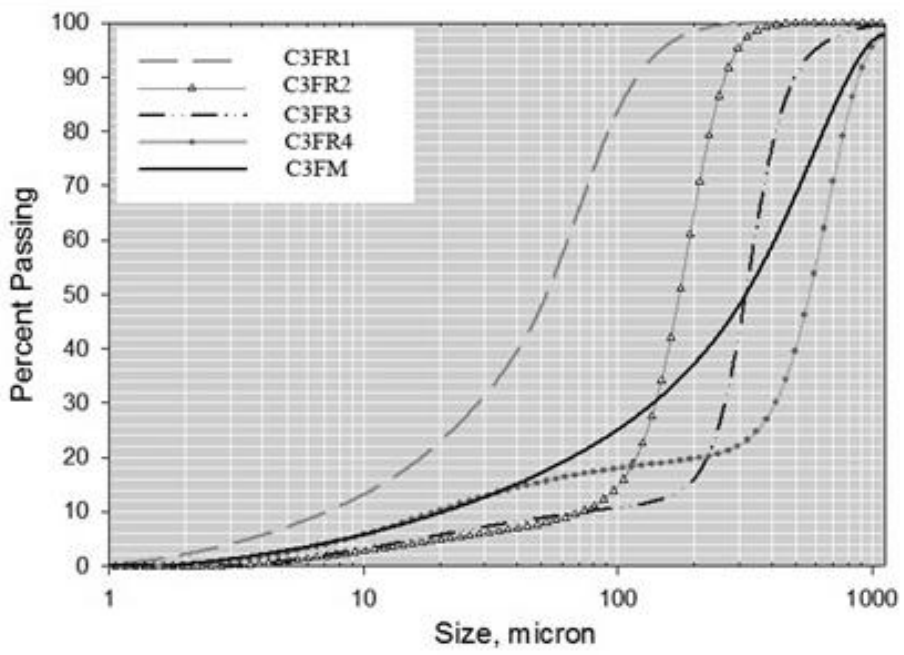

Figure 4.28. CVUSCs of C3FM and Mono-Sized Subsamples (C3FR1through C3FR4)

The CVUSCs of products comminuted at different conditions are presented in Figures 4.29 - 4.33. To illustrate the particle size change as a function of operational pressure, each of these figures also includes the CVUSC of the corresponding feed.

www.manaraa.com

C3FR1 had a median particle size (D_{50}) of 52.51 microns. It was the finest feed used in this study (see Figure 4.28). In the case of identical comminution pressures, the size reduction ratio of the C3FR1 was very low when compared to other feeds. This has been attributed to higher strength of fine particles explained in previous sections. As seen in Figure 4.29, the fineness of the product obtained from the feed C3FR1 increased as the pressure increased.

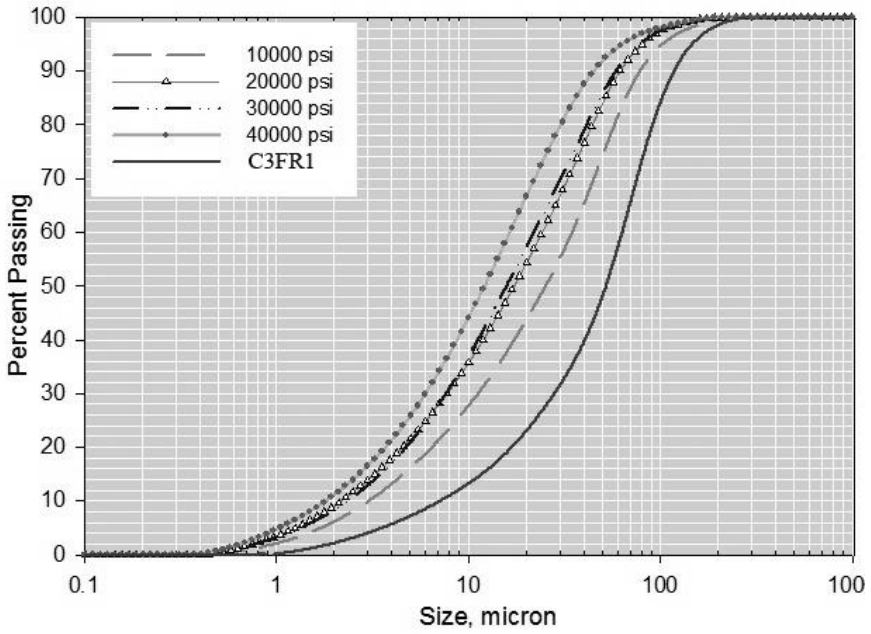

Figure 4.29. CVUSCs of Products for C3FR1 Comminuted at Different Operational Pressures

The response of the feed C3FR2 to the action of a waterjet at four different operational pressures is displayed in Figure 4.30.

The median particle size (D_{50}) of C3FR2 was 174.10 microns which is almost 3 times greater than that of the C3FR1. The comminution efficiency of the C3FR2 was higher than that of C3FR1 in terms of the size reduction ratio. The highest size reduction, obtained at 40,000 psi, was approximately 11 for the feed C3FR2. As the applied

www.manaraa.com

operational pressure increased from 10,000 to 40,000 psi, the median particle sizes (D_{50}) of the ground products were decreased from 63.36 to16.12 microns.

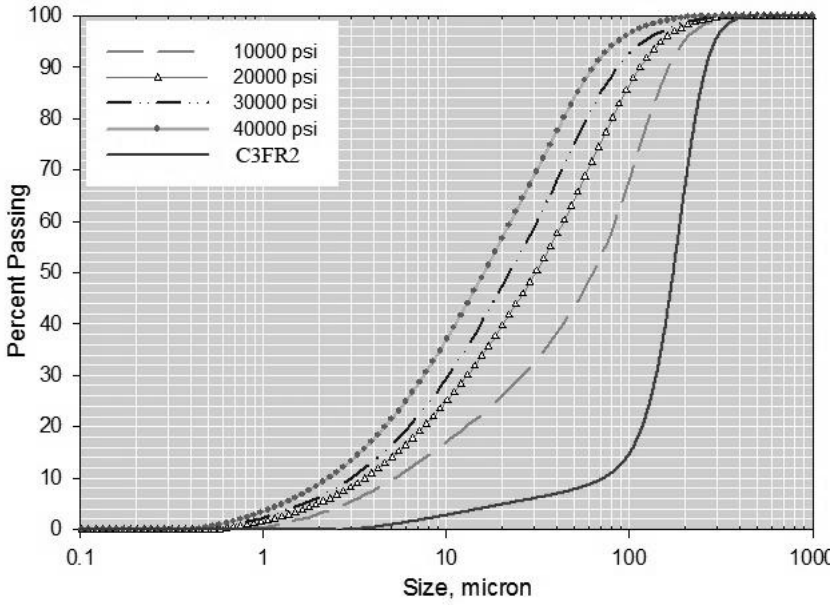

Figure 4.30. CVUSCs of Products for C3FR2 Comminuted at Different Operational Pressures

The behavior of the feed C3FR3 subjected to the action of a waterjet at four different operational pressures is presented in Figure 4.31. The feed material of the C3FR3 with a median particle size (D_{50}) of 318.20 microns was coarser than C3FR2. The highest size reduction ratio, obtained at 40,000 psi, was near 13 for this feed size suggesting a higher efficiency of comminution than that of C3FR2. As the operational pressure increased from 10,000 to 40,000 psi, the median particle sizes (D_{50}) of the ground products were decreased from 109.20 to 24.05 microns. This data confirms the effect that higher pressures led to finer products.

www.manaraa.com

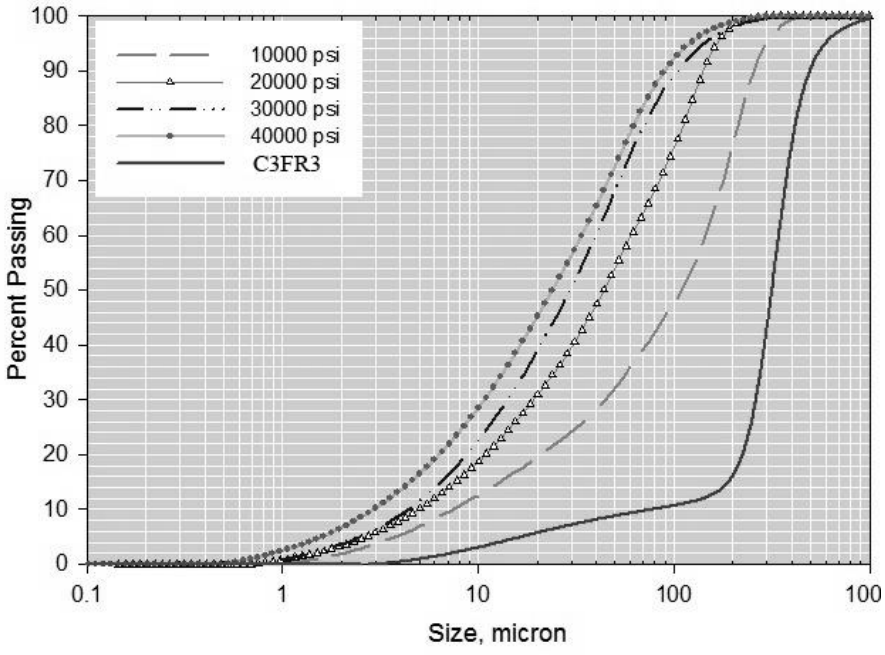

Figure 4.31. CVUSCs of Products for C3FR3 Comminuted at Different Operational Pressures

The feed C3FR4 was the coarsest feed used in these experiments (see Figure 4.28). Its response to the action of a waterjet with different pressures is presented in Figure 4.32. The median particle size (D_{50}) of the feed C3FR4 was two times greater than C3FR3's median particle size. The median particle sizes of C3FR4's products were very close to the products of the C3FR3 (see Figure 4.31 and Figure 4.32). This means that the highest size reduction ratio was obtained using the coarsest feed C3FR4 under identical pressures. The median particle sizes of the comminution products obtained from C3FR4 ranged from 115.80 to 22.96 microns. The finest product was obtained by applying a 40,000 psi operational pressure. However, the cumulative volume undersize curves of 30,000 and 40,000 psi began to overlap near 20 microns. This phenomenon suggests that the probability of coarser particles breaking was higher than smaller particles. This is in agreement with the findings of Palaniandy (2008) for the opposed fluidized bed jet mill.

www.manaraa.com

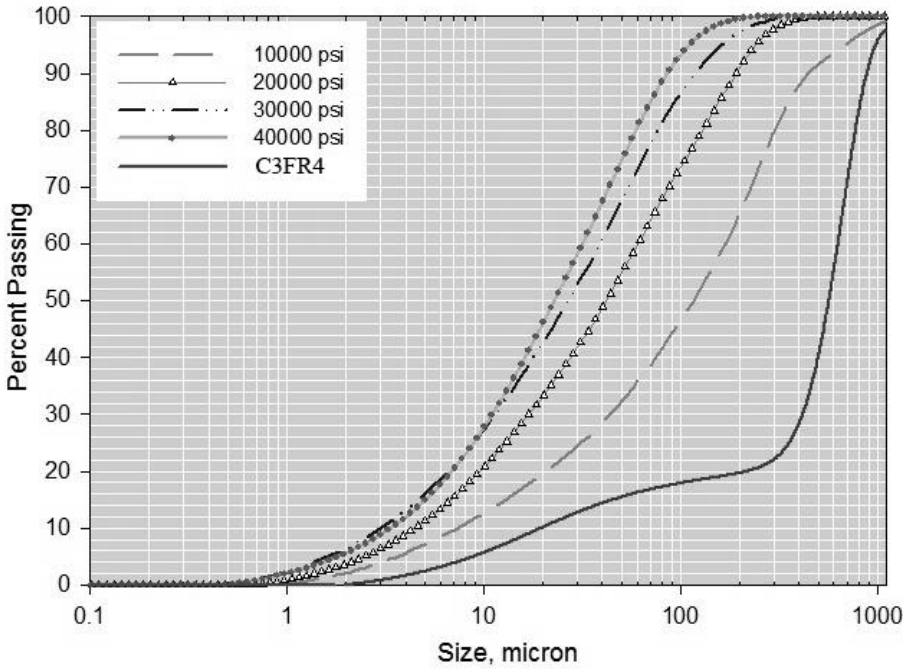

Figure 4.32. CVUSCs of Products for C3FR4 Comminuted at Different Operational Pressures

The last group of comminution tests was conducted on the original feed material C3FM to investigate whether the size classification affects the process of comminution. The results are presented in Figure 4.33. The feed C3FM contained both coarse and very fine particles together (see Figure 4.28). It had a median particle size (D_{50}) of 318.40 microns. The CVUSCs in Figure 4.33 indicates that the median particle size (D_{50}) of the product, ground at the lowest pressure (10,000 psi), was 98.26 microns. As the operational pressure increased, the median particle sizes (D_{50}) of products decreased gradually to 20.37 microns. This change trend correlates with the result observed from its mono-sized subsample experiments: higher operational pressures led to finer products.

www.manaraa.com

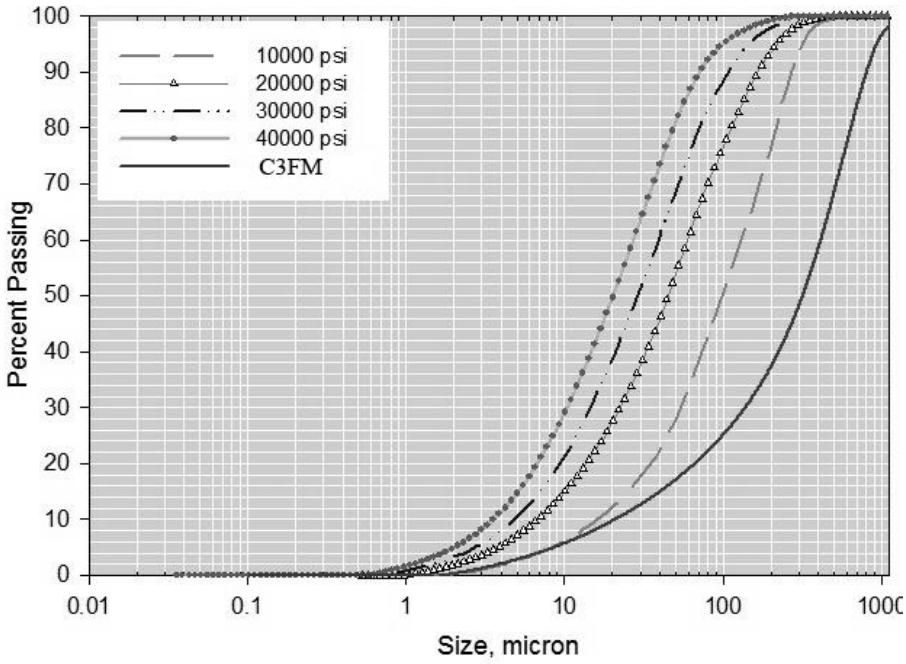

Figure 4.33. CVUSCs of Products for C3FM Comminuted under Different Operational Pressures

Based on results presented in Figures 4.28 - 4.33, it can be summarized that finer products resulted from higher pressures. For the effect of the feed size, it can be stated that higher size reduction ratios were obtained for the coarser feeds. This correlates with the theory of comminution that smaller particles were more difficult to break than larger ones.

4.4.2. Surface Area Change. In this subsection, the effect of waterjet-based C3 coal comminution was further analyzed based on the calculated surface area change. The summary of results is given in Figure 4.34.

It can be seen that the highest calculated surface area ratios (CSARs) were obtained for the coarsest feed. This observation follows the general trend in comminution: the smaller the particle size the harder it is to further reduce its size. This effect is also closely related to the finding that higher pressure leads to finer products.

www.manaraa.com

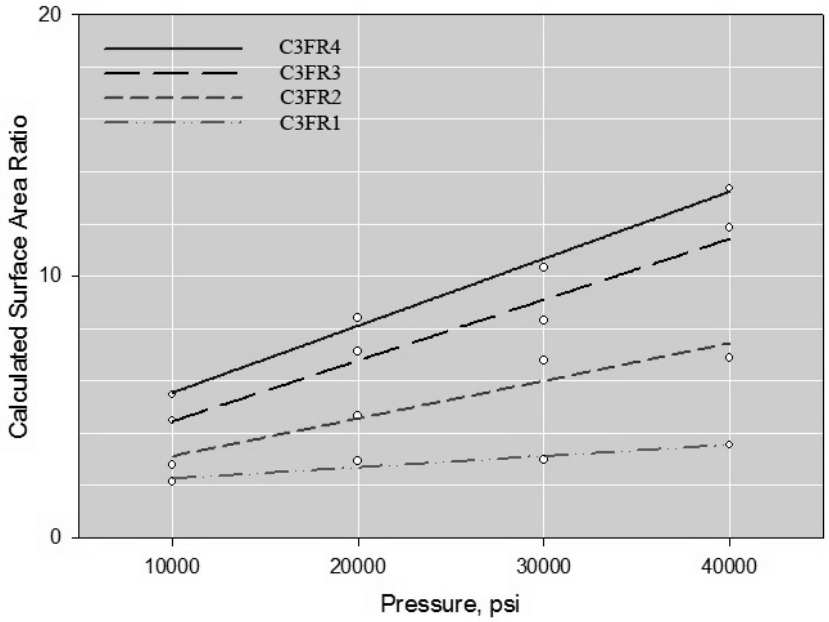

Figure 4.34. CSARs versus Operational Pressures for Mono-Sized Subsamples of C3FM

As explained earlier, a higher calculated surface area indicates a smaller particle size for the same amount of material. Following this explanation to Figure 4.34 leads to the statement that increasing the pressure from 30,000 to 40,000 psi resulted in generation of fine particles for the feeds C2FR3 and C2FR4. The CUVSCs presented in Figure 4.31 and Figure 4.32 indicated that increasing pressure in this range led to a minimum change of the median particle sizes (D_{50}). Based on these observations, it is concluded that abrasion became the prevailing mechanism of particle size reduction when the pressure was greater than 30,000 psi for C3 coal. Detailed explanation of this effect was given in Subsection 4.3.2.

4.4.3. Particle Size Distribution. The effect of operational pressure on the size distribution of C3FM exposed to the action of a waterjet is given in Figure 4.35.

It can be observed that the size distribution of the original feed material, C3FM, was very wide before grinding by the high-pressure waterjet mill. The particle size distribution (PSD) curve clearly shrank after undergoing a 10,000 psi grinding. The sizes of the particles are shifting to smaller values synchronously. However, the majority of

www.manaraa.com

particles were coarser than 10 microns. As the pressure increased to 20,000 psi, two peaks with sizes of 5 and 65 microns can clearly be observed in the PSD curve of the product. Under this pressure, the amount of particles concentrated around 5 microns was not as significant as the amount of particles concentrated around 65 microns. With further increasing the pressure to 30,000 psi, the size of the peak located around 65 microns became smaller combined with progressively decreasing in the amount of particles concentrated around this peak. Simultaneously, a greater population of 5 micron particles was developed. Finally, almost all particles concentrated around 5 microns after a 40,000 psi pressure was applied. The change trend of the PSD as a function of pressure demonstrates that the high-pressure waterjet mill with 40,000 psi pressure has the capacity to generate ultrafine coal particles below 10 microns with narrow size distribution for C3 coal.

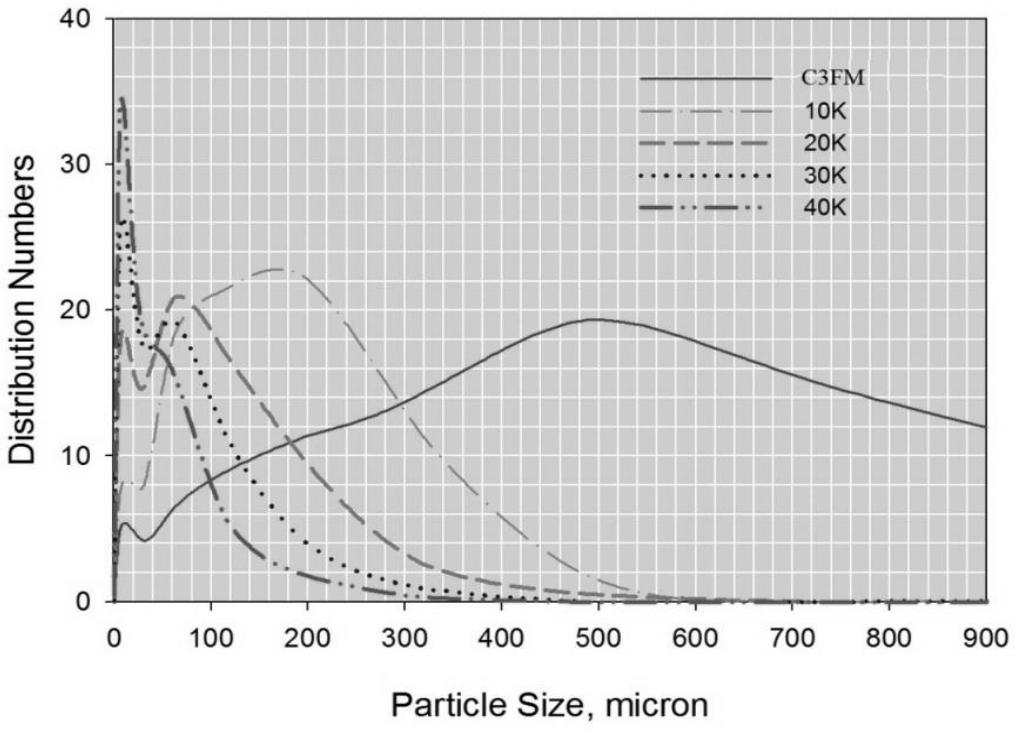

Figure 4.35 PSD Curves of C3FM as a Function of the Operational Pressures

www.manaraa.com

4.4.4. Morphological Properties of Feeds and Comminution Products. In order to provide a comprehensive evaluation of the effects of pressure on the behavior of the C3 coal, SEM studies were conducted on the original feed material, C3FM, and its resulting products. The results are given in Figures 4.36 - 4.40.

As seen in Figure 4.36, coal particles of the original feed material C3FM exhibit a poor quality shape with irregularities and non-uniform surface texture. Additionally, these particles had a variety of sizes.

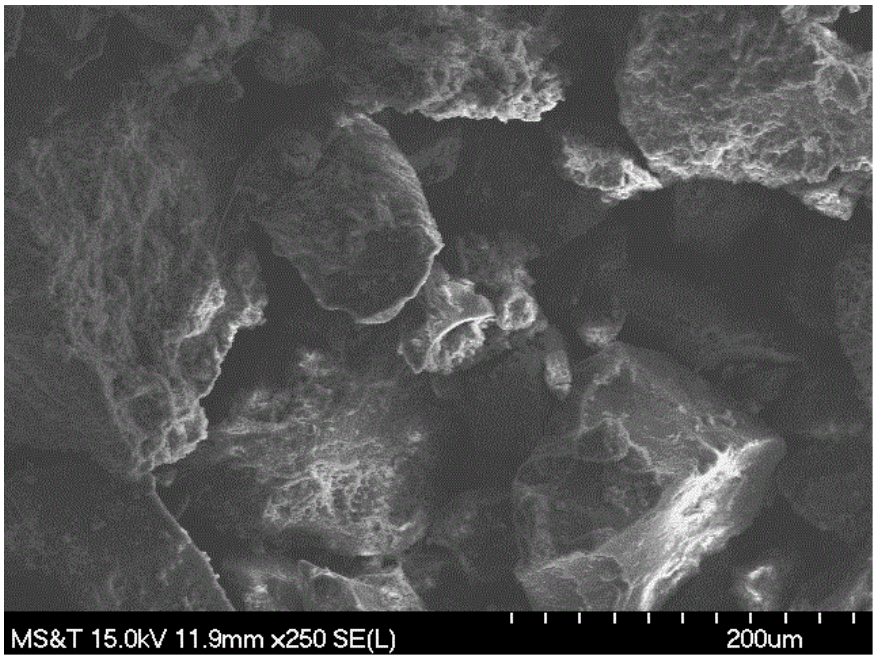

Figure 4.36. Morphological Properties of the Original Feed Material (C3FM)

The ground particles of 10,000 psi in Figure 4.37 display improvement in the particle's overall morphology compared to the feed material (Figure 4.36). Flaky coal particles covered with fine clay minerals are noticeable. The presence of fine clay on the surface of the 10,000 psi product confirmed that C3 coal has a high content of clay. It is worth noting that particles in Figure 4.37 still present an irregular shape.

www.manaraa.com

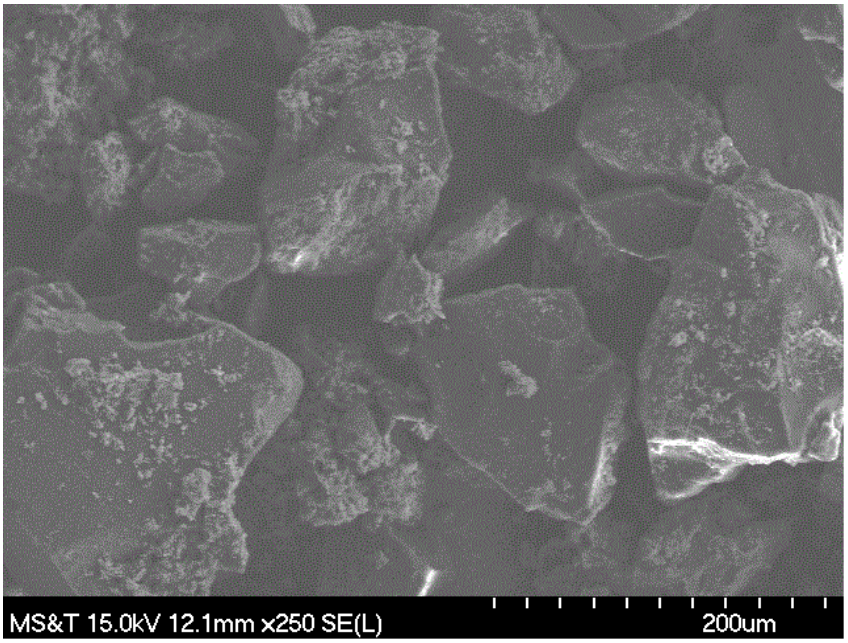

Figure 4.37. Morphological Properties of the Product Obtained from C3FM (10,000 psi Operational Pressure)

Trimming of sharp edges and corners of the particles was observed in most of the particles after the pressure was increased to 20,000 psi (see Figure 4.38). According to Sri Raj Rajeswari et al. (2011), a particle having one or more sharp angles on its surface is believed to possess an angular shape. The cubical shape indicates a shape that particles have smooth angles on their surface compared to angular shape. According to these definitions, it can be said the shape of the particles in Figure 4.38 are generally cubical. However, a few particles with the angular shape were still noticed.

Figure 4.39 shows the morphological properties of the product after being ground under a 30, 000 psi operational pressure. Particles with different sizes are visible in the picture. The majority of particles are mostly isometric in shape with rounded edges. The number of the cubic shaped particles is higher in Figure 4.39 than in Figure 4.38. This indicates that the degree of particle-particle interaction was further enhanced when the pressure increased from 20,000 to 30,000 psi.

www.manaraa.com

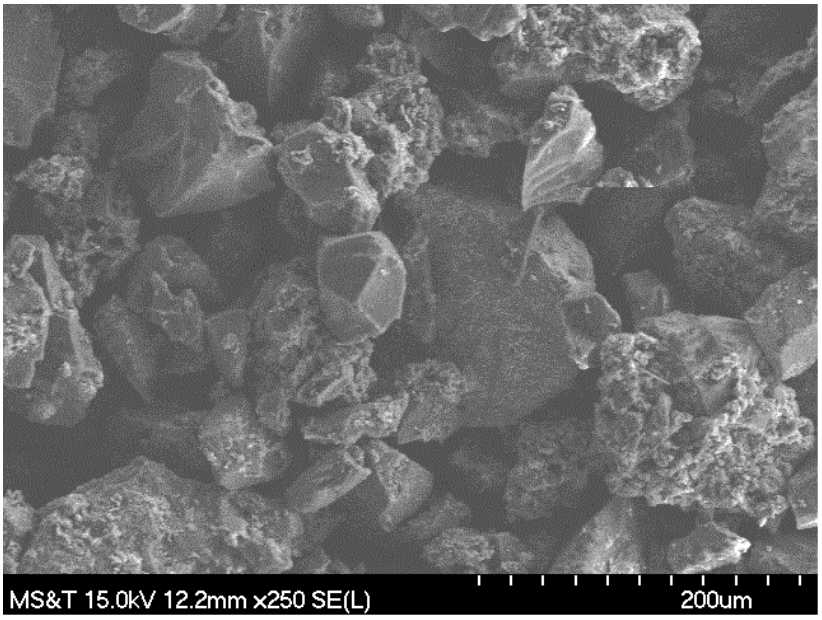

Figure 4.38. Morphological Properties of the Product Obtained from C3FM (20,000 psi Operational Pressure)

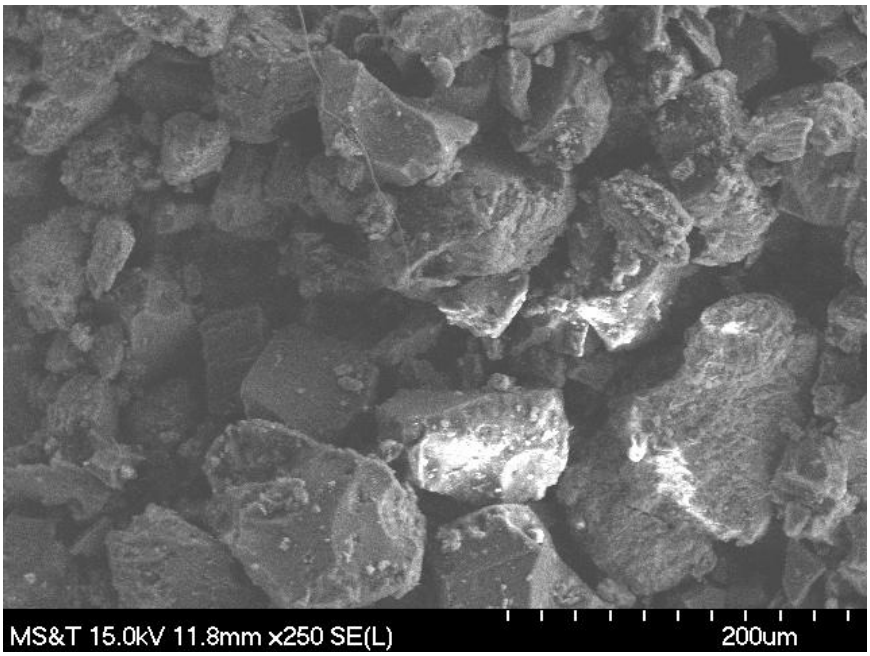

Figure 4.39. Morphological Properties of the Product Obtained from C3FM (30,000 psi Operational Pressure)

www.manaraa.com

The product of the 40,000 psi shown in Figure 4.40 contains mostly fine, cubical and semi-spherical particles. A few particles with larger size are still presented. These particles either had higher strength than the smaller surrounding particles or did not impact against the anvil. To eliminate this effect, the waterjet-based mill can be operated in series with a classifier.

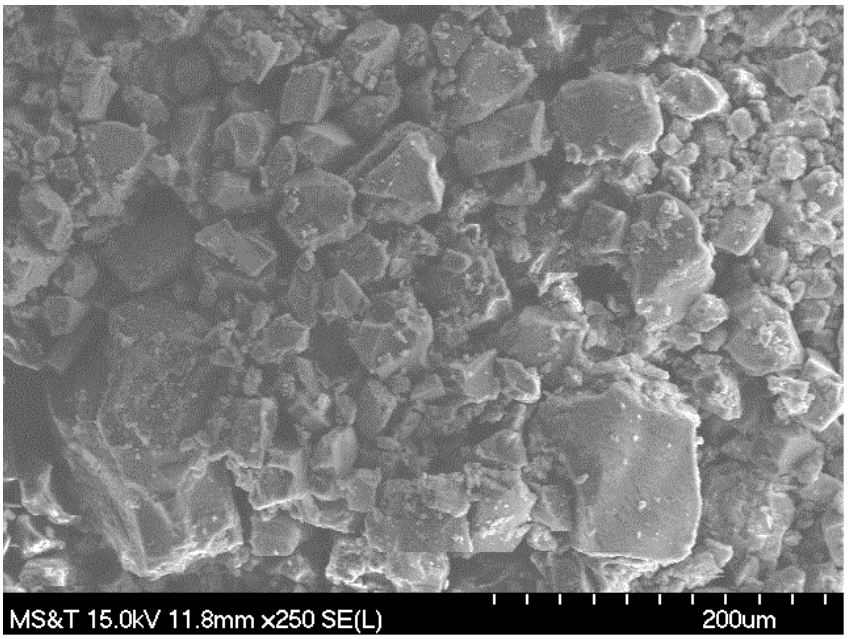

Figure 4.40. Morphological Properties of the Product Obtained from C3FM (40,000 psi Operational Pressure)

Results presented in Figures 4.36 to 4.40 indicate that the shapes of the particles are altered from irregular shapes with non-uniform surface texture toward more spherical shapes by increasing the pressure. This effect indicates that the particles underwent a higher level of particle-particle interaction when higher pressure was applied. Further, it can be said that the abrasion breakage mechanism became more important for size reduction as the pressure increased. This is in agreement with C1 and C2 coal. Detailed discussion is given in Subsection 4.2.4.

www.manaraa.com

4.5. OVERVIEW OF SECTIONS 4.2, 4.3, AND 4.4

In Sections 4.2, 4.3, and 4.4, the effects of coal comminution using a waterjet were thoroughly investigated using three coals with different properties. The comminuted products were characterized using four approaches including cumulative size curves, surface area change, particle size distribution curves, and morphological properties.

After a rapid overview of these tests results, major test observations are reported in this section.

4.5.1. Particle Size Analysis. To assess the full significance of the comminution results, the cumulative volume undersize curves (CVUSCs) were, firstly, used to characterize the feeds and their resulting products. As a valuable quantity for routine control of the grinding circuit, the median particle size (D_{50}) was set as a criterion to represent the fineness of the products. The comminution efficiency of the waterjet-based comminution was compared based on the particle size reduction ratio.

The median particle sizes (D_{50}) of the products comminuted at different conditions are summarized in Tables 4.1 to 4.3. As seen in these tables, the median particle size of the product decreased with an increase of the pressure regardless of the coal properties. This finding carries a practical recommendation for conditions generating finer products. Additionally, it is noteworthy that the effect of the pressure increase on the median particle size decrease exhibited a diminishing return. This can be clearly visualized in Figures 4.41 to 4.43. This diminishing return indicates that the efficiency of the waterjet mill decreases with increasing operational pressure. The reason for this is that the input energy wasted in the production of heat increased as the operational pressure increased. This is strongly supported by Figure 4.44.

As seen in Figure 4.44, the temperature of the products that exited from the cavitation cell was proportional to the pressure. The proportionality of the pressure to the temperature of the products indicates that the efficiency of the high-pressure waterjet mill for coal comminution decreases as the applied pressure is increased.

www.manaraa.com

Table 4.1. C1 Coal: The Median Particle Size of the Products Comminuted at Different Comminution Conditions

Samples	Median Particles Sizes (D_{50}) of Products, µm			
	10,000 psi	20000 psi	30,000 psi	40,000 psi
C1FR1	28	21	16	10
C1FR2	32	25	18	12
C1FR3	57	29	20	18
C1FR4	87	35	28	21
C1FM	79	43	16	11

Table 4.2. C2 Coal: The Median Particle Size of the Products Comminuted at Different Comminution Conditions

Samples	Median Particles Sizes (D_{50}) of Products, µm			
	10,000 psi	20000 psi	30,000 psi	40,000 psi
C2FR1	30.00	22.13	18.51	16.10
C2FR2	70.77	36.41	28.56	21.32
C2FR3	115.30	49.97	30.86	27.06
C2FR4	129.40	50.01	37.50	31.40
C2FM	58.18	36.72	27.68	20.37

Table 4.3. C3 Coal: The Median Particle Size of the Products Comminuted at Different Comminution Conditions

Samples	Median Particles Sizes (D_{50}) of Products, µm			
	10,000 psi	20000 psi	30,000 psi	40,000 psi
C3FR1	25.43	17.39	15.92	12.25
C3FR2	63.36	30.13	21.89	16.12
C3FR3	109.20	41.14	29.89	24.05
C3FR4	115.80	41.62	28.36	22.96
C3FM	98.26	46.57	29.97	20.37

www.manaraa.com

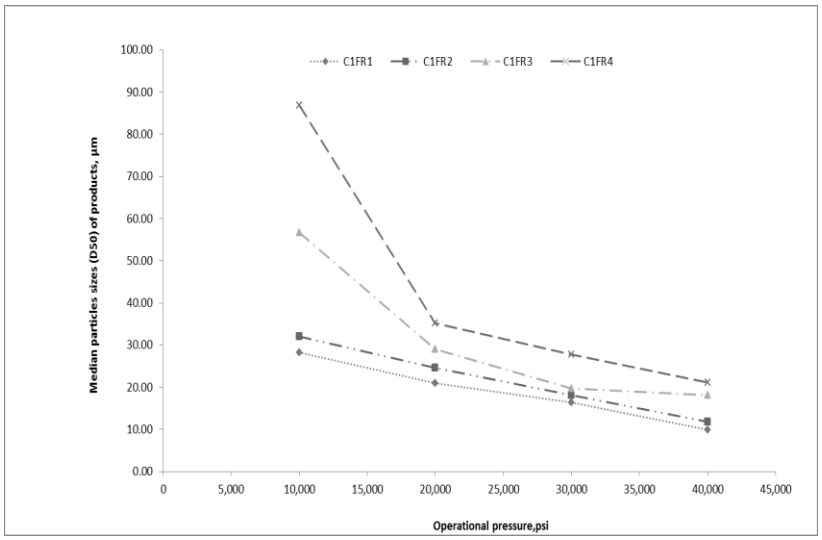

Figure 4.41. C1 Coal: Median Particle Sizes of the Products as a Function of Operational Pressures

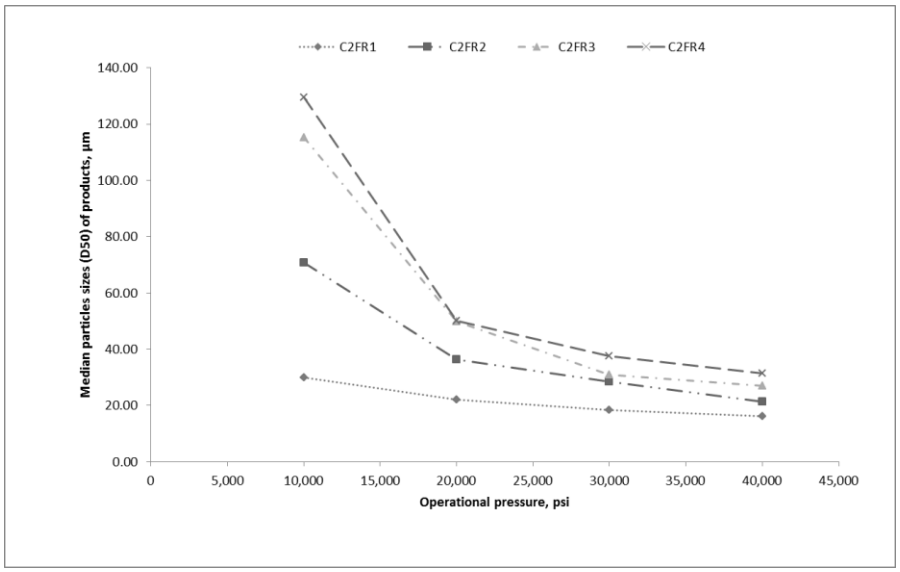

Figure 4.42. C2 Coal: Median Particle Sizes of the Products as a Function of Operational Pressures

www.manaraa.com

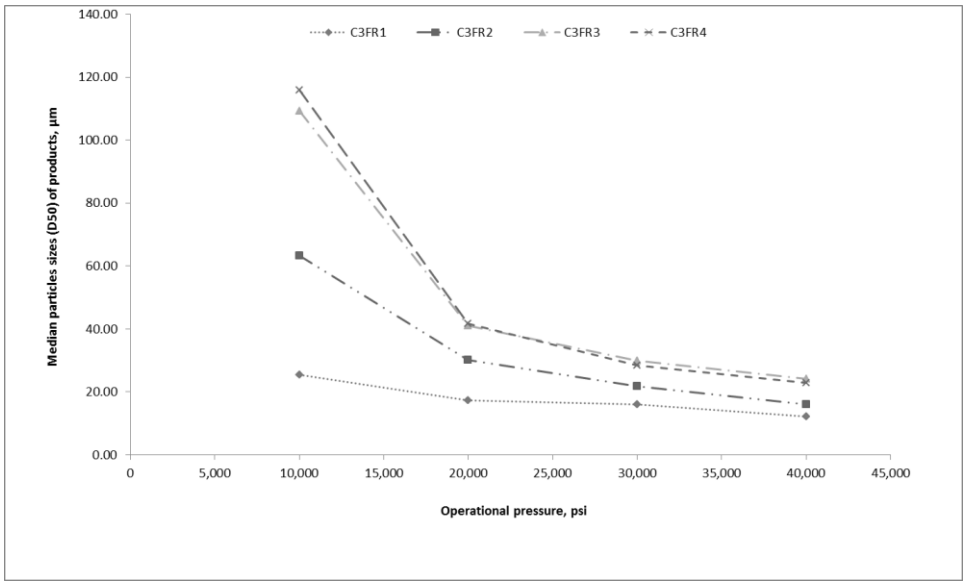

Figure 4.43. C3 Coal: Median Particle Sizes of the Products as a Function of Operational Pressures

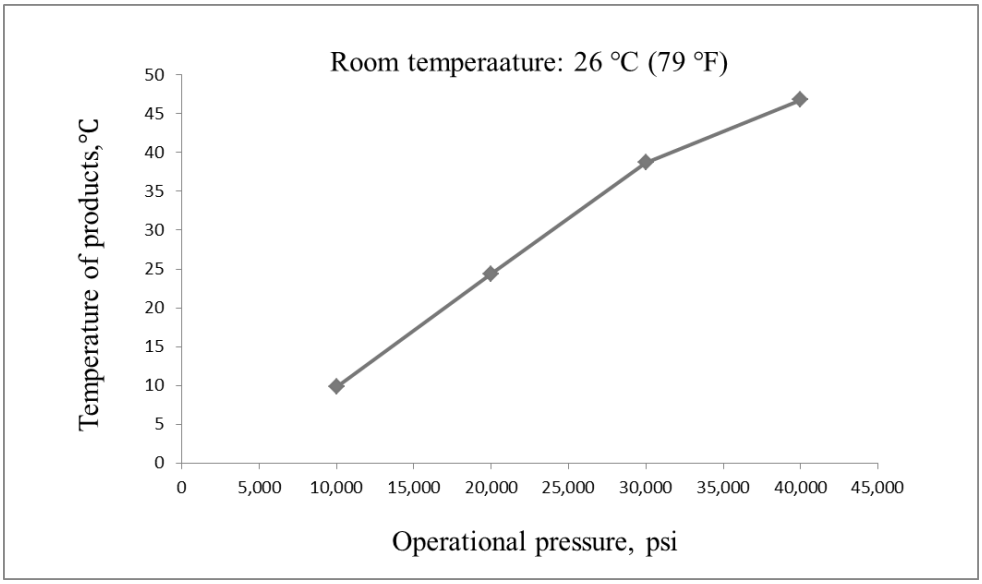

Figure 4.44. Temperature of Comminuted Products as a Function of the Operational Pressure

www.manaraa.com

Based on the median particle sizes of the feeds and their corresponding products, the particles size reduction ratios are calculated and are summarized in Tables 4.4 through 4.6. Data listed in these tables indicate that the size reduction ratios are affected by the operational pressure, feed size, and properties of coal samples. Regardless of coal properties, the higher operational pressure led to higher size reduction ratios. This statement is connected with the observation that higher size reduction ratios were obtained for coarser feed. This is in correlation with the theory of comminution: the smaller the particle size the harder it is to further reduce its size.

By comparing the data listed in Tables 4.4 through 4.6, it is found that the lowest size reduction ratio was obtained for the C2 coal. As explained in Section 4.3.1, the lower efficiency of the C2 coal than that of C1 coal was attributed to the higher ash content of C2 coal. Following this explanation, it is expected that C2 coal should be more efficiently comminuted than C3 coal (see Table 3.1). The data listed in Tables 4.5 and 4.6 is in contradiction to this expectation. This contradiction is possibly a result of the difference of the composition and occurrence of impurities presented in these two coals.

According to previous analysis, clay is the main mineral of C3 coal. Although the type and occurrence mode of clay in coal varies with its origins, analysis of Section 4.4 indicated that clay presented in C3 coal had lower hardiness and can dissolve into water spontaneously. Additionally, the flaky shape of coal particles existed in the products of C3FM indicates that the clay occurs in C3 coal as layers. Therefore, it can be easily comminuted by the high-pressure waterjet mill. For C2 coal, quartz and pyrite are the main minerals (see Figures 4.45). They are much harder than clay. In addition, the physical occurrence of pyrite in C2 coal appears in the modes of disseminated as individual grains (see 4.45 (b)). These disseminated grains of pyrite are thought to have crystallized from inorganic matter inherited from the original plant material. More directly, the pyrite is the syngeneic mineral of C2 coal and there are consequently no clear boundaries between these pyrite grains and carbon. Thus, there are some composited particles (mixture of pyrite minerals and coal) that have higher hardness values presented in C2 coal. For these reasons, C3 coal can be earlier comminuted than C2 coal by the waterjet mill even though C3 coal has much higher ash content.

www.manaraa.com

Table 4.4. C1 Coal: Particle Size Reduction Ratios of Different Comminution Conditions

Samples	Size Reduction Ratios			
	10,000 psi	20000 psi	30,000 psi	40,000 psi
C1FR1	1	2	3	4
C1FR2	5	6	9	13
C1FR3	5	9	14	15
C1FR4	5	14	17	23
C1FM	1	2	6	9

Table 4.5. C2 Coal: Particle Size Reduction Ratios of Different Comminution Conditions

Samples	Size Reduction Ratios			
	10,000 psi	20000 psi	30,000 psi	40,000 psi
C2FR1	1	2	2	3
C2FR2	2	4	5	7
C2FR3	3	6	10	11
C2FR4	5	12	16	19
C2FM	3	4	6	8

Table 4.6. C3 Coal: Particle Size Reduction Ratios of Different Comminution Conditions

Samples	Size Reduction Ratios			
	10,000 psi	20000 psi	30,000 psi	40,000 psi
C3FR1	2	3	3	4
C3FR2	3	6	8	11
C3FR3	3	8	11	13
C3FR4	5	15	22	27
C3FM	3	7	11	16

www.manaraa.com

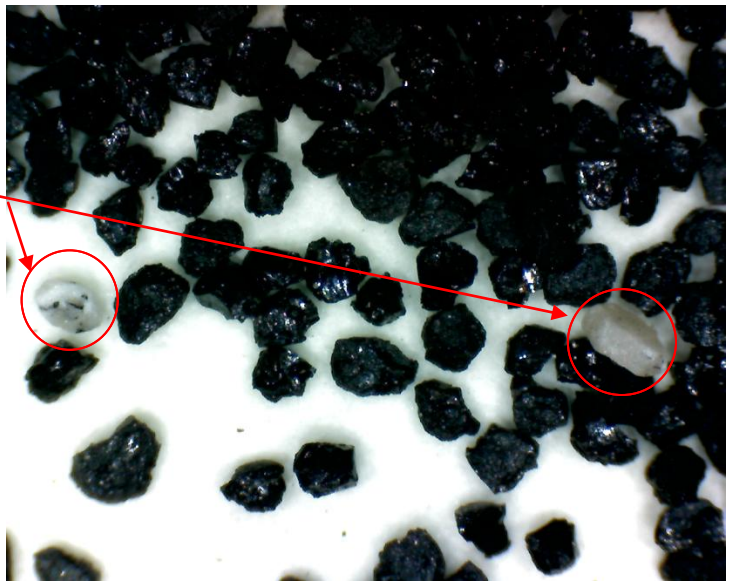

(a) Particle Size Larger than 300 Microns

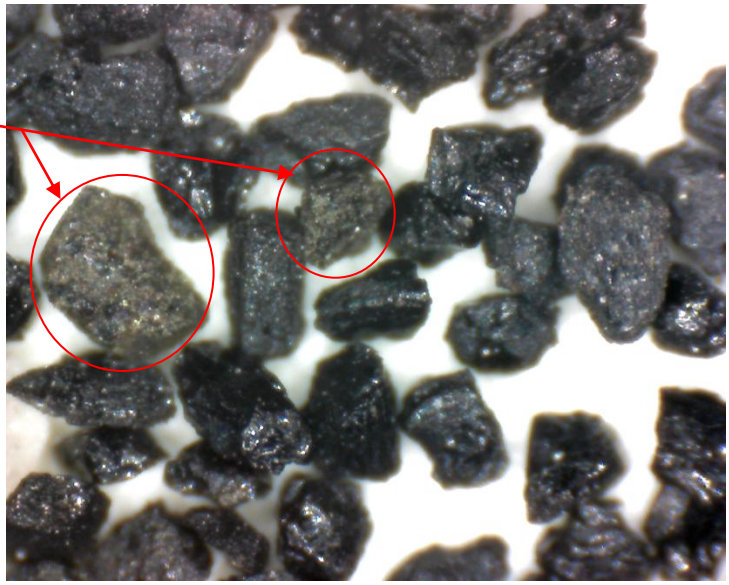

(b) Particles Sizes Fell within A Range from 212 to 300 Microns.

Figure 4.45 Photomicrograph of C2 Coal

www.manaraa.com

4.5.2. Surface Area Change. Analysis of the surface area change further proved that the effect of coal comminution using a waterjet is strongly affected by the operational pressure and feed sizes. The pressure is the key factor to determine the fineness of the products while the efficiency of the coal comminution strongly depends on the coarseness of the feed. Regardless of coal properties, higher operational pressures generate finer products. This conclusion connected to the result that the smaller the particle size, the harder it is to further reduce its size. In addition to these two conclusions, it was found that the abrasion breakage mechanism was becoming more important for size reduction as the pressure increased.

4.5.3 Particle Size Distribution. The effects of operational pressure on the particle size distribution (PSD) of three different coal samples indicated that, as the pressure increased, the size distribution of products became narrower and further reduction of particle sizes occurred as pressure increased. Despite the fact that C1, C2, and C3 coal had different properties, higher populations of fine particles less than 10 microns with tight size distribution developed when the pressure was greater than 30,000 psi. This technique has potential applications since the development of coal water fuel for commercial utilization of superfine coal slurries in high-speed diesel engines is currently limited by insufficient grinding process where are unable to produce ultrafine coals powder with a diameter less than 10 microns (Cui et al., 2008).

4.5.4. Morphological Properties of Feeds and Comminution Products. The results of morphological analysis indicate that the morphological properties of the products were strongly affected by the pressure. Regardless of coal properties, the shapes of the particles changed from irregular shapes with sharp edges toward to blocky and/or spherical shapes as a result of the pressure increase. This change tendency indicates that the abrasion mechanism became more pronounced for size reduction as the applied pressure increased. This is in accordance with analysis of the surface area change (Section 4.5.2).

www.manaraa.com

4.6. WATERJET-BASED COMMINUTION OF C3 COAL IN THE FEED FORM OF COAL-WATER SLURRY

The objective of this study was to show the effects of feed mode (dry/wet) on the effectiveness of coal comminution using a waterjet mill. To achieve this objective, the feeds were fed into the mill in the form of coal-water slurry.

Despite the fact that C1, C2, and C3 coals have different properties, the experimental results in Sections 4.2, 4.3, and 4.4 indicate that the responses of these three coals to the action of the waterjet were similar. For this reason, only C3 coal was used for the comminution study. In order to compare with the results of Section 4.4, where crushed C3 coal powders were directly fed into the mill, the standoff distance used in this study remained constant at 19 millimeters. The operational pressures, varied from 10,000 to 40,000 psi with a10,000 increment, was the first variable. Feed sizes with -106 (C3FR1), - 212 + 106 (C3FR2), - 355 + 212(C3FR3), - 850 + 355 (C3FR4) was the other variable.

4.6.1. Particle Size Analysis. As previously mentioned, some valuable quantities for routine control of the grinding circuit can be determined from the cumulative size curves. It is the most widely used method to record the result of the particle size analysis. For this reason, the cumulative volume undersize curves (CVUSCs) are firstly used to characterize the feeds and their resulting products in this study.

Figure 4.46 illustrates the CVUSCs of feeds used in this study. The median particle sizes (D_{50}) of the C3FR1, C3FR2, C3FR3, and C3FR4 were determined to be 51.45, 161.80, 296.70, and 555.10 microns, respectively. An abnormally high content of fine particles can be observed even for the coarsest feed C3FR4. This is consistent with the behaviors of mono-sized subsamples used in Section 4.4 (Figure 4.28). Consequently, it can be said that this abnormal phenomena is the result of clay dispersion. A detailed explanation is given in Section 4.4.1. The contrast of the CVUSCs from mono-sized subsamples presented in Figures 4.28 and 4.46 leads to the conclusion that mono-sized subsamples used in this study are the same as those used in Section 4.4.

www.manaraa.com

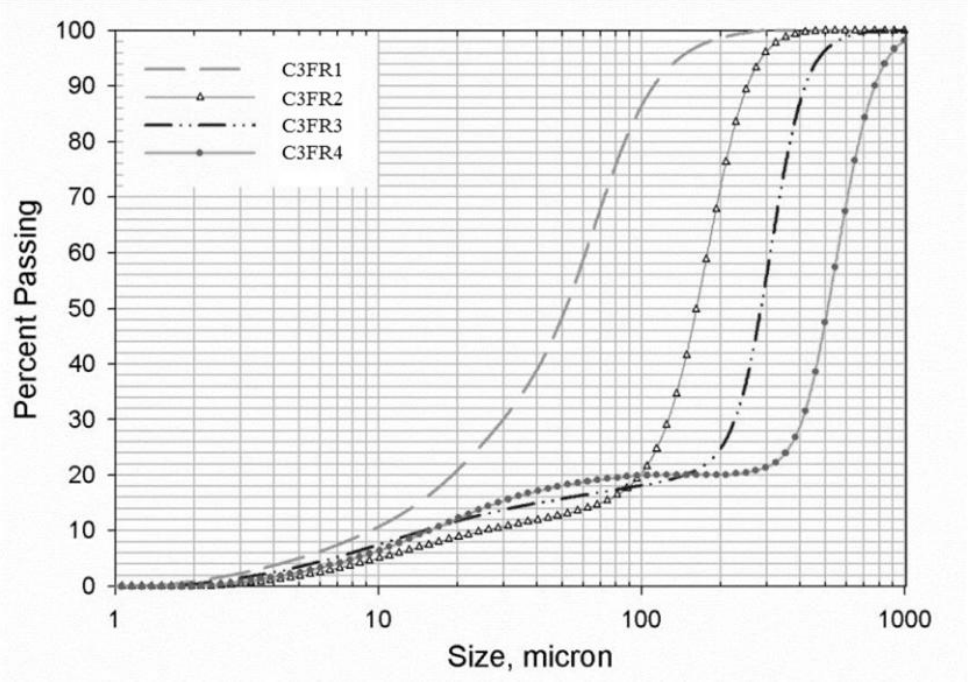

Figure 4.46. Wet Feed: CVUSCs of Mono-Sized Subsamples of C3FM (C3FR1through C3FR4)

Figures 4.47 to 4.50 give the CVUSCs of the products ground under different comminution conditions. The CVUSC of the corresponding feed is also included in these figures to illustrate the particle size change as a function of operational pressure.

The C3FR1 was the finest feed. The median particle sizes (D_{50}) of the products were 34.28, 29.06, 22.88, and 20.17 microns as the operational pressure increased from 10,000 to 40,000 psi respectively (see Figure 4.47). This data indicates that finer products resulted from higher pressures. This follows the general trend obtained from previous studies. For this feed, the highest size reduction ratio of 3 was obtained at 40,000 psi.

As seen in Figure 4.48, the feed C3FR2 was coarser than C3FR1. The size reduction ratio of the C3FR2 was slightly higher than that of the C3FR1 under equal pressure. The maximum size reduction ratio obtained at 40,000 psi was approximately 5 for this feed compared with 3 for the feed C3FR1. As the applied pressure increased from 10,000 to 40,000 psi, the median particle sizes (D_{50}) of the products from C3FR2 varied from 113.5 to 33.35 microns.

www.manaraa.com

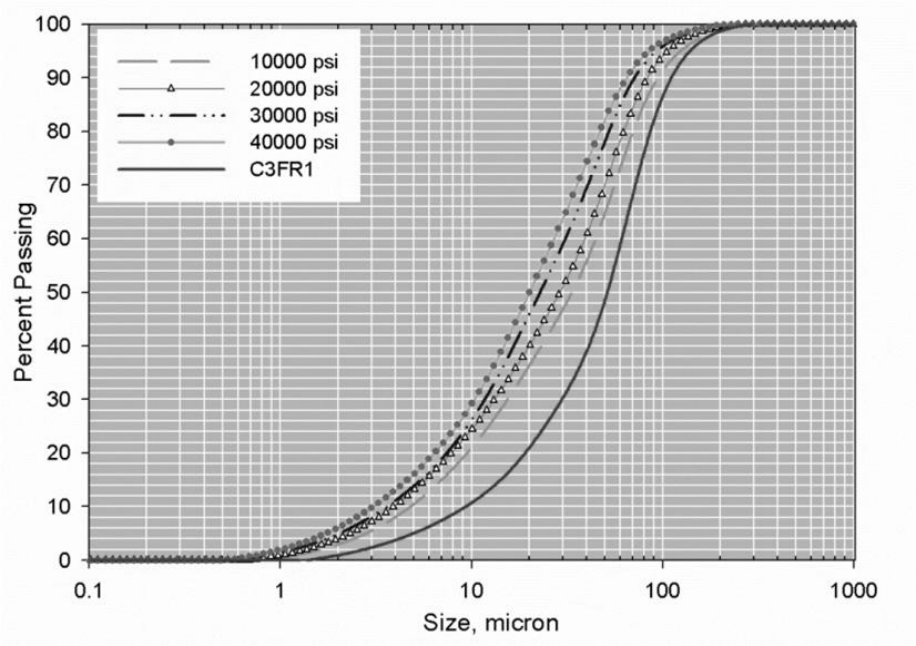

Figure 4.47. Wet Feed: CVUSCs of Products for C3FR1 Comminuted at Different Operational Pressures

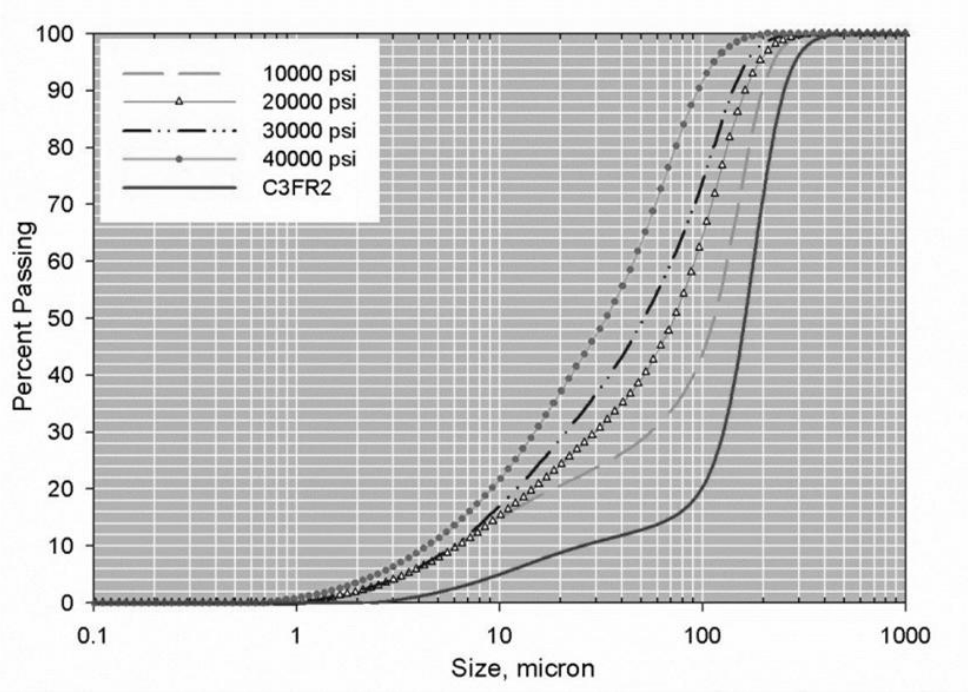

Figure 4.48. Wet Feed: CVUSCs of Products for C3FR2 Comminuted at Different Operational Pressures

www.manaraa.com

The response of the C3FR3 to the action of the waterjet at different pressures is presented in Figure 4.49. The feed C3FR3 was even coarser than C3FR2 (see Figure 4.46). The median particle sizes (D_{50}) of the ground products were determined to be 211.30, 125.90, 70.14, and 42.30 microns as the pressure increased (see Figure 4.44). The maximum size reduction of 7 was obtained at 40,000 psi.

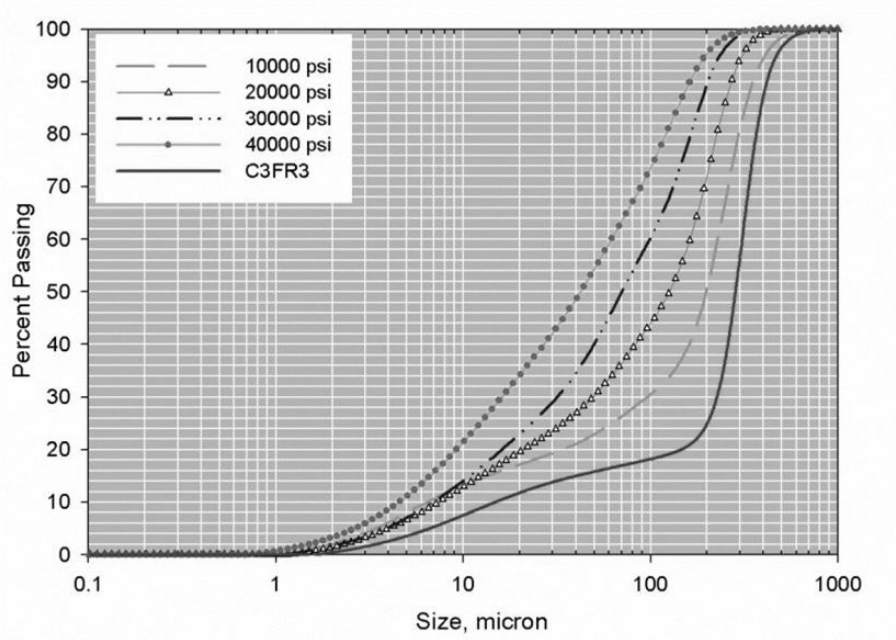

Figure 4.49. Wet Feed: CVUSCs of Products for C3FR3 Comminuted at Different Operational Pressures

C3FR4 was the coarsest feed material used in this study. The grinding results of this feed are illustrated in Figure 4.50. The highest size reduction ratios were obtained for this feed when compared to other feeds. The size reduction ratio was approximately 15 at 40,000 psi for this feed. The median particle sizes (D_{50}) of the ground products decreased from 389.90 to 37.00 microns as pressure increases. It is noteworthy that the feed (C3FR4) contained a higher amount of particles finer than 176 microns than the product of 10,000 psi. This abnormal phenomenon is the result of clay disperses into water.

www.manaraa.com

Because clay can disperse into water spontaneously, some clay was removed after undergoing the waterjet grinding. As a result, a smaller amount of ultrafine particles were detected in the product of 10,000 psi.

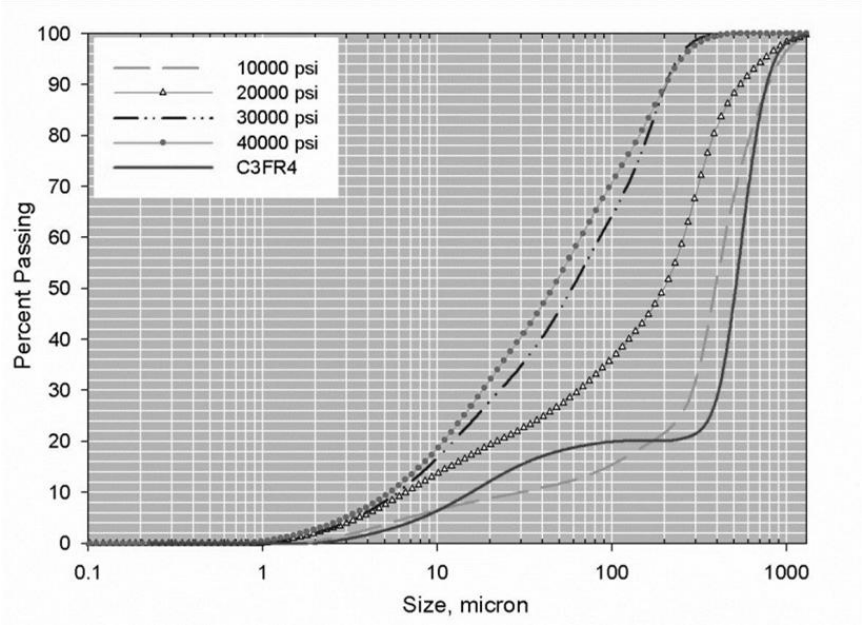

Figure 4.50. Wet Feed: CVUSCs of Products for C3FR4 Comminuted at Different Operational Pressures

4.6.2. Summary of Section 4.6. As it has already been explained in Section 4.5.1, the median particle size and size reduction ratio are selected as criteria to evaluate the effect of coal comminution using a waterjet. The results are summarized in Tables 4.8 and 4.9.

As seen in Tables 4.8 and 4.9, the increase in the operational pressure resulted in an increase in the fineness of the products. This conclusion is connected with the observation that progressively increasing the coarseness of feeds leads to increased size reduction ratios. These findings are in accordance with general trends drawn from previous experiments, Sections 4.2 through 4.4.

www.manaraa.com

By comparing Table 4.9 with Table 4.6, it was found that feeding samples into the mill as a coal suspension resulted in lower size reduction ratios when compared to dry feeding (crushed coal powder). This can be attributed primarily to the reduced probability of particle-particle interaction. When compared to dry feeding, the solid concentration in the mixing tube and cavitation cell was lower when samples are fed into the mill as a coal suspension. As a result, the effect of the abrasion between particles was reduced due to the lower probability of collision between particles. Additionally, the cushioning effect produced by a bed of water on the particle surface is believed to be another explanation for the lower size reduction ratios of the wet feed.

Table 4.7. C3 Coal- Wet Feeding: The Median Particle Size of the Products Comminuted at Different Comminution Conditions

Samples	Median Particles Sizes (D_{50}) of Products, µm			
	10,000 psi	20000 psi	30,000 psi	40,000 psi
C3FR1	34.28	29.06	22.88	20.17
C3FR2	113.50	66.58	51.38	33.35
C3FR3	211.30	125.90	70.14	42.30
C3FR4	389.90	197.70	45.74	37.00

Table 4.8. C3 Coal- Wet Feeding: Size Reduction Ratios Obtained at Different Comminution Conditions

Samples	Size Reduction Ratios			
	10,000 psi	20000 psi	30,000 psi	40,000 psi
C3FR1	1	2	2	3
C3FR2	1	2	3	5
C3FR3	1	2	4	7
C3FR4	1	3	12	15

www.manaraa.com

4.7. THE EFFECT OF STANDOFF DISTANCE ON WATERJET-BASED COAL COMMINUTION

The standoff distance is defined as the distance from the mixing nozzle to the anvil. To analyze the effect of standoff distance on the behavior of coal particles exposed to the action of the waterjet, comminution experiments were carried out by varying the placement of the anvil in the cavitation cell. The original feed material of C3 coal (C3FM) and its mono-sized subsamples were used. For the purpose of these experiments, the operational pressure was kept constant at 10,000 psi for four mono-sized subsamples. However, the pressure varied from 10,000 to 40,000 psi with a 10,000 increment for the original feed material, C3FM.

4.7.1. C3 Coal Comminution with 100 Millimeter Standoff Distance. As the subtitle suggests, the anvil is placed 100 millimeters away from the mixing nozzle along the on-axis of the cavitation cell in this study. The feed sizes with -106 (C3FR1), - 212 + 106 (C3FR2), - 355 + 212 (C3FR3), - 850 + 355 (C3FR4), and -850 microns (C3FM) were used as the first variable. The second variable was the operational pressure. The operational pressure varied from 10,000 to 40,000 psi with a 10,000 increment.

4.7.1.1 Particle size analysis. To quantitatively characterize the behavior of the coal particles exposed to the action of a waterjet, the cumulative volume undersize curves (CVUSCs) were used firstly to analyze the feeds and resulting products. The results are given in Figures 4.51 to 4.53.

Figure 4.51 displays the CVUSCs of the C3FM and its mono-sized subsamples. It can be observed that the feeds from fine to coarse are in the order of C3FR1, C3FR2, C3FR3, and C3FR4. The original feed material C3FM contains very fine and coarse particles together.

Figure 4.52 displays the behavior of the mono-sized subsamples (C3FR1 through C3FR4) subjected to the action of the waterjet at 10,000 psi. As seen in Figure 4.52, a particle size decrease was observed as the feeds became finer. On the contrary, increasing fineness of feeds resulted in reduced size reduction ratio. A size reduction of 4 was obtained for the coarsest feed C3FR4. This value decreased to 2 for the finest feed C3FR1. The median particle sizes (D_{50}) of the ground products were determined to be 25.91, 61.10, 118.40, and 145.00 microns as the coarseness of feeds increased, respectively.

www.manaraa.com

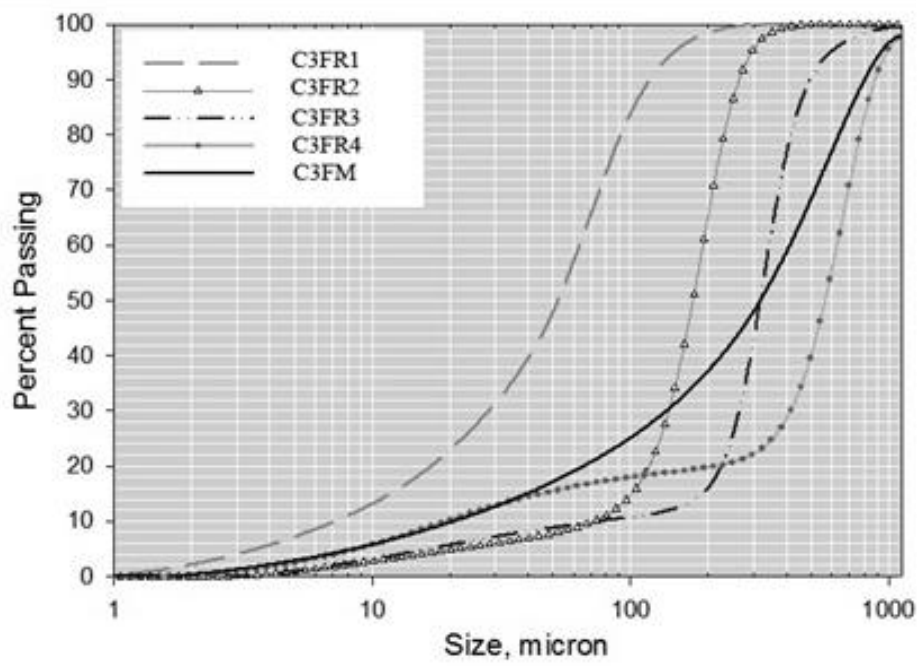

Figure 4.51. CVUSCs of C3FM and Mono-Sized Subsamples (C3FR1through C3FR4)

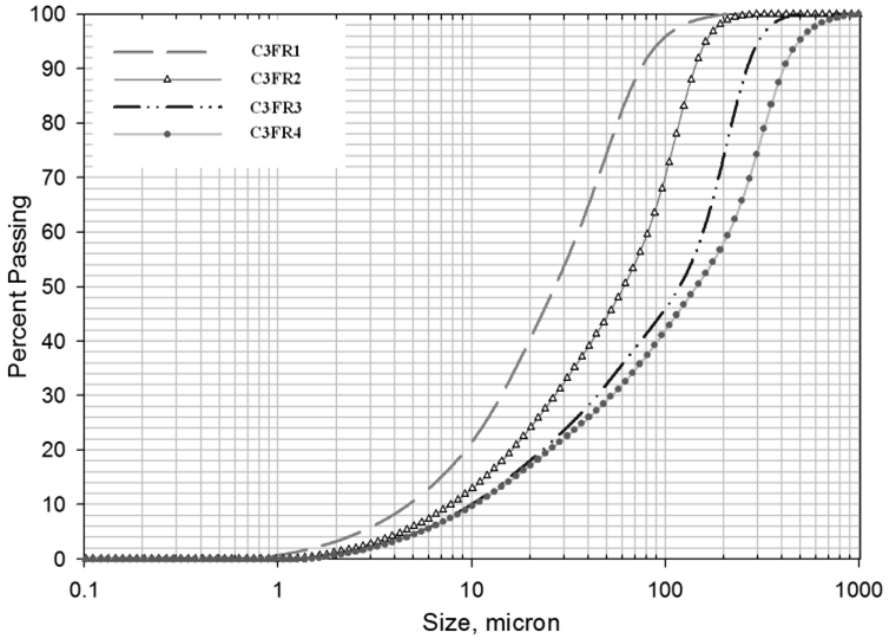

Figure 4.52. 100 mm Standoff Distance: CVUSCs of Products Obtained from Mono-Sized Subsamples Comminuted at 10000 psi

www.manaraa.com

Results of previous experiments proved that the effect of pressure on the response of coal comminution using a waterjet is independent on the size classification. For this reason, the original feed material, C3FM, was used to investigate the effect of pressure on the particle size change. The results are given in Figure 4.53. Curves presented in Figure 4.53 indicate that an increase in the pressure resulted in a decrease in the sizes of the products. In the situation where applied pressure increased from 10,000 to 40,000 psi, the median particle sizes (D_{50}) of the products decreased from 101.70 to 23.30 microns.

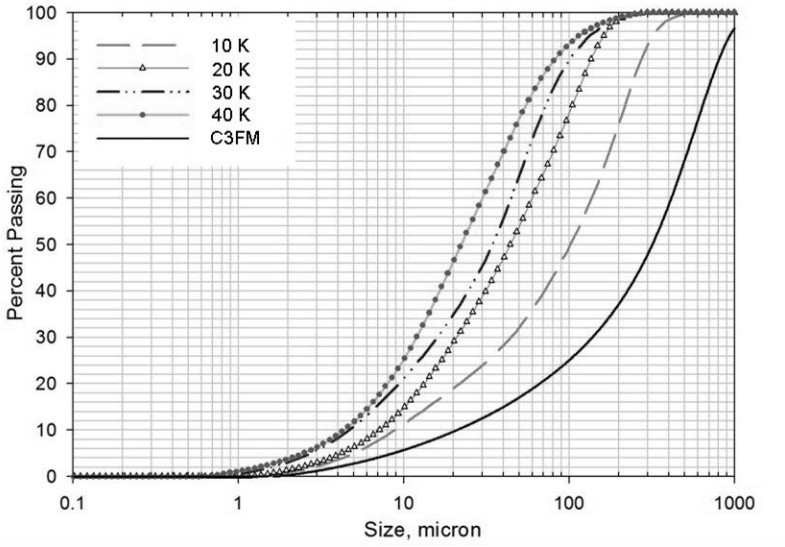

Figure 4.53. 100 mm Standoff Distance: CVUSCs of Products Obtained from C3FM Comminuted at Different Operational Pressures

4.7.1.2 Particle size distribution. The particle size distribution (PSD) of the original feed material, C3FM, as a function of pressure is illustrated in Figure 4.54.

As seen in Figure 4.54, the PSD of the original feed material C3FM was very wide. After undergoing a 10,000 psi pressure fragmentation, the PSD clearly shrank. However, the majority of particles were coarser than 10 microns. Further increasing pressure resulted in decreasing particle sizes and shrinking size distribution. However,

www.manaraa.com

the amount of particles concentrated near 5 microns was not significant until the pressure increased to 30,000 psi. When the operational pressure increased to 40,000 psi, a distinct peak near 5 microns combined with a narrower size distribution was developed. However, there is still another peak with coarser size in the ground product. This finding indicates that 40,000 psi can generate a relatively high population of particles smaller than 10 microns. However, the distribution of the particle size is not narrow enough under these circumstances.

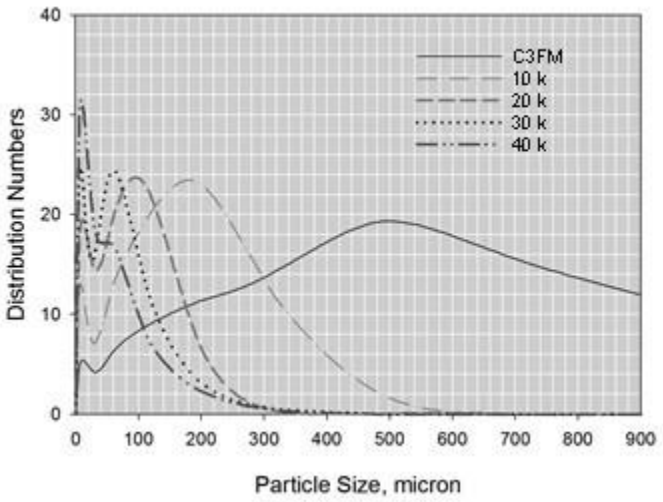

Figure 4.54. 100 mm Standoff Distance: PSD of C3FM as a Function of the Operational Pressure

4.7.2. C3 Coal Comminution with 98 Millimeter Standoff Distance. To display the effects of the standoff distance, the only difference in the comminution conditions between Subsections 4.7.2 and 4.7.1 was the location of the anvil. In this subsection, the anvil is located 98 millimeters away from the mixing nozzle along the on-axis of the cavitation cell.

4.7.2.1 Particle size analysis. Since feeds used in this subsection are exactly the same as those of Subsection 4.7.1.1, only the resulting products are characterized using

www.manaraa.com

the cumulative volume undersize curves (CVUSCs). The results are given in Figures 4.55 and 4.56.

Figure 4.55 illustrates the particle size changes of the mono-sized subsamples comminuted at 10,000 psi. The median particle sizes (D_{50}) of the comminution products ranged from 25.39 to 91.27 microns as the coarseness of the feed material increased. The size reduction ratio was still 2 for the finest feed sample, increasing to 6 for the coarsest feed under these parameters. This data indicates that the tendency of particle size change as a function of the pressure is in accordance with findings of Subsection 4.7.1.1. However, the fineness of the product and the size reduction ratio were higher in this situation than the situation where 100 mm standoff distance was used under equal pressure.

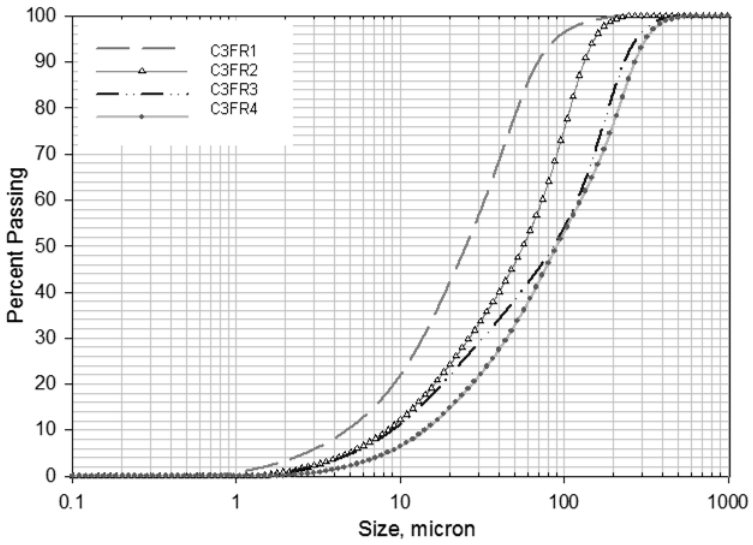

Figure 4.55. 98 mm Standoff Distance: CVUSCs of Products Obtained from Mono-Sized Subsamples Comminuted at 10000 psi

Figure 4.56 gives the results of the original feed material, C3FM, comminuted under different pressures. Overall, a particle size decrease was observed by increasing the

www.manaraa.com

operational pressure. The median particle sizes of the ground products were determined to be 68.34, 31.30, 22.86, and 19.30 microns as the operational pressure increased from 10,000 psi to 40,000 psi respectively. Accordingly, the size reduction ratio increased from 5 to 16. In situations where the standoff distance was 100 millimeters, the size reduction ratio varied from 3 to 14. This data indicates that shorter standoff distance benefits the efficiency of coal comminution using a waterjet.

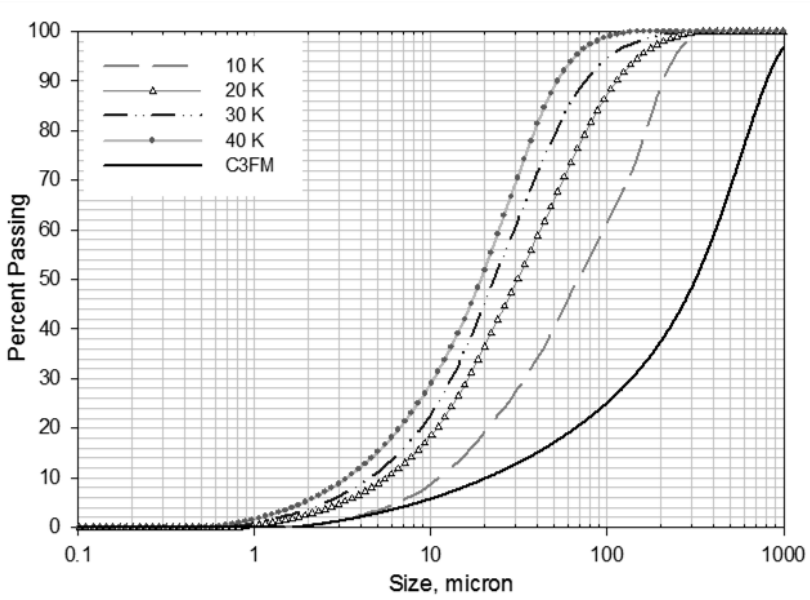

Figure 4.56. 98 mm Standoff Distance: CVUSCs of Products Obtained from C3FM Comminuted at Different Operational Pressures

4.7.2.2 Particle size distribution. The effect of pressure on the relative frequency of particle sizes presented in comminution products is illustrated in Figure 4.57. Similar observation were made in Subsection 4.7.1.2, the sizes of the original feed material, C3FM, was widely distributed with larger sizes. After being subjected to the 10,000 psi grinding, the sizes of the original feed material C3FM was significantly reduced. Simultaneously, the homogeneity of the particle sizes was clearly improved.

www.manaraa.com

However, the majority of particles were still coarser than 10 microns. When the pressure increased to 20,000 psi, a high population of 5 micron particles with a narrower size distribution was observed. It is worth noting that the amount of particles concentered around 5 microns was already higher than the amount of particles concentrated around the larger size peak. As the pressure increased to 30,000 psi, an even higher population of 5 micron particles was generated and remaining particles are all concentrated around 5 microns. When the pressure is further increased to 40,000 psi, the population of 5 micron particles was further increased. Additionally, the PSD curve became narrower, centered around 5 microns. Comparison of the PSD curves presented in Figures 4.54 and 4.57 leads to the conclusion that, in terms of producing ultrafine particles with tight size distribution, decreasing the standoff distance from 100 to 98 mm improved the efficiency of the waterjet mill.

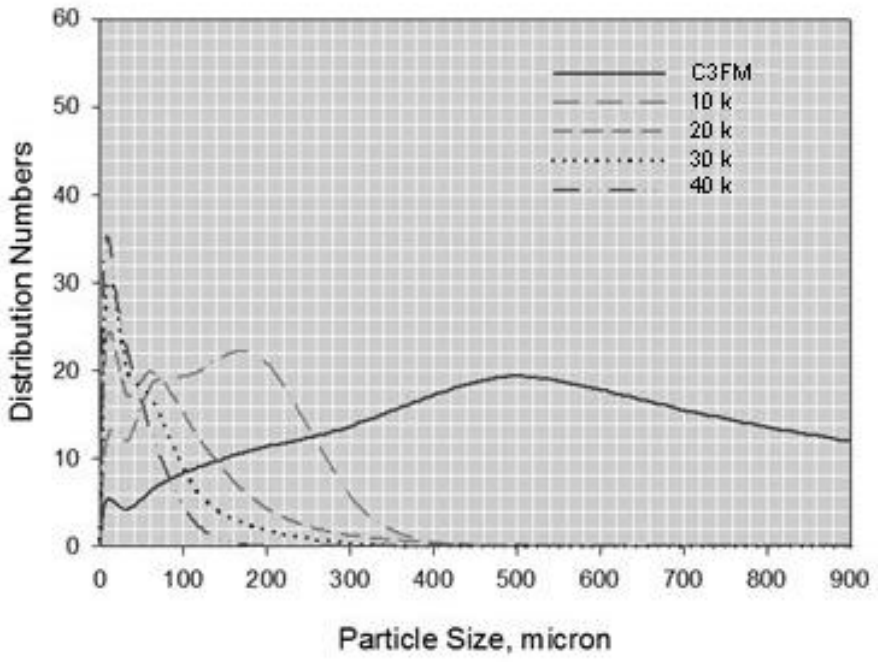

Figure 4.57. 98 mm Standoff Distance: PSD of C3FM as a Function of the Operational Pressure

www.manaraa.com

4.7.3. C3 Coal Comminution with 3 Millimeter Standoff Distance. The methodology used in Subsections 4.7.1 and 4.7.2 is adopted in this subsection with the exception that the standoff distance was changed to 3 millimeters.

4.7.3.1 Particle size analysis. The cumulative volume undersize curves (CVUSCs) of the products are given in Figures 4.58 and 4.59.

Figure 4.58 illustrates mono-sized subsamples of C3FM fractured under 10,000 psi operational pressure. The median particle sizes (D_{50}) of the ground products were determined to be 21.39, 39.17, 42.43, and 51.54 microns as the coarseness of feeds increased. The size reduction ratio of 11 was obtained for the coarsest feed C3FR4. This value is almost three times larger than the size reduction ratio with a 100 millimeter standoff distance. This increase in size reduction ratio by a factor of 3 indicates a significant improvement in the efficiency of the waterjet mill.

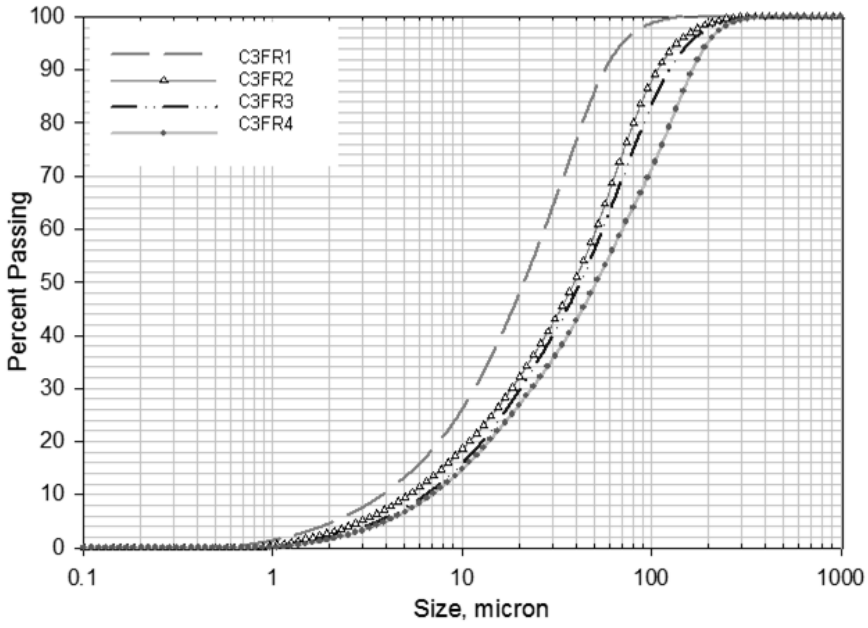

Figure 4.58. 3 mm Standoff Distance: CVUSCs of Products Obtained from Mono-Sized Subsamples Comminuted at 10000 psi

www.manaraa.com

The results of the original feed material, C3FM, comminuted at different operational pressures are summarized in Figure 4.59. Progressively increasing the pressure from 10,000 to 40,000 psi resulted in a decrease of the median particle size from 40.55 to 16.18 microns. This follows the general trend revealed in previous experiments.

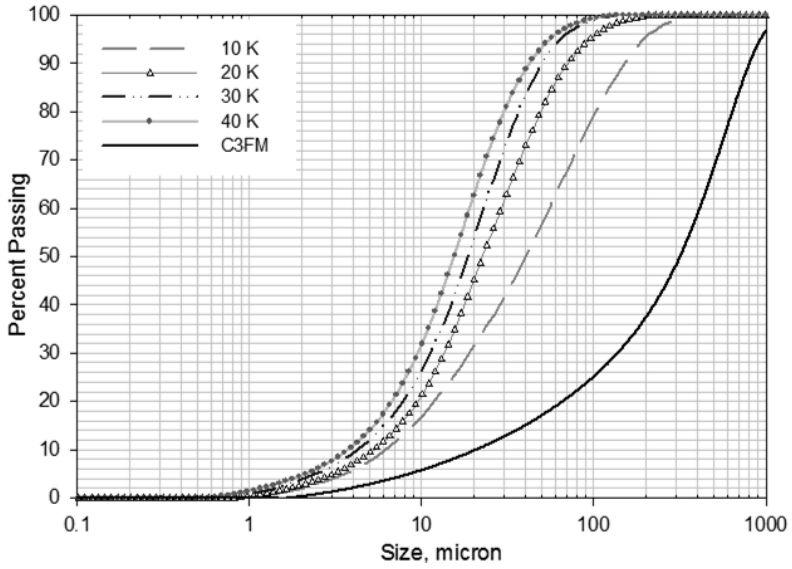

Figure 4.59. 3 mm Standoff Distance: CVUSCs of Products Obtained from C3FM Ground at Different Operational Pressures

4.7.3.2 Particle size distribution. The effects of operational pressure on the size distribution of the C3FM exposed to the high-pressure waterjet mill are given in Figure 4.60.

As seen in Figure 4.60, the size distribution of the original feed material C3FM was again very wide before it was ground by the waterjet mill. In similar to observations in Subsections 4.7.1.2 and 4.7.2.2, increasing pressure resulted in reduced particles sizes with a narrowed size distribution. It is worth noting that in this situation, the amount of particles accumulated around 5 microns was already significant when a 10,000 psi jet was applied. When the pressure increased to 20,000 psi, only one peak around 5 microns can

www.manaraa.com

be observed. These findings indicate that a 3 mm standoff distance is more efficient in terms of product quality when compared to standoff distances of 100 and 98 millimeters.

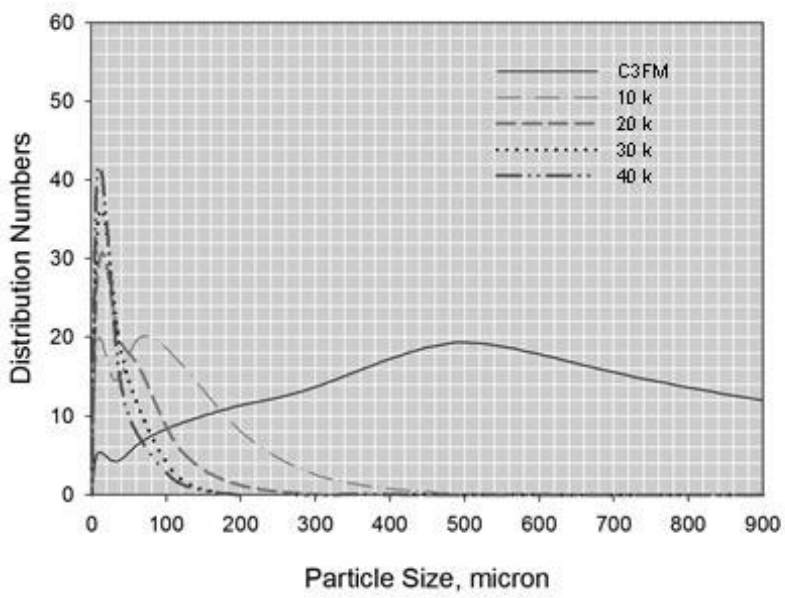

Figure 4.60. 3 mm Standoff Distance: PSD of C3FM as a Function of the Operational Pressure

4.7.4. Section Summary. The results presented in this section are consistent with previous finding regarding the pressure and feed size. Since the objective of this study is to investigate the effect of the standoff distance, the focus of discussion here is on the comparison of results obtained at different standoff distances. Since the size reduction ratio is a key factor to evaluate the comminution efficiency, it is selected as the first criterion for evaluating the influence of standoff distance.

Based on the median particle sizes of the feeds and their resulting products, the particle size reduction ratios obtained at different comminution conditions are calculated and summarized in Tables 4.10 and 4.11. Data presented in Tables 4.10 and 4.11 indicates that the decrease of standoff distance from 100 to 3 mm resulted in a significant

www.manaraa.com

increase in the size reduction. This effect can be explained by the kinetic energy that coal-water jet impacts against the anvil. In the comminution process of the high-pressure waterjet mill, the primary collision of the waterjet and coal particles takes place inside the abrasive cutting head (see Figure 3.3 for reference). During this collision, the coal particles are accelerated by absorbing partial kinetic energy of the waterjet and mixed with it together. This coal water slurry jet then travels into the cavitation cell and impacts against the anvil. A further size reduction therefore results. The efficiency of this impact comminution is determined by the kinetic energy of the coal-water slurry jet when it impacts the anvil. As the standoff distance increases, the impact energy decreases. Therefore, the size reduction ratio decreases as the standoff distance increases.

Based on particle size distribution analysis, it was found that smaller standoff distance benefits the generation of fine particles below 10 microns with a tight size distribution. This also can be attributed to the influence of the standoff distance on the impact energy. The major kinematic parameter in the impact comminution is the impact velocity. An increase in the impact velocity fractures smaller particles (Yashima et al., 1986). Higher impact energy resulted in higher impact velocity. In situation where applied pressure is equal, sizes of particles subject to milling at a shorter standoff distance smaller than those at larger standoff distance. In addition to this effect combined with the finding that shorter standoff distances resulted in higher size reduction ratios leads to the conclusion that a smaller standoff distance is more capable of generating ultrafine coal particles with tight size distributions.

Table 4.9. Mono-Sized Samples: Size Reduction Ratios as a Function of Standoff Distance

Samples	Standoff Distance, mm		
	100	98	3
C3FR1	2	2	2
C3FR2	3	3	4
C3FR3	3	3	7
C3FR4	4	6	11

www.manaraa.com

Table 4.10. Original Feed Material (C3FM): Size Reduction Ratios as a Function of Standoff Distance

Pressure, psi	Standoff Distance, mm		
	100	98	3
10000	3	5	8
20000	7	10	14
30000	9	14	17
40000	14	16	20

www.manaraa.com

5. APPLICATION OF THE FRACTAL THEORY FOR EVALUATING EFFECTS OF WATERJET-BASED COAL COMMINUTION

5.1. GENERAL INTRODUCTION

As seen in Section 4, quantitatively assessing the sizes of the comminution products is a key parameter in evaluating the comminution process. There are several methods available for representation and evaluation of particle size analysis data. Usually, the particle size analysis results are graphically presented, as those graphs used in Section 4. Those graphs are very useful and widely accepted method for presenting the particle size distribution of granular material. However, quantification of particle size of comminution products by only considering a few points such as P_{80} or P_{50}, or a limited portion of the particle size distribution curve has inherent limitations. To address this problem, fractal theory is introduced to characterize the sizes of the comminution products.

Fractal theory provides a mean that quantify the entire particle sizes of the comminution products through a specific and exact value. At the moment, most applications of the fractal concept for PSD analysis are the mass-based fragmentation model developed by Turcotte (1986). However, the use of laser particle size analyzers is a very convenient method for particle size analysis of fine and ultrafine particle coal particles generated with the use of high pressure waterjet grinding. It provides volume-based size distribution of particles. To directly use the data from the laser particle size analyzers, a volume-based fractal model is proposed to characterize PSD of coal ground in a waterjet mill in this section. The model was validated by comminution experiments for the range of operational pressures up to 40,000 psi. Also, the effect of the operational pressure on the size distribution was investigated by the proposed fractal model.

5.2. FRACTAL MODEL FOR PARTICLE SIZE DISTRIBUTION

According to self-similar fractal theory, the size distribution of elements in a fractal system is given by the following equation (Chen, 2005):

$$n_{(R \geq r)} = cr^{-D} \tag{5.1}$$

www.manaraa.com

where, r is a defined equivalent radius of particles

$n_{(R\geq r)}$ is the number of particles greater than r in radius

c is a constant, D is the fractal dimension.

When r is equal to the minimum radius r_0, the total number of fragments n_0 with minimum radius is,

$$n_0 = c{r_0}^{-D} \tag{5.2}$$

Combining Eq. (1) and Eq. (2) gives the following relationship,

$$\frac{n_{(R\geq r)}}{n_0} = \frac{r}{r_0}^{-D} \tag{5.3a}$$

or

$$n_{(R\geq r)} = n_0(r/r_0)^{-D} \tag{5.3b}$$

After derivation, Eq. (3) becomes,

$$dn_{(R\geq r)} = -n_0 r_0^D D r^{-(D+1)} dr \tag{5.4}$$

The cumulative volume of particles whose radius greater than r is:

$$dV_{(R\geq r)} = kr^3 dn_{(R\geq r)} \tag{5.5}$$

Substituting Eq. (4) into Eq. (5) yields,

$$dV_{(R\geq r)} = -kn_0 r_0^D D r^{2-D} dr \tag{5.6}$$

where, k is the coefficient of volume. Taking integration of Eq. (6), Eq. (7) can be formulated,

$$\int_{V_0}^{V_{(R\geq r)}} dV_{(R\geq r)} = \int_{r_0}^{r} -kn_0 r_0^D D r^{2-D} dr \tag{5.7}$$

www.manaraa.com

Mathematically, the relationship between accumulated volume of particles whose radius is greater than defined radius r and total volume of all particles yields the following equation,

$$V_0 - V_{(R\geq r)} = \frac{kn_0 r_0^D D}{3-D} r^{3-D} \tag{5.8}$$

According to the definition of integration, V_0 is the accumulated total volume of all fragments. $V_{(R\geq r)}$ is the volume of particles whose radius greater than r. Term of $\frac{\mathrm{kn_0 r_0^D D}}{\mathrm{3-D}}$ is the coefficient depending on the properties of materials, and will be referred as K_V later. Since K_V is a constant for a given coal sample, then Eq. (8) simplifies to,

$$V_0 P\% = K_V r^{3-D} \tag{5.9}$$

where, P % is the accumulative volume percentage of particles with radius smaller than r. Then Eq. (9) can be transformed into a linear relationship as,

$$LogP = \ 3 - D \ \ logr + logK_V - logV_0 + 2 \tag{5.10a}$$

Further this equation can be simplified to the following form,

$$LogP = alog\ r + logK \tag{5.10b}$$

Where, a is the slope coefficient of the linear regression lines. If the size distribution of the fragments is a fractal, log P should correlate log r linearly. Each fractal dimension (D) representing a particular PSD could be calculated from the slope of the best-fit linear regression line using Eq. (11),

$$D = 3 - a \tag{5.11}$$

www.manaraa.com

5.3. CHARACTERIZATION OF THE COMMINUTION PRODUCTS BY THE PROPOSED MODEL

To validate the proposed mode in characterization of the PSD of the products comminuted by the waterjet mill, the original feed material of C1 coal, C1FM, was used. The cavitation cell was operated at various operational pressures. These pressures varied from 10,000 to 40,000 psi with a 10,000 psi increment. The standoff distance was kept constant at19 millimeters for all tests. The particle sizes of the comminution products were determined by a laser diffraction Microtrac S3500 series particle size analyzer.

In order to use the fractal model for particle size distribution, data obtained from Microtrac S3500 size analyzer was presented on logP - logr scale, Figure 5.1. Curves in Figure 5.1 represent particle size distribution as a function of operational pressure varied in this series of experiments.

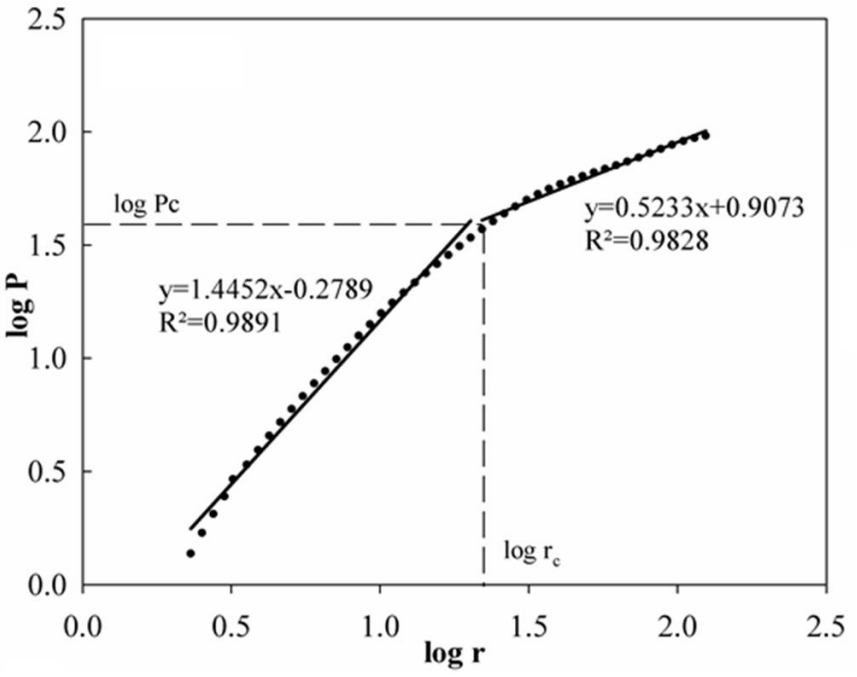

(a) Comminution Product of 10,000 psi

Figure 5.1. Regressive Curves of PSDs for Products Comminuted at Different Pressures

www.manaraa.com

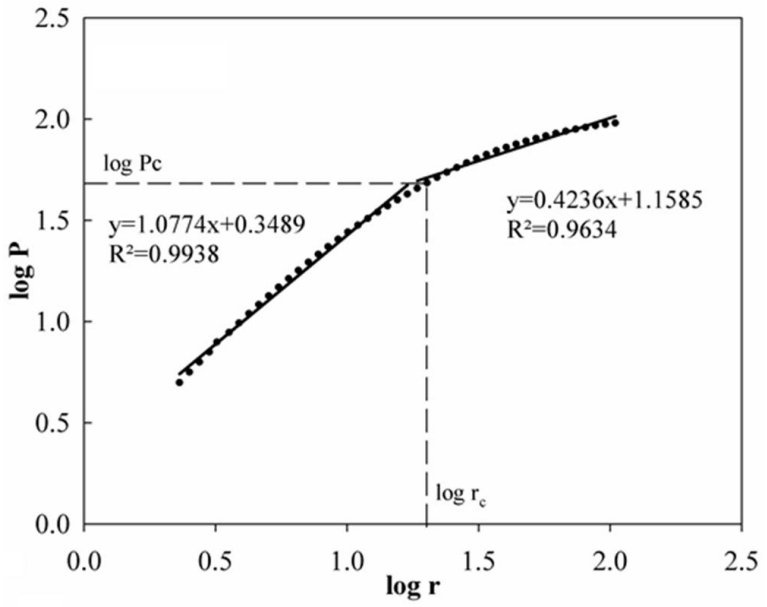

(b) Comminution Product of 20,000 psi

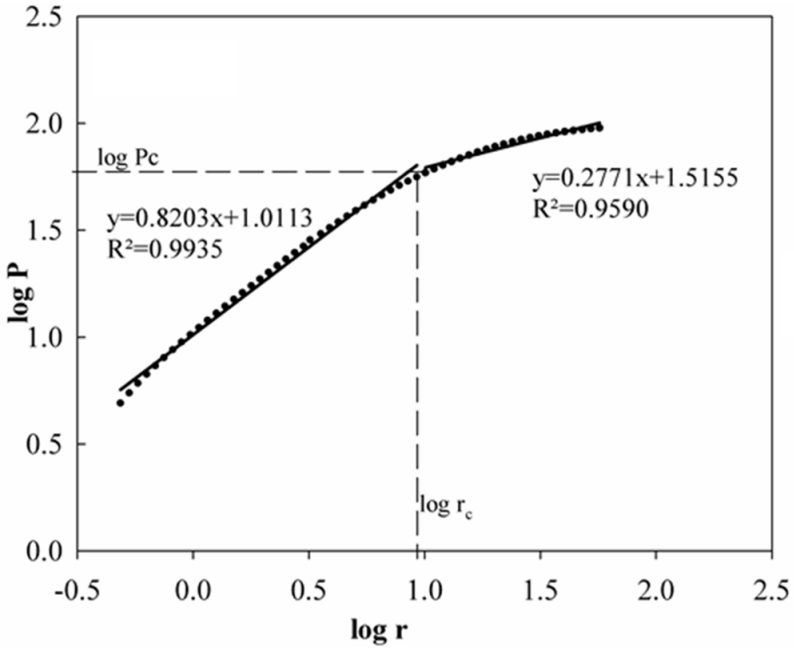

(c) Comminution Product of 30,000 psi

Figure 5.1. Regressive Curves of PSDs for Products Comminuted at Different Pressures Cont.

www.manaraa.com

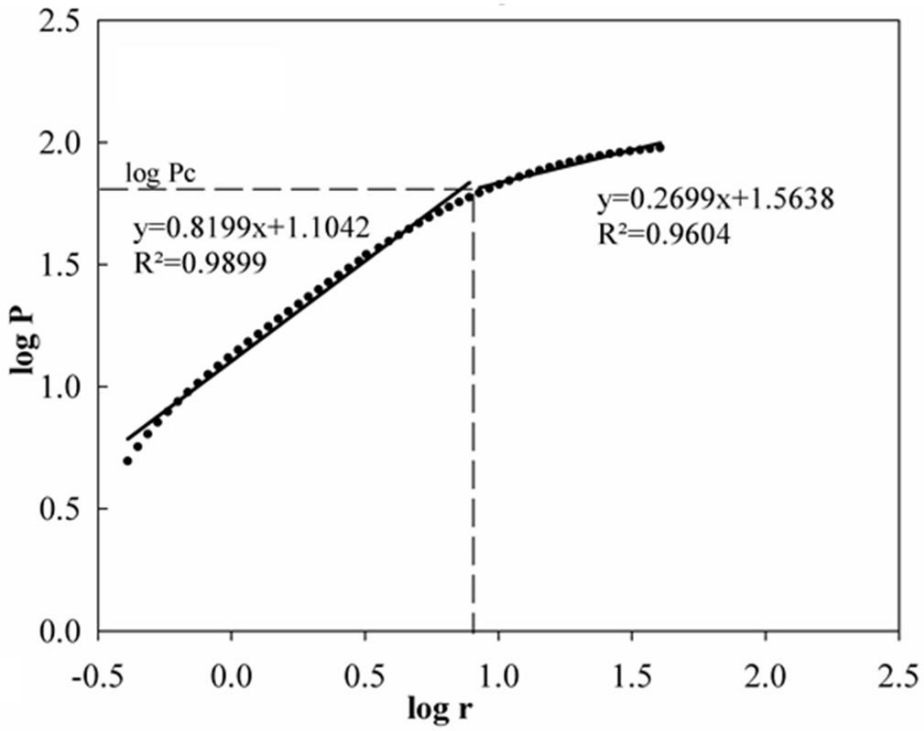

(d) Comminution Product of 40,000 psi

Figure 5.1. Regressive Curves of PSDs for Products Comminuted at Different Pressures Cont.

The particle size distribution curve, when presented on a log-log scale, consists of two linear segments (see Figure 5.1), as introduced by Tasdemir (2009). Following his interpretation, these segments represent fine and coarse particle fractal domains. This method was adopted for data analysis of coal comminution by waterjets with the exception, that the authors introduced a volume-based fractal model instead of a mass-based model used by Tasdemir.

Since the data presented on log-log scale consisted of two linear segments, each slope represented a different fractal domain. The first segment represents the fine particles. This segment was determined by solving for the highest linear regression coefficient (R2) for contiguous data points starting from the first data point. Then the remaining data was fit into a line representing the second domain. The fractal dimensions of these two domains were calculated using the slopes of the best fitting lines, as

www.manaraa.com

summarized in Table 5.1. The point that separated these two domains is defined as the cutoff point. The values of the cutoff points ($\log r_c$) with a corresponding logP were also included in Table 5.1.

Table 5.1. Fractal Dimensions Calculated From the Slopes of the Best Fitting Lines

Operational Pressure, psi	First Domain		Second Domain		Log r_c	Log P_c
	D_1	R^2	D_2	R^2		
10,000	1.6101	0.9891	2.4767	0.9828	1.3424	1.5684
20,000	1.9226	0.9938	2.5764	0.9634	1.2671	1.6569
30,000	2.1797	0.9935	2.7229	0.9590	1.0036	1.7678
40,000	2.1801	0.9604	2.7301	0.9604	0.9284	1.7921

The fractal dimensions in mineral fragmentation should fall within a range from 1.44 to 3 as suggested by Turcotte (1998) and Cui et al. (2006). The experimental results presented in Table 5.1 are in agreement with this statement. According to previous studies by Lu et al. (2003) and Cui et al. (2006), each fractal dimension indicates a particular PSD and a higher value of fractal dimension represents a higher amount of fine particles. In our experiments, it was observed that the fractal dimension increases with the increasing operational pressure (see Table 5.1). This observation indicates that higher operational pressures led to higher amount of fine particles. This is consistent with the conclusion observed in Section 4.

It is worth noting in Table 5.1 that fractal dimensions in the first domain (D_1) fell between 1.6101 and 2.1801. Fractal dimensions in the second domain (D_2) were higher, from 2.4767 to 2.7301, for the same experimental conditions. It seems that these results contravened the statement that higher fractal dimensions indicate finer products. The reason for this contravention is that the breakage mechanisms producing fragments in these two domains are different. As introduced and experimentally confirmed by

www.manaraa.com

Carpinteri and Pugno (2002), Carpinteri and Pugno (2003), and Tasdemir, (2009), the fractal dimension, representing finer particles generated by the abrasion breakage mechanism, was close to 2. The fractal dimension of coarser particles generated by the destructive mechanism should be close to 3. Data presented in Table 5.1 agrees with this statement.

Further analysis of data presented in Table 5.1 reveals that an increase in the operational pressure is associated with an increase in the volume-percentage of particles (log Pc) smaller than the cut-off point size (Log rc). This change trend indicates that, as the operation pressure increases, more particles fell into the first domain. Further, it can be said that, as an increase in the operational pressure, the PSD of the product became narrower and the surface-dominated breakage becomes the predominant size reduction mechanism. To sum up, two conclusions can be drawn from the fractal dimensions listed in Table 5.1. 1) As the operational pressure increased, the particle size distribution became narrower combined with further reduction of particle sizes. 2) The abrasion mechanism became more pronounced for particle size reduction with an increase of the operational pressure. These conclusions are in complete agreements with findings of Subsections 4.2.3 and 4.2.4 (particle size distribution analysis and SEM studies of C1 coal). Therefore, it can be speculated that the proposed fractal model Eq. (5.10) is capable to characterize the coal products comminuted by the high-pressure waterjet mill.

The relationship between the fractal dimension of the comminution products and operational pressure is depicted in Figure 5.2. According to Figure 5.2, fractal dimensions of products increase with increasing operational pressure. However, in the same range of pressures, the upward trend is more obvious for the fractal dimension in first domain (D1). This finding reveals the abrasion breakage which is a result of a surface-dominated phenomenon is the prevailing mechanism for the generation of ultrafine particles. This correlates with the results of the surface area change analysis in Section 4. Based on the experimental results, it is clear that the fractal dimension, as a single parameter, retains most information. It reflects the combined results of the cumulative volume size curves, particle size distribution curves, and calculated surface area change.

www.manaraa.com

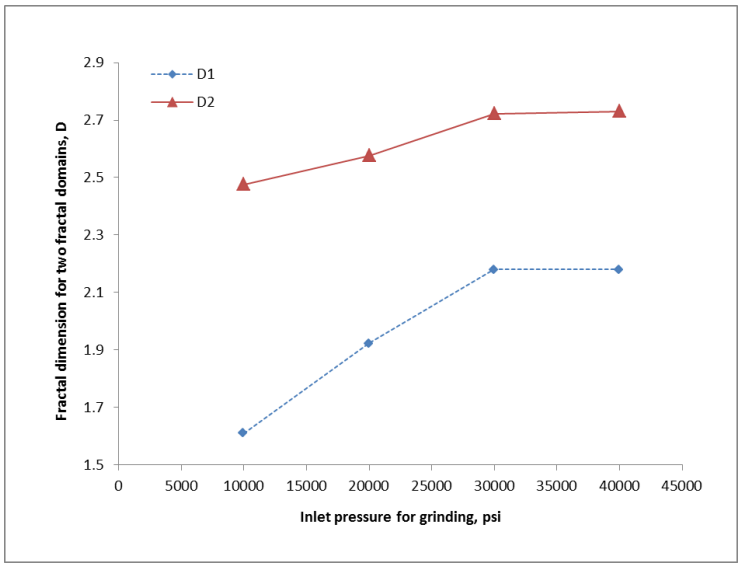

Figure 5.2. Fractal Dimensions of Particle Size Distribution versus Operational Pressure

5.4. SUMMARY OF SECTION 5

Results obtained in this Section indicate that the fractal theory is a useful tool to characterize the PSDs of coal products with a signal parameter. The proposed fractal model's use in characterizing the particle size distribution of coal comminuted in a high-pressure waterjet mill was well validated by the experimental results.

Experimental results indicate the particle size distribution of coal products comminuted by the high pressure waterjet mill exhibited bi-fractal performance. This bi-fractal performance suggests that there are two different breakage mechanisms at the waterjet-based comminution process. The abrasion mechanism predominantly produces smaller particles. The generation of relatively coarse particles is more dependent on the destructive mechanism.

Analysis of fractal dimensions indicates that, for the same fractal domain, the higher fractal dimension indicates a higher amount of fine particles. Additionally, it was found that the fractal characteristic of the products was strongly dependent on the operational pressure. The dependence on the operational pressure is acutely correlated to the transition of the breakage mechanism from destructive to abrasion combined with the

www.manaraa.com

change of the PSD curve. Higher operational pressures led to finer products with narrower size distribution. This effect connected to the observation that the abrasion breakage becomes the predominant size reduction mechanism as the operational pressure increased.

www.manaraa.com

6. CONCLUSIONS AND RECOMMENDATION FOR FUTURE WORK

6.1. CONCLUSIONS

To advance coal-water fuel preparation, a new method of waterjet-based coal comminution has been investigated. Results analysis of this study was the basis for drawing the following conclusions:

- Waterjet-based coal comminution offers a promising method for preparation of ultrafine coal particles for CWF. Analysis of experimental results demonstrated that regardless of coal properties, this comminution method can effectively develop a greater population of fine particles below 10 microns with a tight size distribution.
- Regarding jet properties, the waterjet-mediated coal comminution was strongly affected by the operational pressure and standoff distance. Regardless of feed properties, the higher operational pressure led to finer products with more spherical shape. The decrease of the standoff distance from 100 to 3 millimeters resulted in a significant increase in the size reduction as a result of increased impact energy.
- The properties of the feeds also have significant effects on the process of waterjet-based coal comminution. Feed size was the major factor affecting the size reduction ratio. Due to greater intensity of flaws and cracks in larger particles, coarser feeds resulted in higher size reduction ratios. Coal-water slurry feed resulted in lower size reduction ratios than crushed coal powder feed due mainly to the reduced solid concentration in the cavitation cell and mixing tube. The effect of the ash content on the performance of the waterjet mill varies with the type and occurrence mode of the minerals. For coal containing harder minerals and/or minerals occurring in the mode of disseminated individual grains, the waterjet mill was less efficient.
- Based on surface area change and morphological properties analysis, two major mechanisms for size reduction in the waterjet mill were identified. Additionally, it was found that the abrasion mechanism became more pronounced as the pressure increased.

www.manaraa.com

- To quantitatively assess the particle size distributions of the comminution products, a volume-based fractal model was deduced based on fractal theory. Based on this model, it was found that the particle size distributions of the coal products exhibited bi-fractal performance. The bi-fractal performance confirmed that there were two mechanisms involved in size reduction in the high-pressure waterjet mill. Further analyzing fractal dimensions leads to the conclusion that that the surface-dominant phenomena is the major mechanism for producing smaller particles, while the generation of larger particles depends on the volume-dominant mechanism.

6.2. RECOMMENDATIONS FOR FUTURE WORK

This research provides results of coal comminution with selected properties in relation to the waterjet parameters. Based on the experimental results, it is proposed to continue the work to further investigate the economic and environmental benefits of the novel comminution method. Therefore, the future work will focus on:

6.2.1. Construction of Mathematical Models for Waterjet-Based Comminution. Since there is currently no accurate model to quantitatively asses the efficiency of the waterjet mill for ultrafine coal comminution, more detailed further experiments will permit the construction of mathematical relationship between the process parameters and comminution efficiency.

6.2.2. Conduction of Comparative Experiments. Based on the literature review, waterjet-based coal comminution is a selective process. Thus, it is expected that the waterjet-based comminution method will improve the carbon separation in the following froth flotation process. To explore this, the conventional coal comminution methods will be replaced by a waterjet mill. Then, comparisons of coal combustion products will be made between the new method of feed stock preparation for powder generation and the conventional one.

6.2.3. Energy Consumption Analysis. Since the comminution theories are not suitable for estimating the energy consumption of the waterjet mill, it is proposed to use the specific surface energy for the process efficiency analysis.

www.manaraa.com

BIBLIOGRAPHY

Anonymous, 2011.New report power Generation from coal. *Coal News*, December 2011, pp.2.

Austin, G.L., 1984. Gaudin lecture: concepts in process design of mills. *Mining Engineering*, V.36 (n:6), pp. 628–635.

Bartoli, F., Philippy, R., Doirisse, M., Niquet, S., and Dubuit, M., 1991. Silty and sandy soil structure and self-similarity: the fractal approach. *Journal of Soil Science*, vol. 42, pp. 167-185.

Boltik, L., 2011. The future of mining. *Coal News*, December 2011, pp.11.

Carpiniteri, A., Pugno,N., 2002. A fractal comminution approach to evaluate the drilling energy dissipation. *International Journal for Numerical and Analytical Methods in Geomechanics*, vol.26, pp. 499-513.

Carpinteri, A., Pugno, N., 2003. A multifractal comminution approach for drilling scaling laws. *Powder Technology*, vol.131, pp. 93–98.

Caton, J.A., 1993. The development of a coal-fuel diesel engines: a brief review, 1992 Enenrgy Information Annual, 17, A89-A97.

Charles, W.D., Gallagher, A.E.J., 1982. Comminution energy usage and material wear. In: Mular, A.L., Jergensen, G.V., (II) (Eds.), Design and Installation of Comminution Circuits. S.M.E – A.I.M.E., New York, pp. 248–274.

Chen, Y., 2005. Fractal Geometry (2ed edition). The Earthquake Press, Beijing, 289 pp.

Corbit, D. J. and Garbary, J., 1995. Proceedings: Biological Sciences, vol. 262 (n:1363) , pp. 1-6.

Coulson, J. M., Richardson, J. F., 1980. Chemical Engineering, Pergamon Press, Great Britain.

Crawford, L.W., and Young, I.M., 1993. Quantification of fungal morphology, gaseous transport and microbial dynamics in soil: an integrated framework utilizing fractal geometry. *Geoderma*, vol. 56, pp. 157-172.

www.manaraa.com

Cui, L., An, L,, Jiang, H., 2008. A novel process for preparation of an ultra-clean superfine coal-oil slurry. *Fuel*, vol. 87, pp. 2296-2303.

Cui, L., An, L. Q., Gong, W. L., and Jiang, H. J., 2007. A novel process for preparation of ultra-clean micronized coal by high pressure water-jet comminution technique. *Fuel*, vol. 86, pp.750-757.

Cui, L., An, L., and Gong, W., 2006. Effects of process parameters on the comminution capability of high pressure water jet mill. *International Journal of Mineral Processing*, vol. 81, pp. 113–121.

Falconer, J.K., 1990. Fractal geometry: Mathematical Foundations and Applications. New York, Wiley.

Friesen, W. I., and Ogunsola, O. I., 1995. Mercury porosimetry of upgraded western canadian coals. *Fuel*, vol. 74 (n: 4), pp. 604-609.

Fu, S., Duan, X., and Gao, Y., 2001. Development of high–pressure water jet comminution. *Journal of Coal Science and Engineering* (China), vol. 1.

Fuerstenau, D.W., and Abouzeid, A. Z. M., 2002. The energy efficiency of ball milling in comminution. *International Journal of Mineral Processing*, vol. 67, pp. 161–185.

Galecki, G, Akar, G, Sen, S, and Li, Y., 2011. Enhanced cleaning of the coal feedstock for power generation. Mining engineering conference on *Innovations in Mining Engineering*, 30 Aug - 1 Sept. Rolla, United States.

Galecki, G., et al., 2009. Coal comminution with waterjets for diesel engine power generation. Poster session at the Missouri Energy Summit, 22-23 April, Columbia, MO, United States.

Galecki, G., and Mazurkiewicz, M., 1987a. Effectiveness of coal comminution by high pressure waterjet. 8th Miami International Conference on *Alternative Energy Sources*, 14-16 December, Miami Beach, Florida.

Galecki, G., and Mazurkiewicz, M., 1987b. Hydro abrasive cutting head - energy transfer efficiency. 4th U.S. *Waterjet Conference*, 26-28 August, University of California-Berkeley, pp. 109-117.

www.manaraa.com

Galecki, G., and Mazurkiewicz, M., 1988. Direct injection of coal into cavitation cell for the purpose of comminution. 9th International Symposium on *Jet Cutting Technology*, 4-6 October, Sendai, Japan.

Galecki, G., and Mazurkiewicz, M., 1998. Comminution by waterjets. *Book of water jet applications in construction engineering.* Momber, A. (eds). Rotterdam, Netherlands, A. A Balkema Publishers Press, 424pp.

Gee, J. M., and Warwick, R. M., 1994. Metazoan community structure in relation to the fractal dimensions of marine macroalgae. *Marine Ecology Progress Series*, vol.103, pp. 141-150.

Gong, W., and Fang, M., 1998. New development of jet mill technology and study on mechanism of comminution with high pressure water jet. *Chemical Engineering Processing*, vol. 6, pp. 30-33.

Gunnarsson, B.B., 1992. Fractal dimension of plants and body size distribution in spiders. *Functional Ecology*, vol. 6, pp. 636-641.

Gong, C., and Dong, L., 2007. Energy consumption in comminution of Mica with Cavitation Abrasive Water Jet. *Journal of China University of Mining and Technology*. vol. 17 (n: 2), pp. 251-254.

Guo, C.W., Liu, L., Li, A., and Zhang, D., 2002. Comminution of mica by cavitation abrasive water jet. *Journal of Jet Flow Engineering*, vol, 49 (n: 3), pp. 10-14.

Hlavac, M.L., et al., 2010a. Material grinding by waterjets–feasibility and limits. *Journal of Scientific Conference Proceedings*, vol. 2, pp. 8-14.

Hlaváč, M.L., Hlaváčová, I.M., Jandačka, P., Zegzulka, J., and Viliamsová, J., 2010b. Comminution of material particles by water jets-Influence of the inner shape of the mixing chamber. *International Journal of Mineral Processing*, vol. 25, pp.25-29.

Hou, S., and Sun, Z., 2003. High-pressure water jet technology. *Journal of Coal Science & Technology*, vol. 29, pp. 1-4, In Chinese.

Huang, G., Xu, S., and Li, X., 2003. Characterizations of PSD fractal of porous medium. *Transactions of Tianjing University*. vol. 9.

www.manaraa.com

Huang, K.F., 1994. Selective crush by high speed liquid jet. *Metallic Ore Dressing Abroad*, vol. 2, pp. 1-6.

Hyslip, P.J., Vallejo, E.L., 1997. Fractal analysis of the roughness and size distribution of granular materials. *Engineering Geology*, vol. 48, pp. 231-244.

Karmis, M., 2011. Research on environmental impacts of coal operations. *Coal News*, December 2011, pp. 19.

Kelly, E.G., and Spottiswood, D.J., 1995. Introduction to mineral processing. The Australian Mineral Fpundation press, Australia.

Kost, K., 2011. From Challenge, rises opportunity. Coal News, December 2011, pp. 9.

Kozak, E., Ya, A., Sokolowski, S., Sokolowska, Z., and Stepniewski, W., 1996. A modified number-based method for estimating fragmentation fractal dimensions of soils. *Soil Science Society of America Journal*, vol. 60, pp. 1291–1297.

Kwade, A., and Bernotat, S., 2002. Present and future treads in dry fine grinding. *Industrial Minerals*, January, pp. 69-71.

Laskowski, J.S., 2001. Coal flotation and fine coal utilization (first edition). Elsevier Science Publisher,368pp.

Lek, S., Kalayanee, K., Noparit, M., and Thammasak, P., 2008. Fine grinding of brittle minerals and materials by jet mill. *Songklanakarin J. Sci. Technol*, vol. 30 (n: 3), pp. 377-384.

Liu, Z., Sun, Z., 2005. Wet comminution of raw salt using high-pressure fluid jet technology. *Powder Technology*, vol.160, pp. 194 – 197.

Lu, P., Jefferson, I.F., Rosenbaum, M.S., and Smalley, I.J., 2003. Fractal characteristics of loess formation: evidence from laboratory experiments. *Engineering Geology*, vol. 69, pp. 287–293.

Mandelbrot, B. B., 1977. Fractals: Form, Chance and Dimension. W H Freeman and Co, 1977; ISBN 0716704730.

Mandelbrot, B. B., 1982. The Fractal Geometry of Nature, W.H. Freeman and Company, New York, 497 pp.

www.manaraa.com

Mazurkiewicz, M., 2001. Method of creating ultra-fine particles of materials using a high-pressure mill. United States Patent No: 6318649.

McCabe,W.L., Smith, J.C., and Harriott,P., 1993. Unit Operation of Chemical Engineering. McGraw Hill Inc., Singapore.

Morse, D, R., Lawton, J.H., Dodson, M., and Willamson, M.H., 1985. Fractal dimension of vegetation and the distribution of arthropod body lengths. *Nature*, vol. 314, pp.731-733.

Neale, E.A., Bowers, L.M., and Smith, T.G., 1993. Early dendrite development in spinal cord cell cultures: a quantitative study. J. *Neurosci. Res*., vol. 34, pp. 54-66.

Perfect, E., 1997. Fractal models for the fragmentation of rocks and soils: a review. *Engineering Geology*, vol. 48, pp.185-198.

Perfect, E., Rasiah, V., and Kay, B.D., 1992. Fractal dimensions of soil aggregate-size distributions calculated by number and mass. *Soil Science Society of America Journal*, vol. 56, pp. 1407–1409.

Perry's., 1984. Perry's chemical engineers' handbook. McGraw Hill Press, Singapore.

Rieu, M., and Sposito, G., 1991. Fractal fragmentation, soil porosity, and soil water properties: II. Application. *Soil Science Society of America Journal*, vol. 55, pp. 1239-1244.

Smith T.G Jr, Marks W.B, Lange G.D, Sheriff W.H. Jr., Neale E.A., 1989. A fractal analysis of cell images. *Journal of Neuroscience Methods*, vol. 27 (n:2), pp.173-80.

Sri Raj Rajeswari, M., Azizli, K.A.M., Hashim, S.F.S., Abdullah, M.K., Abdul Mujeebu, M., and Abdullah, M.Z., 2011. CFD simulation and experimental analysis of flow dynamics and grinding performance of opposed fluidized bed air jet mill. *International Journal of Mineral Processing*, vol. 98, pp.94-105.

Sun, J., 1993. Waterjet cutting technology. China University of Ming and Technology Press.

Sun, Z., and Hou, F., 2002. Orthogonal analysis for factors of water power comminuting raw salt. *Fluid Mach*, vol. 30, pp. 47–50.

www.manaraa.com

Tasdemir, A., 2009. Fractal evaluation of particle size distributions of chromites in different comminution environments. *Minerals Engineering*, vol. 22, pp. 156-167.

Tony Hayward Group Chief Executive, 2010. Coal Can Do That. In Coal: The World's Fastest-Growing Fuel for the Past Decade. Retrieved July 13, 2011, from http://www.coalcandothat.com/content.php?view=571.

Turcotte, D.L., 1986. Fractal and fragmentation. *Journal of Geophysical Research*, vol. 91, pp.1291–1296.

Turcotte, D.L., 1992. Fractals and Chaos in Geology and Geophysics. Cambridge University Press, Cambridge.

Thilagan Palaniandy, S., 2008. A study on ultrafine grinding of silica and talc in opposed fluidized bed jet mill. PhD Dissertation, University Sains Malaysia.

Wang, R., Chen, K., Li, D., and Ma A., 2009. Research of ultra-fine comminuting coal with premixed water jet based on neural network. *Procedia Earth and Planetary Science*, vol.1, pp.1519–1524.

Wang, Y., and Forssberg, E., 2007. Enhancement of energy efficiency for mechanical production of fine and ultra-fine particles in comminution. *China Particuology*, vol. 5, pp. 193-201.

Wills, B.A., 1997. Mineral processing technology. Great Britain by Scotprint Ltd. Press, Musselbrugh, Great Britain, 486pp.

Wu, Q., Borkovec, M., and Sticher, H., 1993. On particle-size distributions in soils. *Soil Science Society of America Journal*, vol. 57, pp. 883-890.

Yashima,S., Kanda, Y., and Sano, S., 1987. Relationship between particle size and fracture energy as estimated for single particle crushing. *Powder Technology*, vol.51, pp.277-282.

Zeng, F., Zhu, S., and Wang, Z., 2002. The fractal characteristics of particle size distribution in coal grinding process. *Mining Science and Technology*. A. A. Balkema Publishers, pp. 493–496.

Zhang, B., and Li, S., 1995. Determination of the surface fractal dimension for porous media by mercury porosimetry. *Industrial & Engineering Chemistry Research*, vol. 34, pp. 1383-1386.

www.manaraa.com

Zhou, F., He, Q., Wang, D., Dai, G., and Lu, W., 2004. Relationship between fractal characteristics of pores in coal and oxygen-adsorbing quantity. *Proceedings of the 5th International Symposium on Mining Science and Technology*, pp.4.

Zulfiquar, H .M., Moghtaderi, B., and Wall, F.T., 2006. Technology assessment report 49 of Co-Milling of coal and biomass in a pilot-scale vertical spindle mill. The university of Newcastle.

www.manaraa.com

VITA

Yaqing Li was born in Shaanxi, China. She graduated with a Bachelor's Chemical Engineering degree in June 2006 from China University of Mining and Technology. Prior to joining Missouri University of Science and Technology she worked in Xuzhou VIC S&T Corporation (China) as a project manager in the Energy Division from October 2006 to December 2008. She joined Missouri University of Science and Technology in the spring of 2010 for her Master's degree in Mining Engineering. Her area of focus is Mineral Processing. She graduated with her Master's degree in Mining Engineering in December 2012.

www.manaraa.com

المنارة للاستشارات
www.manaraa.com